OUKA
Osaka University Knowledge Archive

Title	Analysis of roles of NurA and HerA in DNA repair in Thermus thermophilus
Author(s)	藤井, 裕己
Citation	大阪大学, 2018, 博士論文
Version Type	VoR
URL	https://doi.org/10.18910/70785
rights	
Note	

Osaka University Knowledge Archive : OUKA

https://ir.library.osaka-u.ac.jp/

Osaka University

Analysis of roles of NurA and HerA in DNA repair in *Thermus thermophilus*

Doctoral thesis
September 2018

Yuki Fujii

Graduate School of Frontier Biosciences

Osaka University

Abstract

NurA and HerA are thought to be essential proteins for DNA end resection in archaeal homologous recombination systems. *Thermus thermophilus* HB8, an extremely thermophilic eubacterium, has proteins that exhibit significant sequence similarity to archaeal NurA and HerA. To unveil the cellular function of NurA and HerA in *T. thermophilus* HB8, I performed phenotypic analysis of disruptant mutants of *nurA* and *herA* with or without DNA-damaging agents. The *nurA* and *herA* genes were not essential for survival, and their deletion had no effect on cell growth and genome integrity. Unexpectedly, these disruptants of *T. thermophilus* HB8 showed increased resistance to UV irradiation and mitomycin C treatment. Further, these disruptants and the wild type displayed no difference in sensitivity to oxidative stress and a DNA replication inhibitor. *T. thermophilus* HB8 NurA had nuclease activity, and HerA had ATPase. The overexpression of loss-of-function mutants of *nurA* and *herA* in the respective disruptants showed no complementation, suggesting their enzymatic activities were involved in the UV sensitivity. In addition, *T. thermophilus* HB8 NurA and HerA interacted with each other *in vitro* and *in vivo*, forming a complex with 2:6 stoichiometry. These results suggest that the NurA-HerA complex has a similar architecture to archaeal counterparts, but that it impairs, rather than promotes, the repair of photoproducts and DNA crosslinks in *T. thermophilus* HB8 cells. This cellular function is distinctly different from that of archaeal NurA and HerA.

Table of contents

Abbreviations

ccc	covalently closed circular
CD	circular dichroism
Chi	crossover hotspot instigator
CPD	cyclobutane pyrimidine dimer
DSB	double-strand break
dsDNA	double-stranded DNA
F_D	frequency of DNA uptake
F_H	apparent frequency of HR
GEO	Gene Expression Omnibus
HAS	HerA and ATP synthase
HR	homologous recombination
Hyg	hygromycin-B
Km	kanamycin
MMC	mitomycin C
NA	nalidixic acid
NER	nucleotide excision repair
oc	open circular
OD_{660}	optical density at 660 nm
PBS	phosphate-buffered saline
SSB	single-strand DNA-binding protein
ssDNA	single-stranded DNA
TEV	tobacco etch virus
TLS	translesion DNA synthesis
transjugation	transformation-dependent conjugation
TRCF	transcription-repair coupling factor
T_m	transition temperatures
UV	ultraviolet
WT	wild type

General introduction

For all living organisms, it is essential to guarantee accurate storage and propagation of their genetic informations. However, in living cells, DNA is subjected to various lesions by exogenous and endogenous damaging agents, which generate a large variety of DNA lesions (1). Exogenous damage includes photoproducts, double-strand break (DSB), oxidized bases, and interstrand crosslink (Fig. 1). These damage can be produced by ultraviolet (UV) light, ionizing radiation, reactive oxygen species, and DNA crosslink agents throughout the cell cycle (1). Even under physiological conditions, endogenous damage can occur naturally and persistently through intrinsic instability of chemical bonds in DNA. If the resulting DNA lesions are not correctly repaired, they cause genome alteration and, in the worst case, could lead to cell death.

All organisms have various DNA repair machineries to overcome these DNA lesions (1) (Fig. 1). Several DNA repair pathways have been reported that include direct repair, base excision repair, nucleotide excision repair (NER), mismatch repair, and recombinational repair pathways. Most of these pathways utilize multiple proteins and require their functional interactions. Beside direct repair, there are three steps to all repair processes: recognition of a lesion, removal of the damaged base or nucleotides including the damage, and filling of the gap. For example, in the prokaryotic NER system, UvrABC excinucleases recognize and excise DNA lesions, UvrD helicase removes the nucleotide fragment containing the damage, DNA polymerase I synthesizes the complementary strand, and then DNA ligase completes the repair process (2). NER has two sub-pathways, global genomic repair and transcription-coupled repair. In the latter pathway, stalling of the RNA polymerase is responsible for the initiation of repair. Transcription-repair coupling factor (TRCF) releases the stalled RNA polymerase from the template DNA and then recruits UvrA (3).

The cell utilizes different repair pathways for different kinds of damages. In base excision repair pathway various DNA glycosylases specifically recognize damaged bases. In contrast, NER enzymes have broad substrate specificity: these can recognize and excise DNA lesions such as UV-induced pyrimidine dimers and more bulky adducts, but cannot repair DSB.

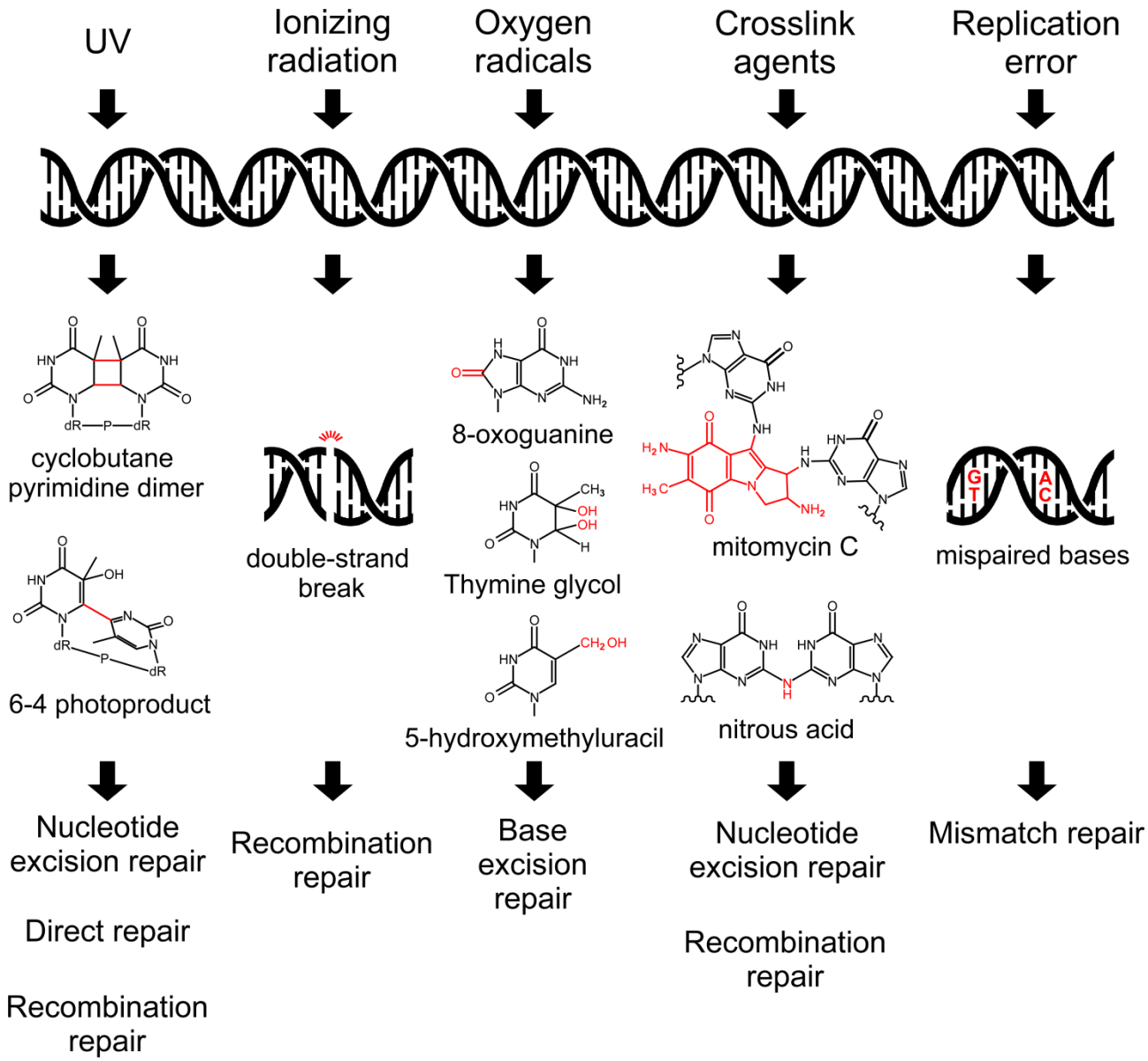

Fig. 1 Instances of DNA damaging agents, DNA lesions, and DNA repair pathways. DNA damages are shown in red. In structural formulas of DNA lesion, dR-P-dR indicates a deoxyribose-phosphate-deoxyribose chain of DNA.

In these DNA lesions, DSBs are one of the most severe types of damage. The pathways for the repair of DSBs are roughly divided into three types: non-homologous end joining, single-strand annealing, and homologous recombination (HR). In contrast to the former two pathways, HR has a role in the repair of DSBs in an error-free manner (Fig. 2). The mechanism of HR is widely conserved in all the domains of life (4). The first event required for the repair of DSB via HR is DNA end resection: resection of one strand at the DNA end by a nuclease and a helicase. On the resultant 3′ overhang, recombinases are recruited and form filaments via mediator proteins, and search the homologous sequences (strand invasion and second-end capture in Fig. 2). Then, a DNA polymerase performs the extension-synthesis of the downstream region from a captured end, and concomitantly a crossover structure (Holliday junction) moves to proceed the strand exchange. Finally, a Holliday junction is resolved by a resolvase, and a nick is sealed by a DNA ligase.

In DNA end resection, the activities of nucleases and helicases are essential to generate 3′ overhang for searching the homologous sequence by recombinases (strand exchange) (5–7). The kinds of enzymes used for end resection are quite different between eukaryotes and bacteria. In eukaryotic cells, MRE11-RAD50-NBS1 (human, MRN) or Mre11-Rad50-Xrs2 (*Saccharomyces serevisiae*, MRX) binds to DSB regions, and recruits CtIP/Sae2 (or Ctp1). MRN/X makes short 5′ overhang in DSBs end, and CtIP/Sae2 process the 5′ end in the limited extent (8–14), followed by generation of long 3′ overhang by EXO1 or DNA2-BLM/Sgs1 complex (9, 10, 12, 15).

On the other hand, bacteria have two kinds of end resection pathways, RecBCD/AddAB pathway and RecF pathway. In RecBCD/AddAB pathway, helicase-nuclease complex RecBCD/AddAB unwinds and digests the duplex DNA from the DSB end until encounter with the recombination hot spot, Chi (crossover hotspot instigator) site (16–18). After Chi recognition, only 5′ strand is digested while RecA proteins are loaded on 3′ overhang by RecBCD/AddAB (19). In *Escherichia coli*, with the absent of RecBCD, SbcB (ExoI) and SbcC background, exonuclease RecJ and helicase RecQ process the 5′ end of DSBs (20, 21). In some bacteria that have no RecBCD/AddAB family proteins (22), end resection is thought to be performed by proteins such as RecJ, RecQ, UvrD and HelD in RecF pathway (23).

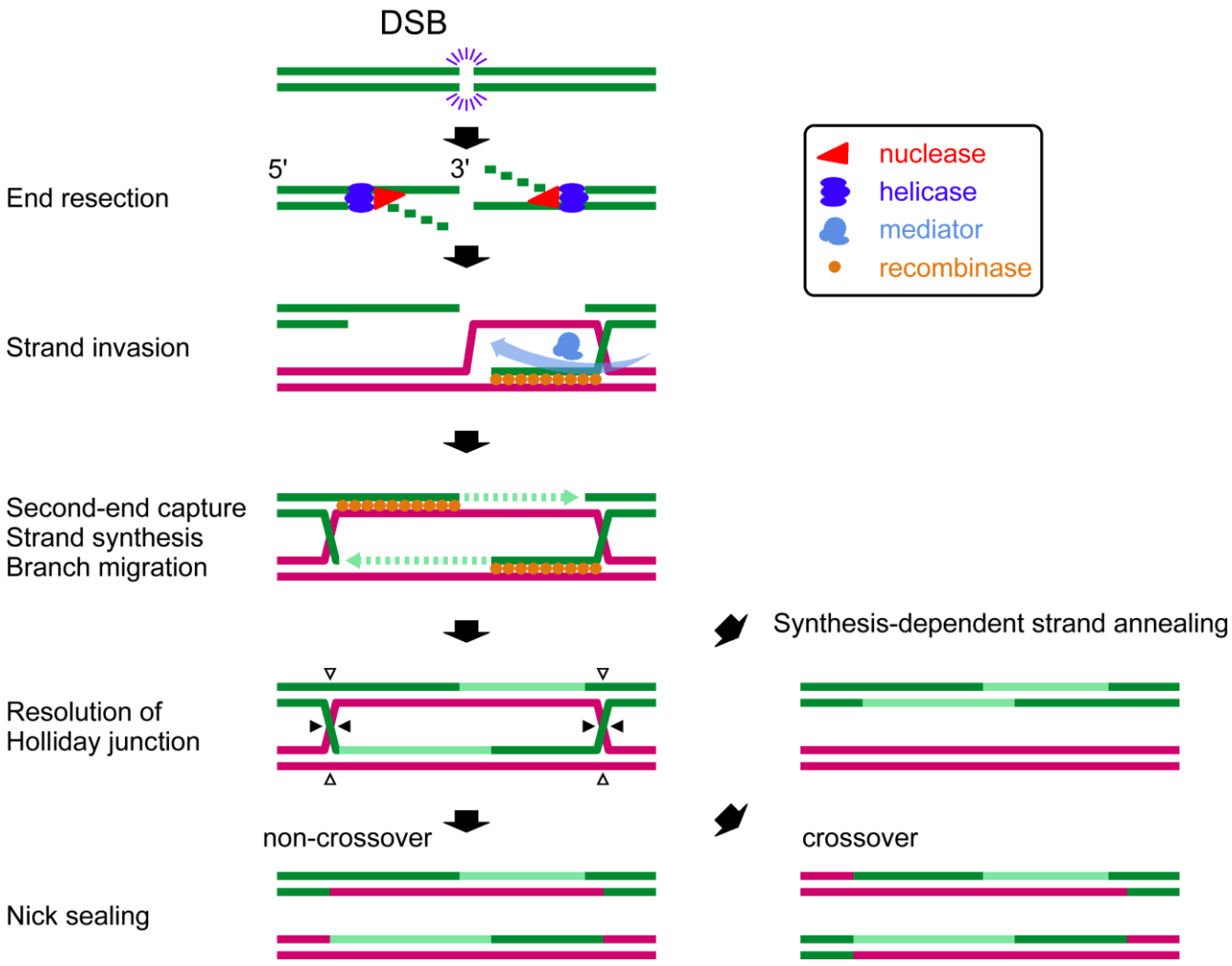

Fig. 2 The overview of DSB repair via homologous recombination. Green lines are damaged strand, and magenta lines are homologous strand to damaged strand. Closed or open triangles in the 5th step indicate the orientation of incision for resolving Holliday junctions. Only when both Holliday junctions are incised at the same direction, non-crossover products are generated.

In archaea, homologs of Rad50/SbcC and Mre11/SbcD were first identified (24, 25) and showed the same activities as their counterparts (26). In contrast, comparative genomic analyses had failed to detect any archaeal homologs of RecBCD or RecFOR. Shortly thereafter, however, new genes encoding a novel type of nuclease (NurA) and helicase (HerA) were identified that might be involved in end resection in archaea (27–29). In the present day, NurA and HerA are well known to be the end resection-related nuclease and helicase in archaea (see Introduction).

In this study, I performed functional analysis of bacterial NurA and HerA homologs of an extremely thermophilic bacterium, *Thermus thermophilus* HB8. In this bacterium, *nurA* and *herA* genes were not essential for survival, in contrast to archaeal homologs. In *T. thermophilus* HB8, disruption of *nurA* and/or *herA* increased resistance to UV irradiation and mitomycin C treatment compared to wild type, but had no effect on sensitivity to H_2O_2 and nalidixic acid treatment. Based on these phenotypes, I suggested that in *T. thermophilus* HB8 NurA and HerA play inhibitory or regulatory roles in repairing photoproducts and DNA crosslinks.

Introduction

Though archaea and eukaryotes share many basic features at the molecular level (30), archaeal cells have clearly different enzymes for end resection compared to eukaryotes, that is, nuclease NurA and helicase HerA. NurA and HerA genes are widely conserved in archaea. The molecular functions of archaeal NurA and HerA have been analyzed in detail. NurA has Mn^{2+}-dependent 5′-to-3′ exonuclease/endonuclease activities to single-stranded DNA (ssDNA) and double-stranded DNA (dsDNA) (27, 31, 32). HerA is a bipolar (5′→3′ and 3′→5′) helicase driven by ATP hydrolysis activity, which is promoted by binding to ssDNA and dsDNA (28). NurA forms the toroidal dimer (PDB ID, 3TAZ and 2YGK) (33, 34) and interacts with the hexameric ring of HerA (PDB ID, 4D2I), which is mediated by the N-terminal HAS (HerA and ATP synthase) domain (34–36) (Fig. 3A and B). The NurA-HerA interaction contributes to high 5′→3′ exonuclease activity of NurA (32–34, 37). In addition, HerA proteins of *Sulfolobus acidocaldarius* and *Sulfolobus tokodaii* interact with Mre11 and/or Rad50 (38, 39). Furthermore, activities of NurA and/or HerA are stimulated by Mre11 or Mre11-Rad50 complex (37, 38). In many archaea, *nurA* and *herA* are encoded next to *mre11* and *rad50* in an operon-like gene cluster (27–29, 40). Like *mre11* and *rad50*, *nurA* and *herA* are also essential genes (41–43), and the involvement of NurA and HerA in HR as a cellular function has been verified by the experiments using wild-type (WT) strains (39, 44, 45). These findings support the notion that archaeal NurA and HerA are involved in end resection (Fig. 3C), although that is incompletely proved. In some archaea, NurA and HerA may function as CRISPR-associated proteins (46, 47).

In addition to RecJ and/or RecBCD/AddAB homologs, NurA and HerA homologs are conserved in many kinds of bacteria, and especially often found in *Cyanobacteria*, *Actinobacteria*, *Firmicutes*, and *Deinococcus-Thermus* (Fig. 4). The bacterial NurA and HerA homologs are less well understood, and have been studied only in a part of *Deinococcus-Thermus* species. Although *Deinococcus radiodurans* NurA alone has no nuclease activity, it shows 5′-to-3′ ssDNA/dsDNA exonuclease/endonuclease activities in the presence of *D. radiodurans* HerA (40). Also, the ATPase activity of *D. radiodurans* HerA is stimulated by interaction with *D. radiodurans* NurA (40). Furthermore, in the case of *D. radiodurans*, HerA interacts with RecJ and stimulates the 5′-to-3′ exonuclease activity of RecJ (48). In the *D. radiodurans* genome, NurA and HerA genes are tandemly arranged but do not form a gene cluster with *sbcD* and *sbcC*, homologous genes of *mre11*

and *rad50*, respectively. *D. radiodurans nurA* and *herA* genes are not essential, but these single- and double-gene disruptant mutants show rapid growth cycle compared to WT (40). In addition, these disruptants show a low frequency of inter-molecular recombination, which suggests that *D. radiodurans* NurA and HerA may be involved in HR (40). In contrast, the disruptant mutant of the *nurA* gene alone shows increased resistance to mitomycin C (MMC) (48), which shows no involvement of NurA in repair of damaged DNA. NurA can block RecJ nuclease activity (48). Therefore, *D. radiodurans* NurA and HerA are thought to modulate RecJ activity. However, cellular components known so far to be involved in end resection are different between bacteria and archaea. Thus, the involvement of NurA and HerA in end resection is still unclear in bacteria.

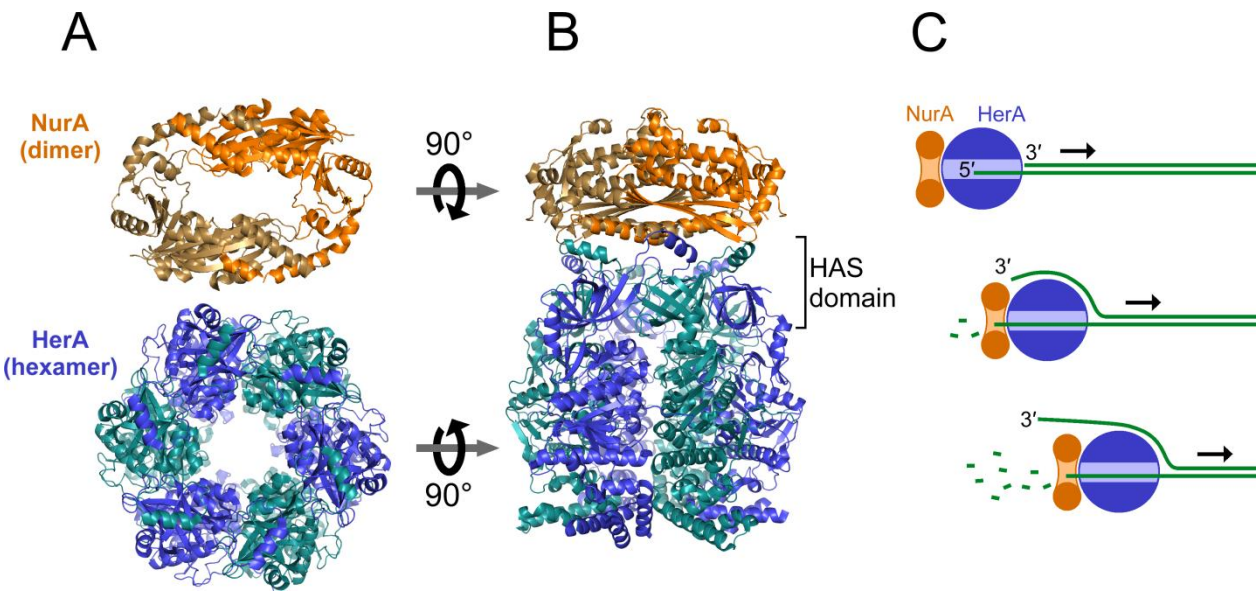

Fig. 3 The structure and molecular function of NurA and HerA. (A) Structures of NurA (PDB ID, 2YGK) and HerA (PDB ID, 4D2I). (B) A model of the structure of NurA-HerA complex. (C) A model of end resection by NurA-HerA complex. These figures were modified from Blackwood *et al.* (34), and Byrne *et al*. (36).

We have studied the HR system in *Thermus thermophilus* HB8, an extremely thermophilic eubacterium that belongs to the same phylum as *D. radiodurans* (49–53). In *T. thermophilus* HB8, RecJ has been thought to be the only enzyme that can perform the processing of the 5′-ends of DNA in HR because this bacterium has no *recBCD* and *recQ* homolog (1). However, the *T. thermophilus* RecJ gene can be disrupted (51), indicating the possibility that other nucleases are involved in the 5′-end processing. In fact, recent studies described above showed the essentiality of archaeal *nurA* and *herA* for cell survival (41–43), and the double mutants of *recJ recBCD* and *recJ recD* show lethality in *Acinetobacter baylyi*, which has no other homolog for an end-resection-related exonuclease (54). Interestingly, detailed sequence analysis revealed genes (*ttha0521* and *ttha0522*) coding for nuclease- and helicase-like proteins that are similar to NurA and HerA, respectively.

Although *T. thermophilus* and *D. radiodurans* belong to the same phylum, their homologous proteins may not have the same cellular functions. The genetic background of *T. thermophilus* is different from that of *D. radiodurans*: *D. radiodurans* has several potential nucleases and helicases for end resection, such as nuclease RecJ and XseA (one of the two subunits of exonuclease ExoVII), and helicase RecQ, UvrD, RecD, and HelD (55–58), whereas *T. thermophilus* HB8 has only RecJ. *T. thermophilus* HB8 also has UvrD, but its disruptant shows similar UV sensitivity to WT (59). There may be a significant overlap of function among the nucleases and helicases in *D. radiodurans*. The difference in genetic background raises the possibility that NurA and HerA in *T. thermophilus* have different functions from those in *D. radiodurans*. In addition, the genome size of *T. thermophilus* HB8 (2.20 Mbp) is smaller to that of *D. radiodurans* R1 (3.28 Mbp). These offer significant advantages for basic research in genetics and molecular biology in *T. thermophilus*.

In this study, I performed mainly phenotypic analysis of gene disruptants of *nurA* and *herA* in *T. thermophilus* HB8 for unveiling the cellular function of NurA and HerA. The *nurA* and *herA* genes were not essential for survival, and their disruption had no effects on proliferation under optimal growth conditions. Unexpectedly, the disruptant mutants showed increased resistance to UV irradiation and MMC treatment but did not show a significant increase in sensitivity to oxidative stress and DNA replication inhibitor. I propose a model in which NurA and HerA in *T. thermophilus* HB8 play a role in the repair of photoproducts and DNA crosslinks in an interfering manner.

Fig. 4 (next pages) Molecular phylogenetic trees of NurA (A) and HerA (B) in bacteria. The indicated strains and gene IDs were obtained by searching the database Pfam 31.0 (https://pfam.xfam.org/) and EggNOG 4.5.1 (http://eggnogdb.embl.de/#/app/home). All amino acid sequences were aligned by multiple-alignment tool MUSCLE and molecular phylogenetic trees were generated by maximum likelihood method with a phylogenetic analysis software MEGA7 (https://www.megasoftware.net/). NurA (TTHA0521) and HerA (TTHA522) of *T. thermophilus* HB8 are shown in red. NurA(-like) and HerA(-like) proteins of *T. thermophilus* HB27 are shown in blue. Boot strap values more than 70 are shown on the branches and expressed in percentages.

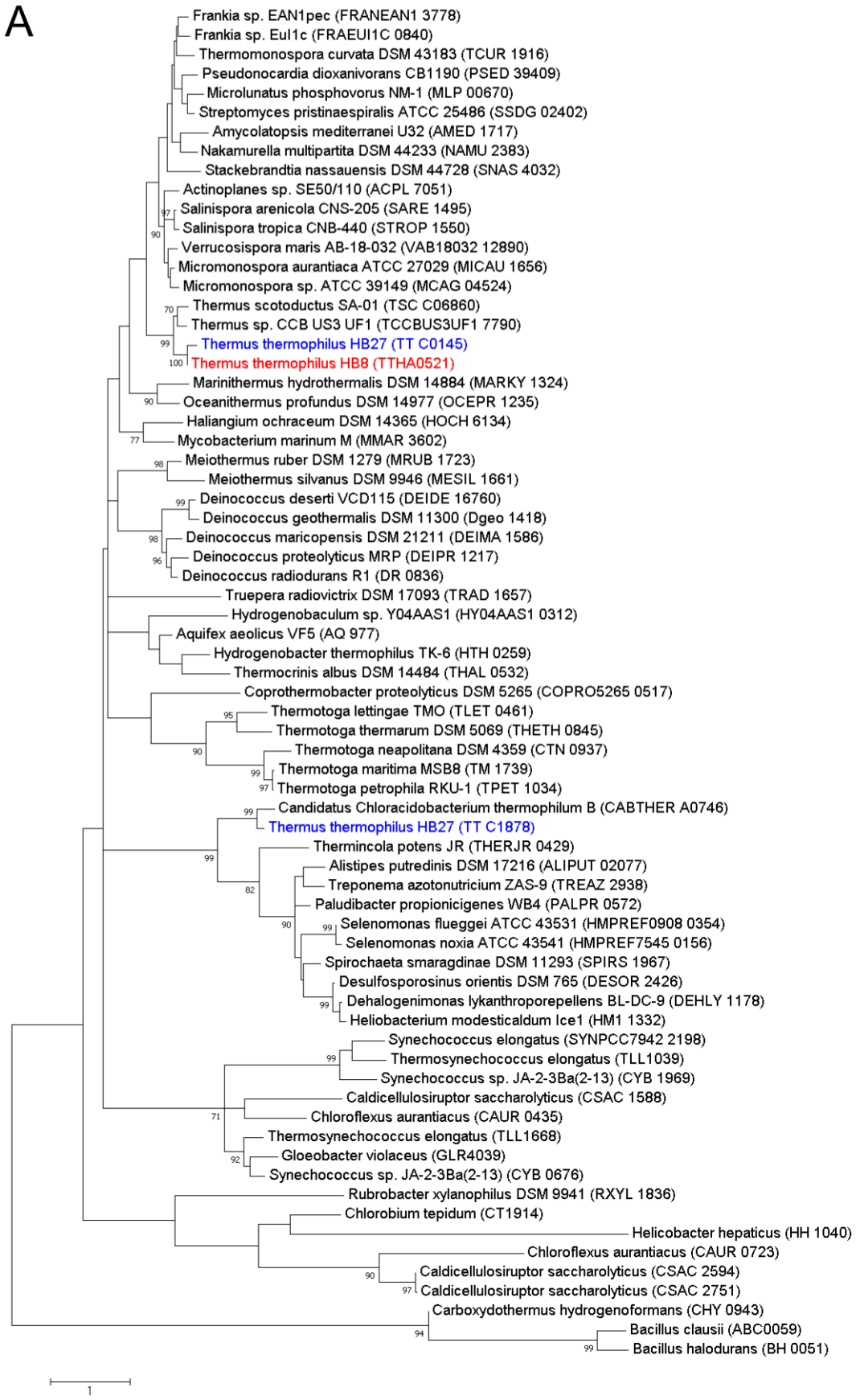

Fig. 4 (continued)

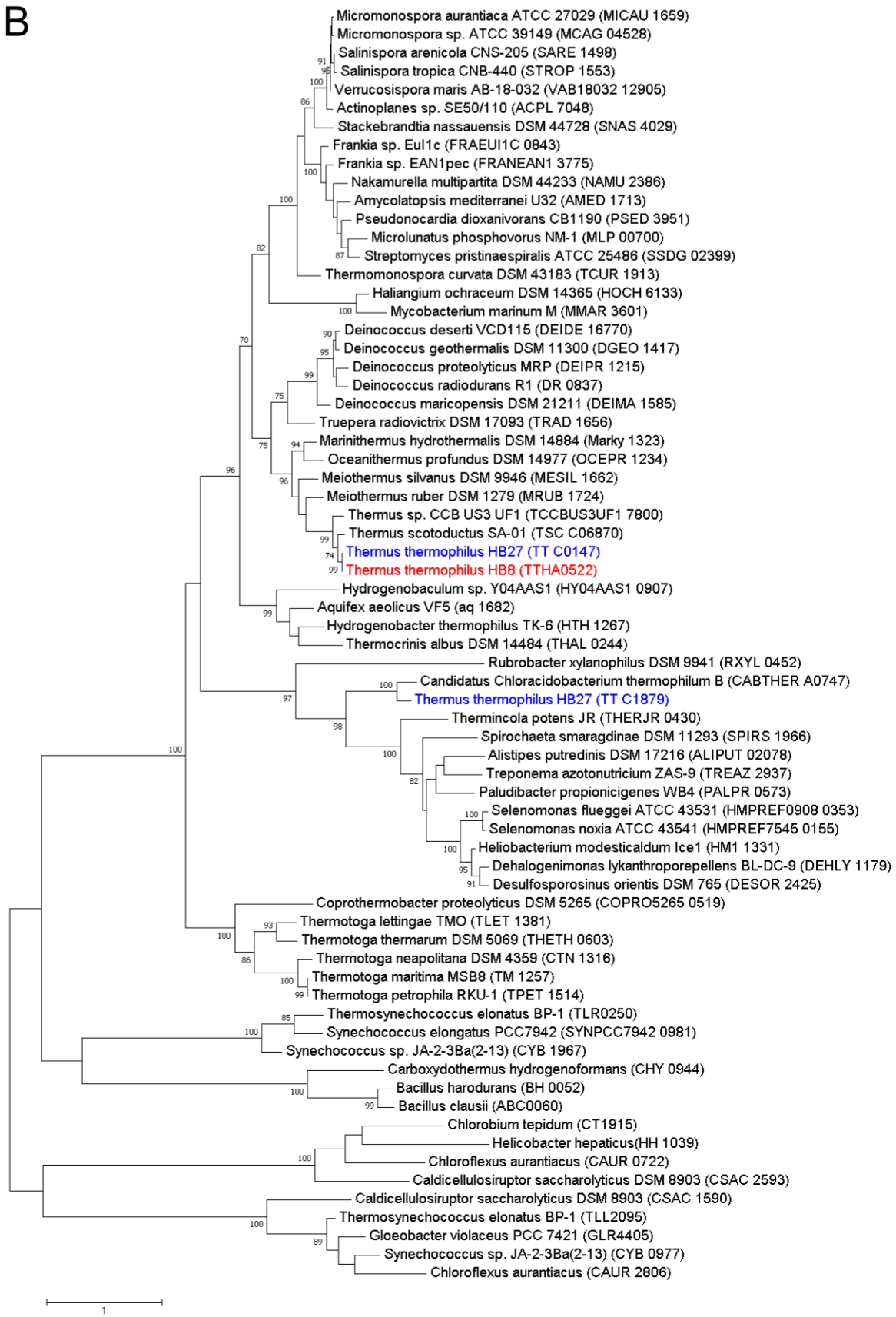

Fig. 4 (continued)

Materials and Methods

Cultivation of *T. thermophilus* HB8

T. thermophilus HB8 was grown at 70°C in TR broth: 0.4% (w/v) tryptone (Difco Laboratories, Detroit, MI, USA), 0.2% (w/v) yeast extract (Oriental Yeast, Tokyo, Japan), and 0.1% (w/v) NaCl (pH 7.5) (adjusted with NaOH). For transformation experiments, *T. thermophilus* HB8 was grown in TT broth, which was made by adding of 0.4 mM $CaCl_2$ and 0.4 mM $MgCl_2$ to TR broth. To make plates, 1.5% (w/v) Phytagel (Sigma-Aldrich, Tokyo, Japan), 1.5 mM $CaCl_2$, and 1.5 mM $MgCl_2$ were added to TR broth (TT plate). To make TT agar plates, 1.5% (w/v) agar (Nacalai Tesque, Kyoto, Japan) was added to TR broth. For phenotypic analysis, cells in log phase were prepared as follows (unless otherwise noted): *T. thermophilus* HB8 cells were inoculated in 3 mL of TR broth and incubated for 16 h at 70°C, and the cultures were diluted at 1:60 in 3 mL TR broth and further incubated at 70°C for about 3 h up to log phase (0.8–2.0 × 10^8 cells/mL). The cell density was confirmed by counting under a microscope. When *T. thermophilus* HB8 cells were incubated on TT or TT agar plates, all plates were protected from drying and light by covering them with aluminum foil.

Transcriptome data analysis

Transcriptome data were obtained from data sets about the *T. thermophilus* HB8 WT strain on the NCBI Gene Expression Omnibus (GEO) web site. The data set about transcriptional changes in cell growth (Accession: GSE21290) was normalized as followed: the raw data values of expression signals from all time points were divided by their arithmetic means. The ratio of each normalized datum to the arithmetic mean indicated the fold change. Other data sets were normalized by the method described previously (60).

Disruptions of target genes

Disruptants of *nurA*, *herA*, *recJ*, *recR*, *uvrA*, and *trcf* (Δ*nurA*, Δ*herA*, Δ*recJ*, Δ*recR*, Δ*uvrA*, and Δ*trcf*, respectively) were generated by substitution of the target gene with the thermostable kanamycin-resistance gene, *HTK* (61), or thermostable hygromycin B-resistant gene, Hyg^R (Accession: AB470102.1), via HR. The plasmids for gene disruption, pGEM-T Easy/Δ*nurA*::*HTK* and pGEM-T Easy/Δ*herA*::*HTK*, pGEM-T Easy/Δ*recJ*::*HTK*, pGEM-T Easy/Δ*recR*::*HTK*, pGEM-T

Easy/Δ*uvrA*::*HTK*, and pGEM-T Easy/Δ*trcf*::*HTK*, were derivatives of pGEM-T Easy Vector (Promega, Madison, WI, USA) and were constructed by inserting *HTK* flanked by approximately 500-bp upstream and downstream sequences of each gene. The plasmid for double-gene knockout of *nurA* and *herA* was constructed from these plasmids: in the *T. thermophilus* HB8 genome sequence, *nurA* and *herA* are arranged in tandem, and thus these were disrupted simultaneously. Both pGEM-T Easy/Δ*nurA*::*HTK* and pGEM-T Easy/Δ*herA*::*HTK* have a PstI site and an NdeI site on 5′ and 3′ termini of the downstream sequences. These plasmids were digested with PstI and NdeI, and the resultant larger fragment from pGEM-T Easy/Δ*nurA*::*HTK* and the smaller fragment from pGEM-T Easy/Δ*herA*::*HTK* were ligated together to construct pGEM-T Easy/Δ*nurA*Δ*herA*::*HTK*. The plasmid for gene disruption containing Hyg^R was constructed as follows. The pHG305 and each plasmid containing *HTK* (except for the plasmid targeting *recJ*) for gene disruption were digested with KpnI and PstI. The resultant smaller fragment from the former and the larger fragment from the latter were ligated to construct pGEM-T Easy/Δ*recR*::Hyg^R, pGEM-T Easy/Δ*uvrA*::Hyg^R, and pGEM-T Easy/Δ*trcf*::Hyg^R. The plasmid pGEM-T Easy/Δ*recR*::Hyg^R was constructed in previous study by Shimada *et al*. (51).

For gene disruption, *T. thermophilus* HB8 cells were transformed with these plasmids as follows. *T. thermophilus* HB8 cells in log phase in 400 μL of TT broth were cultivated at 70°C for 2 h after the addition of the plasmid for gene disruption in 50 μL distilled water. Transformants were selected on TT plates containing 500 μg/mL kanamycin (Km; TT+Km plate) or 100 μg/mL hygromycin-B (Hyg; TT+Hyg plate). Since *T. thermophilus* HB8 is a polyploid bacterium (62), incomplete disruption of the target gene is often observed through single selection step. For complete disruption of target genes, obtained colonies were re-cultured in TR broth containing 50 μg/mL Km or 100 μg/mL Hyg. This cultured cells were isolated on TT+Km or TT+Hyg plate, and incubated at 70°C overnight. Gene disruptions of *nurA*, *herA*, *nurA-herA*, and *recJ* were confirmed by PCR amplification using the purified genomic DNAs (described below) as templates and three types of primer sets: P1-P2, P2-P3, and P1-P10 for Δ*nurA*::*HTK*; P4-P5, P4-P6, and P4-P10 for Δ*herA*::*HTK*; P1-P5, P1-P6, and P1-P10 for Δ*nurA*Δ*herA*::*HTK*; P7-P8, P8-P9, and P7-P10 for Δ*recJ*::*HTK*; and P7-P8, P8-P9, and P7-P20 for Δ*recJ*::Hyg^R. The disruptions of *recR*, *uvrA*, and *trcf* were confirmed by cultured-cell PCR (described below) with the following primer pairs: P11-P12, P11-P13, and P11-P20 for Δ*recR*::Hyg^R; P14-P15, P14-P16, and P14-P20 for Δ*uvrA*::Hyg^R; and

P17-P18, P17-P19, and P17-P20 for Δ*trcf*::*Hyg*^{R} (Table 1).

Multiple gene disruptants were generated as follows. Δ*nurA*Δ*herA*Δ*recJ* and Δ*nurA*Δ*herA*Δ*recR* were generated via transformation of Δ*recJ*::*Hyg*^{R} and Δ*recR*::*Hyg*^{R} strains, respectively, with pGEM-T Easy/Δ*nurA*Δ*herA*::*HTK*. Δ*nurA*Δ*herA*Δ*uvrA* and Δ*nurA*Δ*herA*Δ*trcf* were generated via transformation of Δ*nurA*Δ*herA*::*HTK* strain with pGEM-T Easy/Δ*uvrA*::*Hyg*^{R} and pGEM-T Easy/Δ*trcf*::*Hyg*^{R}, respectively. Δ*uvrA*Δ*recR* was generated via transformation of Δ*uvrA*::*Hyg*^{R} strain with pGEM-T Easy/Δ*recR*::*HTK*. Gene disruptions in these multiple gene disruptants were also confirmed by PCR amplification as described above.

Purification of genomic DNA of *T. thermophilus* HB8

Overnight cultures of *T. thermophilus* HB8 cells in 4.5 mL of TR broth (+Km or +Hyg for gene disruptants) were harvested at 19,000 × *g* at 4°C for 5 min and were washed with 500 μL of phosphate-buffered saline (PBS). These cells were suspended in 0.9 mL of GTE solution (25 mM Tris-HCl (pH 7.5), 1 mM EDTA, and 50 mM D-glucose), and gently mixed with 5 μL of 20 μg/mL Proteinase K (Sigma-Aldrich), 20 μL of 0.5 M EDTA, and 100 mL of 10% (w/v) SDS. This solution was incubated at 37°C for more than 1 h and was treated at 95°C for 20 min for inactivation of Proteinase K. After gradual cooling to room temperature, this solution was mixed with 5 mL of 10 mg/mL RNaseA and was incubated at 37°C for 30 min. The solution was gently deproteinized using PCI solution (phenol:chloroform:isoamyl alcohol = 25:24:1) for 3 to 5 times, and was rinsed using CI solution (chloroform:isoamyl alcohol = 24:1). Genomic DNA was collected via isopropanol precipitation, and was finally suspended in 50 μL of 10:1 TE (10 mM Tris-HCl (pH 7.5) and 1 mM EDTA).

Table 1 Primers and substrates used in this study

OligoDNA	Sequence (5′ to 3′)
P1	CGTGATCTTCCCCCTCTCCAAC
P2	TGATGCCGGAGATGTTCACGTG
P3	TCTACTTCGTGGACGGGAGG
P4	CCACTGGGTCCGCTACCTC
P5	TCCTCAAGCTCCACCCTGAAC
P6	GCTTCCCACCACGAACATCTGC
P7	GTGAACTGGCTCCTTTTGGTGTCG
P8	GCTTAAGGAGAACCTGGAGCAGG
P9	CTCGGACCTCTTCCTCACCGTG
P10	CCAACATGATTAACAATTATTAGAGGTCATCGTTCAA
P11	GAAAGCTCCACCTCGGCCAC
P12	CAATGACCAGGCCGTCCATC
P13	ACCTCGTCGGCGTACTCCAG
P14	CTTCCGCGGTCCAGGAGGCC
P15	CGAGGACGGCCCTCCTCCTCTG
P16	CGCTCCTTGGGCACGGGGATC
P17	GCTCGGACTCGTGACCGAC
P18	GATGTCCAGGAGCACCACCG
P19	CTGAAGCGCACGTCCTCCTG
P20	GTGTCGTCCATCACAGTTTGC
P21	GGTGGCGTAGACGGAATTTATGCGG
P22	TAAATTCCGTCTACGCCACCCGCCA
P23	GCGTTACCCAACTTAATCGCCTTG
P24	CCCCTCTAGAAATAATTTTGTTTAACTTTAAG
P25	ATATCTGCAGTTATTACCTGAAGAACTCCCG
P26	ATATGGATCCCGCCTGAAGAACTCCCGGCG
P27	GGCCACGAAGTAGAGGGGCTCGG
P28	GGGAGGGAGCGGGCCGAGG
P29	GCCGCCACCCCGCTGATGC
P30	CGCGACGAGCTACGCCACCTTC
P31	TAATACGACTCACTATAGGG
P32	TATGCTAGTTATTGCTCAGCG
P33	CCCAGTACCTCCTGCCCGTGGGG
P34	ATATCATATGATCCCCGTGAGCCTGGCC
P35	GGAGGGCAAGGAGCCCGTGAGCC
P36	GGCTCACGGGCTCCTTGCCCTCC
P37	GCCGCCACCCCGCTGATGC
P38	GACGCGCTCAACAAGTACGCCCC
P39	GCTTTCCTCCTCCGCGGGGGCGTACTTG
1T21	GGGTGTTGCTTTAGTTGTCAT
2A21	ATGACAACTAAAGCAACACCC
$(dT)_{30}$	TTTTTTTTTTTTTTTTTTTTTTTTTTTTTT
60HJ1	CCGCTACCAGTGATCACCAATGGATTGCTAGGACATCTTTGCCCACCTGCAGGTTCACCC
60LIN2	GGGTGAACCTGCAGGTGGGCAAAGATGTCCTAGCAATCCATTGGTGATCACTGGTAGCGG

Underlines indicate the recognition sites for restriction enzymes for plasmid construction. Primers other than P11–P20 and P26 were generated by BEX Co. (Tokyo, Japan). P11–P20 and P26 were generated by Eurofins Genomics (Tokyo, Japan).

Cultured-cell PCR

The *T. thermophilus* HB8 cells in log phase in 1 mL of TR broth were harvested at 19,000 × *g* at 4°C for 5 min, and were suspended in 1 mL of sterilized distilled water. The cell density of this suspension was adjusted to optical density at 660 nm (OD_{660}) of 0.015 with sterilized distilled water. The suspended cell solution was stored at 4°C until used. The composition of the PCR solution was as follows: 0.1 μL of *TaKaRa LA Taq* (5 unit/μL; TaKaRa Bio, Shiga, Japan), 5 μL of 2×GC Buffer I (TaKaRa Bio), 1.6 μL of dNTP Mixture (2.5 mM each; TaKaRa Bio), 0.5 μL of 10 μM forward and reverse primers, and 1 μL of cultured cell solution (OD_{660} = 0.015) in 10 μL scale. PCR was started by cold-start method, and the initial denaturation was performed at 94°C for 5 min for disrupting cells, and extension was performed at 68°C for 1 min/kbp.

Complementation of Δ*nurA* or Δ*herA*

The plasmid vector, pMK18HK, was constructed based on pMK18::Hyg^R (pMK18H) (63) by deleting the kanamycin-resistant marker *kat* using the inverse PCR method with the primer set, P21-P22 (Table 1), to avoid competition to *HTK*. The deleted region was confirmed by sequencing analysis with a BigDye Terminator v3.1 Cycle Sequencing Kit (Applied Biosystems, CA, USA) and primer P23 (Table 1). To make the NurA-complement plasmid, pMK18HK and pET-HisTEV/*nurA*, which is a derivative of plasmid pET-15b (Novagen, Madison, WI, USA) containing the *nurA* gene and the recognition site for Tobacco Etch Virus (TEV) protease instead of thrombin, were digested by XbaI and HindIII, and the HisTEV-*nurA* fragment and pMK18HK fragment were ligated to form pMK18HK/HisTEV-*nurA*. To make the *herA*-complement plasmid, the fragment containing the *herA* gene was amplified by PCR with a template of expression plasmid pET-11a/*herA*, which is a derivative of pET-11a containing the *herA*, and with the primer set, P24-P25 (Table 1). This fragment and pMK18HK were digested by XbaI and PstI and then ligated to form pMK18HK/*herA*. The product was confirmed by sequencing analysis with primers P6, P24, and P25.

The plasmids containing $nurA_{D51A}$ and $herA_{K168A}$ genes were generated by inverse PCR-based site-directed mutagenesis using pET-HisTEV/*nurA* and pET-11a/*herA* as a template with the primer sets, P27-P28 and P29-P30, respectively. Sequence analysis with the following primers revealed that the construction was error-free: P27, P31, P32, and P33 for $nurA_{D51A}$, and primers P6, P29, P30, P32, and P34 for $herA_{K168A}$ (Table 1). Then, as described above, HisTEV-$nurA_{D51A}$ or $herA_{K168A}$

fragment and pMK18HK were ligated to form pMK18HK/HisTEV-*nurA*$_{D51A}$ or pMK18HK/*herA*$_{K168A}$, respectively.

T. thermophilus HB8 cells were transformed with pMK18HK, pMK18HK/HisTEV-*nurA* (WT or D51A), or pMK18HK/*herA* (WT or K168A) by the same method as the gene disruption, and transformants were selected on TT+Hyg plate. Expression of HisTEV-*nurA* was confirmed by affinity purification with TALON resin (Clontech, Mountain View, CA, USA). Expression of *herA* was confirmed by Western blotting with anti-HerA rabbit antiserum. This antiserum was generated by Kitayama Labes Co. (Nagoya, Japan).

Phenotypic analysis

Unless otherwise mentioned, experimental values were obtained from at least three independent experiments and expressed as geometric means ± standard error. In order to compare the averages, natural-log-transformed data were analyzed by Welch's *t* test, and each *p*-value was adjusted for multiple tests by the Holm-Bonferroni method with statistical software R (https://www.R-project.org/).

Cell growth and viability

The growth of *T. thermophilus* HB8 cells was monitored by measuring OD_{660}. Cells of WT and disruptants were cultured at 70°C for 16 h in 3.5 mL of TR broth. Subsequently, they were diluted down to OD_{660} of 0.01 with 50 mL of TR broth and then further cultivated at 70°C. Experimental values were expressed as the means obtained from at least three independent measurements. Cell viability was calculated as follows: the ratio of CFUs on TT plates to cell densities in log phase counted under the microscope was calculated. These obtained values were normalized by the values of WT. The natural log of the normalized values was analyzed as described above.

Sensitivity to UV irradiation

T. thermophilus HB8 cells in log phase were diluted to an appropriate concentration with TR broth, 100 μL of the diluted solution was spread on a TT plate, and UV light at 254 nm or 312 nm was irradiated at a dose rate of 2.4 $Jm^{-2}s^{-1}$ or 3.2 $Jm^{-2}s^{-1}$, respectively. The CFUs were measured after incubation at 70°C for 24 h, and survival rate was calculated as the fraction of the CFUs under

UV irradiation to those under no irradiation condition. SLUV-4 (254 nm; As One, Osaka, Japan) and EB-160C/J (312 nm; Spectroline, NY, USA) lamps were used as the UV sources.

Sensitivity to mitomycin C and H_2O_2

Mitomycin C (MMC; Nacalai Tesque) was dissolved in 10% (v/v) ethanol and 90% (v/v) ethylene glycol, and this solvent was used as the mock in the MMC sensitivity assay. *T. thermophilus* HB8 cells in log phase were diluted to an appropriate concentration in 500 μL of TR broth, and 5 μL of 0–400 μg/mL MMC solution or 0–400 mM hydrogen peroxide (H_2O_2; Wako Pure Chemical Industries, Osaka, Japan) was added to the culture to a final concentration of 0−4 μg/mL MMC or 0−4 mM H_2O_2, respectively. These cultures were incubated at 37°C for 30 min, and aliquots of 100 μL were spread on TT plates. The CFUs were measured after incubation at 70°C for 24 h, and the survival rate was calculated as the fraction of the CFUs upon treatment with MMC or H_2O_2 to those with no treatment.

Sensitivity to nalidixic acid

Nalidixic acid (NA; Sigma-Aldrich) was dissolved in 1 M NaOH, and this solvent was used as the mock in this assay. To confirm the bactericidal activity of NA against *T. thermophilus* HB8, the cell viability was measured after acute treatment with NA. *T. thermophilus* HB8 cells in log phase in 3 mL of TR broth were incubated at 60°C for 10 min and were mixed with 30 μL of 0 or 180 mg/mL NA. After shaking at 60°C for 0, 2, and 6 h, 100-μL culture samples were collected and diluted to an appropriate concentration with TR broth; then, 100 μL of the diluted solution was spread on a TT plate. The CFUs were measured after incubation at 70°C for 24 h, and the survival rate was calculated as the fraction of the CFUs at 2 and 6 h to those at 0 h after the addition of NA.

Estimation of the mutation frequency

Mutation frequency was estimated based on the frequency of streptomycin-resistant strains measured by the modified Luria-Delbrück fluctuation test (64). *T. thermophilus* HB8 cells were cultured up to the log phase in TR broth, and 500 μL or 100 μL aliquots of the appropriately diluted cultures were spread on TT plates with or without 50 μg/mL of streptomycin (Wako Pure Chemical Industries), respectively. In order to measure the mutation frequency variation induced by UV

irradiation, 10 mL of *T. thermophilus* HB8 cells in log phase in 30 mL of TR broth were dispensed to each of two pre-warmed dishes, and UV light at 254 nm was non-irradiated or irradiated under the conditions, leading to a survival rate of 10%: 4.1 $Jm^{-2}s^{-1}$ UV light was irradiated for 225 s to WT, 240 s to Δ*nurA* or 255 s to Δ*herA* and Δ*nurA*Δ*herA*. One milliliter of these cultures was transferred into 1.5 mL tubes and three milliliters of them into pre-warmed test tubes. To count the cell viability, the former was diluted $1:10^5$ and 100 μL aliquots were spread on TT plates. This enable us to count the CFUs at 0 h from UV irradiation as described below. The latter was cultivated at 70°C for 3 h, and then the cells were spread on TT plates with or without streptomycin as described above. The CFUs were measured after incubation at 70°C for 24 h. Each mutation frequency was calculated as described previously (51). The frequency of mutagenesis by UV irradiation was estimated as the ratio of the mutation frequency with to without UV irradiation. The growth rate was calculated as the ratio of the CFUs on the TT plate at 3 h to those at 0 h from the time point of UV irradiation.

Measurement of the transformation frequency

Two plasmids, pGEM-T Easy/Δ*csp2*::Hyg^R and pMK18HK, were used to measure the frequency of HR (F_H) and of DNA uptake (F_D), respectively. I constructed pGEM-T Easy/Δ*csp2*::Hyg^R in previous study by Tanaka *et al.* (65). *T. thermophilus* HB8 cells were cultured up to log phase in TT broth, and 400 μL aliquots were transferred to other pre-warmed tubes. These cells were cultivated at 70°C for 2 h after the addition of 50 μL of 60, 120, 240, or 480 nM pGEM-T Easy/Δ*csp2*::Hyg^R or pMK18HK. The cultures were diluted to an appropriate concentration in 100 μL of TR broth and were spread on TT plates, and 300 μL aliquots of non-diluted cultures were spread on TT+Hyg plates. The CFUs were measured after incubation at 70°C for 24 h. F_H and F_D were expressed as an average of the ratios of CFUs on the TT+Hyg plate to those on the TT plate, which were obtained from at least three independent experiments. In this method, F_H contains the contribution from F_D. Thus, the efficiency of HR was calculated as a fraction of F_H to F_D. Geometric standard errors of F_H/F_D were calculated according to the law of propagation of error with geometric standard error of F_H and F_D.

Overexpression and purification of NurA and HerA

In order to overexpress NurA and HerA proteins, pET-11a/*nurA* and pET-11a/*herA* were constructed from pET-11a. *Escherichia coli* Rosetta 2(DE3) cells (Merck, Darmstadt, Germany) were transformed with pET-11a/*nurA* and cultured in 150 mL of LBg broth (1.0% polypeptone (Nihon Pharmaceutical, Tokyo, Japan), 0.5% yeast extract (Nihon Pharmaceutical), 0.5% NaCl, and 1.0% D-glucose) containing 50 μg/mL ampicillin sodium salt up to 1×10^8 cells/mL at 37°C. Overexpression of NurA was performed following the Studier method, which is based on the diauxic response of *E. coli* (66). Twenty milliliters of the cultures were diluted with 2 L of the medium for auto-induction (1.5% polypeptone, 1.0% yeast extract, 0.5% NaCl, 0.6% (v/v) glycerol, 0.05% D-glucose, 0.2% lactose, 1.34% $Na_2HPO_4 \cdot 12H_2O$, and 0.17% KH_2PO_4) containing 50 μg/mL ampicillin sodium salt. The cells were cultivated for 24 h at 37°C, harvested by centrifugation at 9,200 × *g* at 4°C, and stored at −30°C until used. The following steps for NurA purification were performed at room temperature unless stated. Frozen cells were suspended in 20 mM Tris-HCl (pH 8.0), 1 mM EDTA, and 5 mM 2-mercaptoethanol (A buffer) and disrupted by sonication after addition of 1 mM phenylmethylsulfonyl fluoride. The supernatant of the cell lysate was recovered by centrifugation at 43,300 × *g* at 4°C for 1 h and applied to a TOYOPEARL SP-650M column (bed volume of 14 mL; Tosoh, Tokyo, Japan) equilibrated with A buffer. The column was washed with A buffer and eluted with a linear gradient of 0–1 M NaCl in A buffer. The eluted fractions containing NurA were collected and applied to a TOYOPEARL SuperQ-650M column (bed volume of 12 mL; Tosoh) equilibrated with A buffer. The flow-through fraction was collected and applied to TOYOPEARL AF-Heparin HC-650M (bed volume of 10 mL; Tosoh) equilibrated with A buffer and eluted with a linear gradient of 0–1 M NaCl in A buffer. The eluted fractions containing NurA were collected, and solid ammonium sulfate was gradually added to the pooled fractions up to 40% of the saturated concentration at 4°C, and the solution was applied to TOYOPEARL Ether-650M (bed volume of 10 mL; Tosoh) equilibrated with 20 mM Tris-HCl (pH 8.0), 1 mM EDTA, 500 mM NaCl, 5 mM 2-mercaptoethanol, and 40% saturated ammonium sulfate (B buffer). The column was washed with B buffer and eluted with a linear gradient from B buffer to A buffer. The buffer of eluted fractions containing NurA were changed to 20 mM Tris-HCl (pH 8.0), 1 mM EDTA, 150 mM NaCl, and 5 mM 2-mercaptoethanol (TES2 buffer), and the resultant fractions were concentrated to 500 μL by ultrafiltration with Vivaspin (10 kDa cut off; Sartorius

Japan, Tokyo, Japan) at 4°C. The concentrated solution was applied to a Superdex 75 10/300 GL column (GE Healthcare, Piscataway, NJ, USA) equilibrated with TES2 buffer and eluted with the same buffer with ÄKTA explorer (GE Healthcare). The fractions containing NurA were collected and concentrated up to 50 μM by ultrafiltration at 4°C. The concentrated solution was frozen in liquid nitrogen, stored at −80°C until used, and stored at 4°C after thawing.

E. coli Rosetta 2(DE3) cells were transformed with pET-11a/*herA* and cultured in 150 mL of LB broth (1.0% polypeptone, 0.5% yeast extract, and 0.5% NaCl) containing 50 μg/mL ampicillin sodium salt up to 1×10^8 cells/mL at 37°C. Twenty milliliters of the cultures were diluted with 2 L of LB broth. The cells were cultivated for 24 h at 37°C, harvested by centrifugation at 9,200 × *g* at 4°C, and stored at −30°C until used. The following steps for HerA purification were performed at room temperature unless stated. Frozen cells were suspended in 20 mM Tris-HCl (pH 8.0), 1 mM EDTA, 50 mM NaCl, and 5 mM 2-mercaptoethanol (C buffer) and disrupted by sonication after addition of 1 mM phenylmethylsulfonyl fluoride. The supernatant of the cell lysate was recovered by centrifugation at 43,300 × *g* at 4°C for 1 h after heat treatment at 70°C for 20 min and was applied to a TOYOPEARL SP-650M column (bed volume of 14 mL) equilibrated with C buffer. The column was washed with C buffer, and flow-through and wash fractions were collected. The collected solution was applied to a TOYOPEARL SuperQ-650M column (bed volume of 12 mL) equilibrated with C buffer and eluted with a linear gradient of 0–1 M NaCl in A buffer. The eluted fractions containing HerA were transferred to a dialysis tube (28.7 mm in diameter, 8,000 MW cutoff; BioDesign, NY, USA), and the protein solution was dialyzed three times against 1.5 L of TES2 buffer containing 30% saturated ammonium sulfate at 4°C. The precipitate was collected from the dialyzed solution by centrifugation at 43,300 × *g* at 4°C and was resuspended with 20 mM Tris-HCl (pH 8.0), 1 mM EDTA, 300 mM NaCl, and 5 mM 2-mercaptoethanol. After dialysis against TES2 buffer, the solution was concentrated by ultrafiltration with Vivaspin (30 kDa cut off). The concentrated solution was applied to a HiLoad 16/600 Superdex 200 pg column (GE Healthcare) equilibrated with TES2 buffer and eluted with the same buffer with ÄKTA explorer. The fractions containing HerA were collected and concentrated up to 400 μM by ultrafiltration at 4°C. The concentrated solution was frozen in liquid nitrogen, stored at −80°C until used, and stored at 4°C after thawing.

The concentrations of the purified proteins were determined using the molar absorption

coefficients of 43,500 $M^{-1}cm^{-1}$ for NurA and of 50,900 $M^{-1}cm^{-1}$ for HerA (67). The purity and sizes of the recombinant proteins were assessed by SDS-PAGE. The purified proteins were confirmed by peptide mass fingerprinting (68), and their molecular masses were analyzed using a Fourier transform ion cyclotron resonance mass spectrometer (69).

Circular dichroism (CD) spectrometry

The CD spectra was recorded with a J-720W CD spectrometer (JASCO, Tokyo, Japan). The samples contained 0.6 μM NurA (as the monomer) and/or 1.8 μM HerA (as the monomer) in 40 mM sodium phosphate (pH 8.3 at 22°C). In order to estimate change of secondary structures by forming NurA-HerA complex, the CD spectra of NurA and/or HerA were measured in a quartz cell with a path length of 1 mm in the far-UV region between 200 and 250 nm at each 0.1-nm interval at 50 nm/min five times. In addition, thermostability was assessed by measuring CD values at 222 nm at 1°C/min from 20 to 98°C in a quartz cell with a path length of 1 mm. Measurements were performed five times for NurA and three times for HerA and NurA-HerA complex. The average values were calculated and were plotted against temperature. Assuming the two-state transition, thermodynamic parameters, transition temperature T_m was determined by fitting Equation 1 and 2 (70) to the experimental data by using Igor Pro 4.03.

$$Y = (Y_n + m_N T)F_N + (Y_U + m_U T)(1 - F_N) \quad \text{Equation 1}$$

$$F_N = (1 + \exp(-\Delta H°(1 - T/T_m)/RT))^{-1} \quad \text{Equation 2}$$

Y is the experimental CD values. Y_N and Y_U represent the signals of native and unfolded states at 0 K, and m_N and m_U are temperature dependencies of CD signals for native and unfolded states, respectively. F_N is the fraction of the native state at temperature T (K), $\Delta H°$ is the transition enthalpy, and R is the molar gas constant.

Size-exclusion chromatography assay

NurA (12.6 μM as the monomer) and/or HerA (20.2 μM as the monomer) dissolved in 300 μL of 20 mM Tris-HCl (pH 8.0), 150 mM NaCl, and 5% glycerol (SEC buffer) were applied to a Superdex 200 10/300 GL column (GE Healthcare) equilibrated with SEC buffer, and they were eluted with the same buffer at a flow rate of 0.5 mL/min with ÄKTA explorer. The elution was monitored by absorbance at 280 nm and fractionated by 0.5 mL. Three hundred microliters of each

fraction were mixed with 900 μL of acetone chilled at −30°C, and proteins were precipitated by centrifugation at 20,400 × *g* for 60 min at 4°C after incubation at −30°C for 24 h. The precipitates were dried and dissolved with 30 μL of TES2 buffer. Proteins in these solutions were separated by SDS-PAGE with 12.5% polyacrylamide gel. As molecular-weight standards for the calibration of size-exclusion chromatography, bovine carbonic anhydrase (29,000), bovine serum albumin (66,000), yeast alcohol dehydrogenase (150,000), and bovine thyroglobulin (669,000) (Sigma-Aldrich) were dissolved in SEC buffer and analyzed by using the method described above. At least three independent experiments were performed.

Preparation of HerA lacking HAS domain

Recombinant HerA (2.2 nmol) was digested by 400 ng of Trypsin Gold (Promega) in 40 μL of TES2 buffer at 37°C for 24 h. The reaction was stopped by the addition of 4 μL of 1 mM phenylmethylsulfonyl fluoride. The digested HerA was then separated by a Superdex 200 10/300 GL column equilibrated with TES2 buffer at a flow rate of 0.5 mL/min with ÄKTA explorer. The major peak contained the N-terminal truncated form that lacked the HAS domain (M1–K75), which was identified by peptide mass fingerprinting (68). This truncated form of HerA (ΔN-HerA) was concentrated by ultrafiltration.

Native PAGE

The mixtures of 1.5 μM HerA (as the monomer) and 0, 0.125, 0.25, 0.375, 0.5, 0.625, 0.75, 0.875, 1.0, 1.2, or 1.5 μM NurA (as the monomer) in 12 μL of TES2 buffer (the molar ratios of HerA to NurA were 6:0, 6:0.5, 6:1, 6:1.5, 6:2, 6:2.5, 6:3, 6:3.5, 6:4, 6:5, or 6:6) were incubated at 55°C for 10 min. The loading buffer was added to the protein solution up to 15 μL, yielding final concentrations of 12.5 mM Tris-HCl (pH 6.8), 2% (v/v) glycerol, and 0.02% bromophenol blue. The samples were applied to 7.5% polyacrylamide gel (acrylamide:*N*,*N*′-methylenebisacrylamide = 29:1) and were electrophoresed at 10 mA/gel at 4°C. Also, the mixtures of 2.5 μM ΔN-HerA (as the monomer) and 0, 0.83, or 12.5 μM NurA (as the monomer) in 12 μL of TES2 buffer (the molar ratios of ΔN-HerA to NurA were 6:0, 6:2, or 6:30) were analyzed in a similar way to the analysis of the full-length HerA. To examine the physical interaction of NurA and/or HerA with single-strand DNA-binding protein (SSB), 4 or 40 μM NurA, 4 μM HerA, and/or 4 μM SSB (as the monomer)

were mixed in the 10 μL of TES2 buffer (the molar ratios among NurA, HerA, and SSB were 1:0:0, 0:1:0, 0:0:1, 1:1:0, 1:0:1, 10:0:1, 0:1:1, or 1:1:1), and incubated at 55°C for 10 min, and analyzed similarly. SSB was prepared by a method modified from that described previously (71). Briefly, SSB was overexpressed in *E. coli*, and was purified using heat treatment of the cell lysate and the following chromatographic resins: TOYOPEARL Buthyl-650M (Tosoh), TOYOPEARL SuperQ-650M, TOYOPEARL AF-Heparin HC-650M, and HiLoad 16/600 Superdex 200 pg. To examine the physical interaction of NurA and/or HerA with RecJ, 0 and 4 μM NurA, HerA, and/or RecJ (as the monomer) were mixed in 10 μL of TES2 buffer (the molar ratios among NurA, HerA, and RecJ were 1:0:0, 0:1:0, 0:0:1, 1:1:0, 1:0:1, 0:1:1, or 1:1:1), and the mixtures were incubated at 55°C for 10 min and analyzed similarly. The recombinant RecJ was a gift from Dr. Yuya Nishida (Osaka university). The buffer system for native PAGE was based on the Laemmli system (72) but without SDS. Proteins in the gel were fixed by 50% methanol and 10% acetic acid, and they were stained by Coomassie Brilliant Blue R-250. Experiments were performed independently at least three times.

Affinity purification assay

An N-terminal His-tagged NurA was prepared using the plasmid pMK18HK/HisTEV-*nurA*, described above for *nurA* complementation. The plasmid for a C-terminal His-tagged HerA was generated as follows. The *herA* gene without the stop codon was amplified by PCR with pET-11a/*herA* as the template and the primer set, P24-P26 (Table 1). In the amplified product, the sequence between the *herA* gene and the BamHI recognition site was changed from 5′ CGC 3′ to 5′ CG 3′ for adjusting the reading frame to the His_6 tag like pET-21b vector. This amplified fragment and the pET-21a vector were digested with NdeI and BamHI, and they were ligated together after purification by gel extraction to form pET-21b/*herA*. The product was confirmed by sequencing analysis with primers from P31, P32, and P35 to P39 (Table 1). pET-21b/*herA* and pMK18HK were digested with NdeI and PstI, and the resultant fragments were ligated together after purification by gel extraction to form pMK18HK/*herA*-His_6.

Disruptants Δ*nurA*, Δ*herA*, and Δ*nurA*Δ*herA* were transformed with pMK18HK, pMK18HK/HisTEV-*nurA*, or pMK18HK/*herA*-His_6. Each complemented strain was cultured in 100 mL of TR broth containing 100 μg/mL of hygromycin B up to log phase. The cultures were rapidly

cooled in ice-cold water, and the cells were collected at 4,400 × *g* at 4°C. Harvested cells were stored at –80°C until use. These cells were thawed and washed by 2 mL of PBS, and they were then suspended in 500 μL of binding buffer (50 mM sodium phosphate, 20 mM imidazole, 1% Triton-X, and 1 mg/mL bovine serum albumin [pH 7.0]). These suspensions were subjected to sonication and centrifuged at 19,000 × *g* at 4°C for 1 h. The supernatants were applied to 20 μL of TALON resin in a spin column and were incubated at 4°C overnight. These columns were washed with 400 μL of binding buffer without bovine serum albumin three times, and bound proteins were eluted with 50 mM sodium phosphate, 300 mM NaCl, and 200 mM imidazole (pH 7.0). The eluted proteins were separated by SDS-PAGE, and candidates for proteins interacting with NurA or HerA were identified by Western blotting or peptide mass fingerprinting.

Nuclease activity assay

Single-stranded oligonucleotides were synthesized (BEX, Tokyo, Japan) and their 5′-termini were labeled with [γ-^{32}P]ATP (MP Biomedical, CA, USA) using T4 polynucleotide kinase (TaKaRa Bio). For the nuclease assay, 1T21 (Table 1) was used as a ssDNA substrate (21-mer), and a dsDNA substrate (21 bp) was obtained by annealing radiolabeled 1T21 with an unlabeled 2A21 (Table 1). The concentrations of these substrates were adjusted to 10 nM with unlabeled substrate. The nuclease reactions using these DNA substrates were performed at 37°C in 4 μM NurA (as the monomer), 1 mM $MnCl_2$, 10 nM substrate, 20 mM Tris-HCl (pH 8.0), 150 mM NaCl, 5 mM 2-mercaptoethanol, and 0.01% BSA. The reaction was started by the addition of a substrate after pre-incubation at 37°C for 10 min. For the stopping reaction, the aliquot of 5 μL was mixed with an equal volume of stop-solution (0.2 % SDS, 20 mM EDTA, and 400 ng/mL Proteinase K (Sigma-Aldrich)) at each time point, and the mixture was incubated at 37°C for 60 min. This solution was combined with the 10 μL of sample buffer (50 mM EDTA, 80% deionized formamide, 10 mM NaOH, 0.1% bromophenol blue, and 0.1% xylene cyanol) and analyzed by electrophoresis through a denaturing 25% polyacrylamide gel containing 8 M urea with 1×TBE buffer (89 mM Tris-borate and 2 mM EDTA). The gel was dried and placed in contact with an imaging plate (GE Healthcare, Piscataway, NJ, USA). The substrates and products were detected and analyzed with a BAS-2500 image analyzer (Fujifilm, Tokyo, Japan).

In the kinetic analysis, the reaction was performed at 37°C in 1 μM NurA (as the monomer), 1

mM $MnCl_2$, 50 nM 5′-radiolabeled $(dT)_{30}$ substrate (Table 1), 0.2–50 μM unlabeled $(dT)_{30}$, 20 mM Tris-HCl (pH 8.0), 150 mM NaCl, 5 mM 2-mercaptoethanol, and 0.01% BSA. The substrates and product were separated and detected as described above. The intensities of the substrate and product bands were quantified by Image Gauge (Fujifilm). The kinetic parameters, k_{cat} and K_M, were determined from time-course analysis by fitting Equation 3 to the experimental data by using Igor Pro 4.03 (WaveMetrics, Oregon, USA).

$$k_{app} = k_{cat} \times [DNA]_{free}/(K_M + [DNA]_{free}) \quad \text{Equation 3}$$

$[DNA]_{free}$ is the concentration of unbound DNA substrate provided by Equation 4, and k_{app} is the apparent rate constant.

$$[DNA]_{free} = [DNA]_0 - [NurA\text{-}DNA] \quad \text{Equation 4}$$

$[DNA]_0$ and [NurA-DNA] are the concentration of total DNA substrate and of DNA-NurA complex, respectively. [NurA-DNA] is provided by Equation 5.

$$[NurA\text{-}DNA] = 0.5 \times \{(K_M + [NurA]_0 + [DNA]_0) - ((K_M + [NurA]_0 + [DNA]_0)^2 - 4[NurA]_0[DNA]_0)^{1/2}\} \quad \text{Equation 5}$$

$[NurA]_0$ is the total concentration of NurA.

Nicking activity assay

A covalently closed circular (ccc) plasmid DNA pUC119 was partially purified by alkaline extraction, and was separated from open circular and linear DNA by CsCl density gradient centrifugation. The nicking activity assay was performed at 37°C in 1 μM NurA (as the monomer), 1 mM $MnCl_2$, 5 μg/mL ccc pUC119, 20 mM Tris-HCl (pH 8.0), 150 mM NaCl, 5 mM 2-mercaptoethanol, and 0.01% BSA. The reaction was started by the addition of $MnCl_2$ after pre-incubation at 37°C for 10 min. At each time point, the aliquot of 5 μL was mixed with 1 μL of 100 mM EDTA and 1 μL of 10×Loading Buffer (TaKaRa Bio) to stop the reaction, and the mixtures were applied to 0.7% agarose gel. The substrate and reaction products were separated by agarose electrophoresis in 0.5×TBE buffer at 25 V for 3 h, and were stained with 0.5 μg/mL ethidium bromide in 0.5×TBE buffer for 30 min. The intensities of the bands were quantified with image analysis software ImageJ (NIH, Bethesda, MD, USA), and the ratio of ccc, open circular, and linear forms were calculated. Experiments were performed independently at least three times. The nicking activity assay was also performed in the presence of 3.5 μM HerA (as the monomer) and the other

conditions that were described above.

ATPase activity assay

HerA ATPase activity was performed at 55°C in 200 nM HerA (as the monomer), 5 mM $MgCl_2$, 0.01–4 mM ATP (Oriental Yeast), 8.9 nM [γ-^{32}P]ATP, 20 mM HEPES-NaOH (PH 8.0), 150 mM NaCl, 1 mM EDTA, 5 mM 2-mercaptoethanol, and 0 or 500 nM DNA. For the reaction in the presence of DNA, 60HJ1 (Table 1) was used as the ssDNA, and a 60 bp dsDNA was obtained by annealing 60HJ1 with 60LIN2 (Table 1). ATPase reaction was started by adding ATP and [γ-^{32}P]ATP mixture after preincubation at 55°C for 5 min. At each time point, 1 μL aliquot of the reaction mixture was added to 1 μL of 500 mM EDTA to stop the reaction and stored at −30°C. Aliquots of 1 μL were spotted on the plastic plate (TLC PEI-Cellulose F, Merck) and separated by thin-layer chromatography in 250 mM LiCl and 500 mM formic acid. The plates were dried and placed in contact with an imaging plate. The substrates and products were detected and analyzed with a BAS-2500 image analyzer. The intensities of the substrate and product spots were quantified with Image Gauge. The apparent rate constant k_{app} was estimated by time-course analysis. The kinetic parameters k_{cat} and K_M were determined by fitting a Michaelis-Menten equation (Equation 6) to the experimental data by using Igor Pro 4.03.

$$k_{app} = k_{cat} \times [ATP]/(K_M+[ATP]) \quad \text{Equation 6}$$

[ATP] is the concentration of ATP.

HerA ATPase activity in the presence of NurA was also analyzed. The reaction was performed in 0 or 0.3 μM HerA (as the monomer), 0–1 μM NurA (as the monomer), 5 mM $MgCl_2$, 5 mM ATP, 10 nM [γ-^{32}P]ATP, 20 mM HEPES-NaOH (pH 8.0), 150 mM NaCl, 1 mM EDTA, and 5 mM 2-mercaptoethanol at 55°C. Other conditions were the same as those described above.

I assumed the following Equation 7 for interaction between hexameric HerA ($HerA_6$) and NurA,

$$HerA_6 + n\text{NurA} \underset{}{\overset{K_d}{<==>}} HerA_6\text{-}NurA_n \quad \text{Equation 7}$$

where n is the number of NurA-binding sites per hexameric HerA and K_d is the dissociation constant defined by Equation 8.

$$K_d = [HerA_6][NurA]^n/[HerA_6\text{-}NurA_n] \quad \text{Equation 8}$$

The total concentrations of hexameric HerA ($[HerA_6]_0$) and NurA ($[NurA]_0$) are related to the respective free concentrations ($[HerA_6]$ and [NurA]) as shown in Equations 9 and 10.

$$[HerA_6]_0 = [HerA_6] + [HerA_6\text{-}NurA_n] \quad \text{Equation 9}$$

$$[NurA]_0 = [NurA] + [HerA_6\text{-}NurA_n] \quad \text{Equation 10}$$

The apparent rate constant k_{app} per hexameric HerA was estimated from time-course analysis. The k_{app} is written as the sum of the rate constants per NurA-free hexameric HerA (k_H) and of hexameric HerA in complex with NurAs (k_{HN}) as follows:

$$k_{app}[HerA_6]_0 = k_H[HerA_6] + k_{HN}[HerA_6\text{-}NurA_n] \quad \text{Equation 11}$$

The k_{app} is obtained from Equations 8–11 to give Equation 12.

$$k_{app} = k_H + (k_{HN} - k_H) \times [NurA]_0^n/(K_d + [NurA]_0^n) \quad \text{Equation 12}$$

Then, the parameters k_{app}, k_{HN}, k_H, n, and K_d were determined from three independent experiments by fitting Equation 12 to the experimental data by using Igor Pro 4.03.

Results

Sequence comparison of NurA and HerA

I searched the *T. thermophilus* HB8 genome for the candidate genes for end resection-related enzymes other than RecJ. A detailed sequence analysis revealed that TTHA0521 and TTHA0522 are significantly similar to *D. radiodurans* NurA (DR_0836) and HerA (DR_0837), respectively. The sequence identity between TTHA0521 (293 residues) and DR_0836 (349 residues) is 36%, although DR_0836 has several insertions compared to TTHA0521. The overall sequence similarity between TTHA0521 and archaeal NurAs is relatively low. However, the residues involved in nuclease activity and DNA-binding ability are conserved among all of these proteins (Fig. 5A). The sequence identity between TTHA0522 (576 residues) and DR_0837 (618 residues) is 52%, and DR_0837 has several insertions. Although the overall sequence similarity between TTHA0522 and archaeal HerAs is also low, the Walker A, Walker B, and Sensor-1 motifs, along with the residue for DNA binding, are conserved among all of these proteins (Fig. 5B). Based on these results, I designated TTHA0521 and TTHA0522 as NurA and HerA of *T. thermophilus* HB8, respectively.

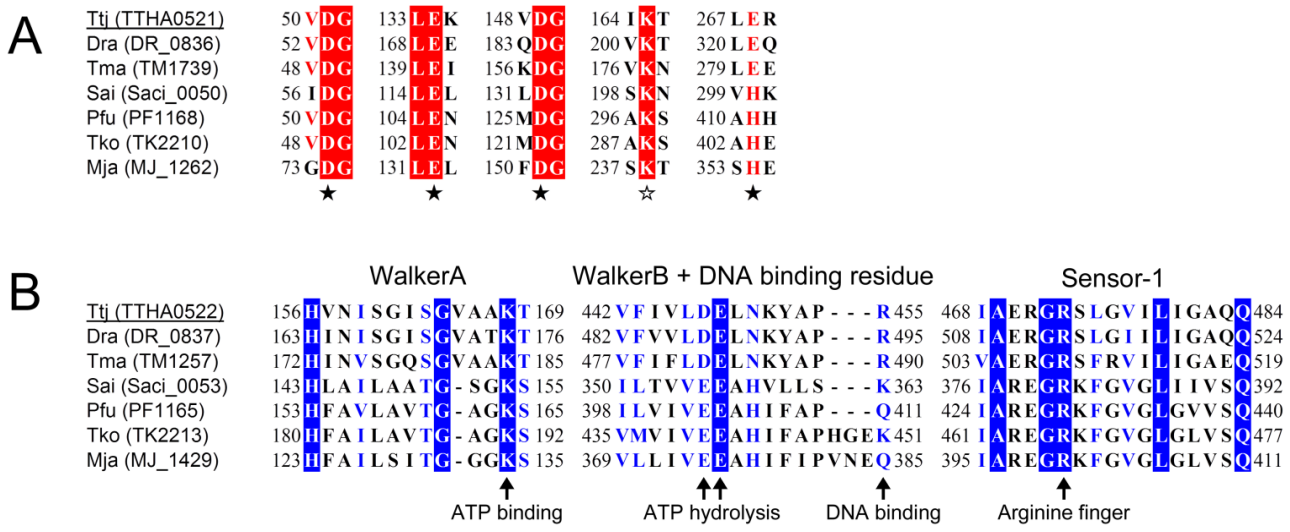

Fig. 5 Conserved residues of NurA and HerA. (A) Sequence alignment of active sites in NurA. Filled stars indicate nuclease activity-related residues, and the open star indicates the DNA-binding residue. (B) Sequence alignment of the Walker A, Walker B, and Sensor-1 motifs, and DNA-binding residues in HerA. Ttj, *Thermus thermophilus* HB8; Dra, *Deinococcus radiodurans*; Tma, *Thermotoga maritima*; Sai, *Sulfolobus acidocaldarius*; Pfu, *Pyrococcus furiosus*; Tko, *Thermococcus kodakaraensis*; Mja, *Methanocaldococcus jannaschii*. Gene IDs are shown in parentheses. Completely conserved residues are shaded by red (NurA) or blue (HerA), and well-conserved residues are indicated by red (NurA) or blue (HerA) letters. Numbers indicate the positions of amino acid residues in each protein.

nurA and _herA_ are constitutively transcribed in _T. thermophilus_ HB8 cells

In the *T. thermophilus* HB8 genome, *nurA* and *herA* form an operon-like gene cluster, suggesting cotranscription. Transcriptome data in the GEO database showed that the expression of *nurA* and *herA* genes showed a similar pattern, supporting the above suggestion. These genes were also constantly detected in an independent manner of growth phase (Fig. 6, Accession: GSE21290). In addition, the transcription levels of *nurA* and *herA* were not changed by long-time cultivation, the treatment of H_2O_2, metal ions (iron or cupper), heat shock, cold shock, exposure to high osmotic pressure, and phage infection (Accession: GSE21183, GSE21430, GSE19508, GSE21288, GSE19723, GSE21289, and GSE21474, respectively) (Fig. 7). These data do not provide valuable information on the physiological function of NurA and HerA.

NurA and HerA are not essential for _T. thermophilus_ HB8

For phenotypic analysis, I tried the disruption of *nurA* and/or *herA* in *T. thermophilus* HB8. The gene disruption was performed via HR (Fig. 8A) as previously described (59), and the disruption was confirmed by PCR-based genotyping (Fig. 8B). The results demonstrated that the deletion mutants of *nurA* and/or *herA*, that is, Δ*nurA*, Δ*herA*, and Δ*nurA*Δ*herA*, were successfully constructed. The elimination of *herA* expression was also confirmed by Western blotting with an anti-HerA antiserum (see Fig. 14B). It was possible that the expression of *herA* was suppressed by the deletion of *nurA* because *nurA* is located just upstream of *herA*. However, HerA protein expression in the Δ*nurA* was verified by Western blotting with the anti-HerA antiserum (Fig. 8C). These results suggest that *nurA* and *herA* are not essential genes in *T. thermophilus* HB8.

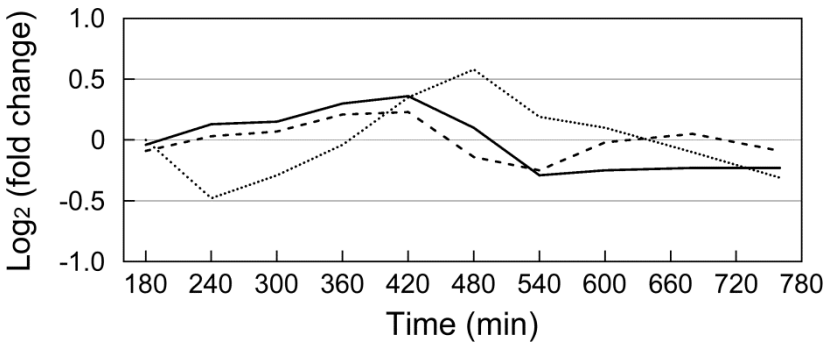

Fig. 6 Transcriptional changes of *nurA* (solid line), *herA* (dashed line), and *recJ* (dotted line) during cell growth. The data were obtained from the data set on the GEO web site (Accession: GSE21290). The horizontal line indicates the cultivation time after dilution.

A

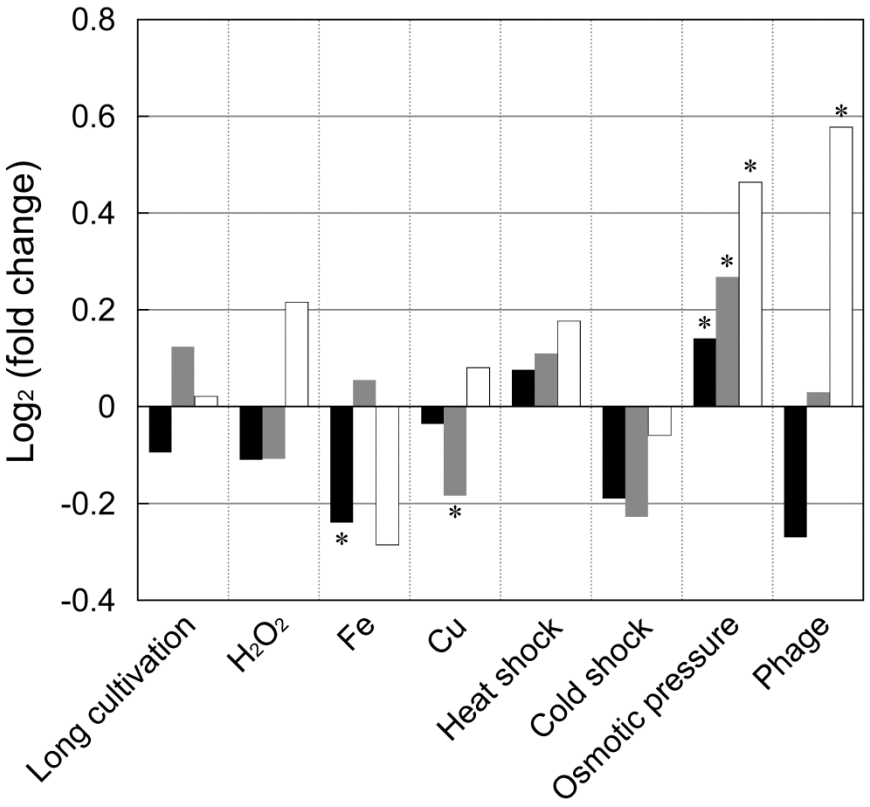

B

GEO accession No.	Stress	Stress condition (harvested time)	Control condition
GSE21183	Long cultivation	20 h cultivation	10 h cultivation
GSE21430	H_2O_2	10 mM H_2O_2 (30 min after addition)	H_2O_2 free
GSE19508	Fe	1.0 mM $FeSO_4$ (30 min after addition)	$FeSO_4$ free
GSE19508	Cu	1.25 mM $CuSO_4$ (30 min after addition)	$CuSO_4$ free
GSE21288	Heat shock	80°C (30 min after temperature change)	No treatment
GSE19723	Cold shock	4°C, 5 min	No treatment (i)
GSE21289	Osmotic pressure	1.5% NaCl (30 min after addition)	No treatment (ii)
GSE21474	Phage	ΦYS40 phage infection (100 min after infection)	No treatment

Fig. 7 Transcriptional responses to various type of stresses. (A) Fold change of expression of *nurA* (black boxes), *herA* (gray boxes), and *recJ* (white boxes) genes. (B) The data sets about the *T. thermophilus* HB8 WT strain on the GEO web site. Asterisks (*) indicate *p* values less than 0.05 under respective conditions. Each commentary indicates the following: (i), Cells were harvested after treatment of cold methanol; (ii), Cells are cultured in 2-fold high concentration of TT broth containing 0.8% polypeptone, 0.4% yeast extract, 0.2% NaCl, 0.4 mM $CaCl_2$, and 0.4 mM $MgCl_2$, which was adjusted to pH 7.2 with NaOH.

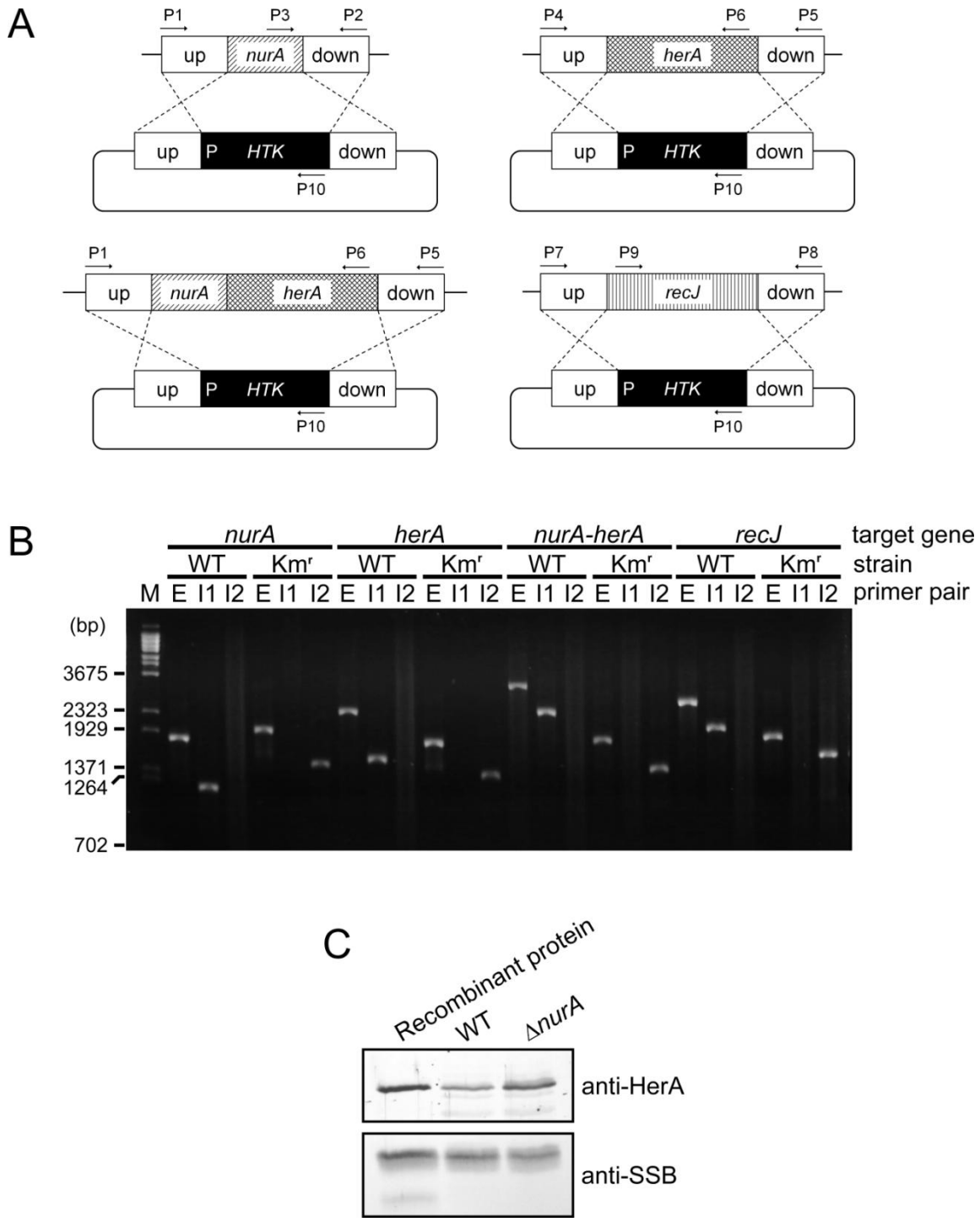

Fig. 8 Gene disruption. (A) Targeted gene disruption by homologous recombination. Arrows indicate the primers used for gene disruption as described in "Materials and Methods" and Table S1. *HTK*, thermostable kanamycin-resistance gene; P, promoter for expression of *HTK*. (B) PCR verification of gene disruption with the external (E) and internal (I1 and I2) primer pairs. E, primers complementary to upstream and downstream regions of target genes; I1, primers complementary to targeted genes and upstream or downstream regions; I2, primers complementary to the *HTK* region and upstream or downstream region. Km^r indicates a kanamycin-resistant strain. M indicates a λ-BstPI DNA size marker. (C) Western blotting of WT and Δ*nurA* cell lysate with anti-HerA antiserum. SSB serves as an internal loading control. As controls for the mobility of HerA and SSB proteins, 50 ng of recombinant HerA and SSB were also applied.

Deletion of *nurA* and *herA* has no effects on cell division and spontaneous mutation frequency

To examine the involvement of *nurA* and *herA* in cell growth and viability, the growth of the disruptants was measured under the optimal growth condition (at 70°C, rich medium). The disruptant of *recJ* (Δ*recJ*) was used as the control because RecJ can process 5′-ends of DSBs (20, 21). Significant differences in cell growth were not detected between WT and the disruptant mutants of *nurA* and/or *herA* (Fig. 9A). Also, no significant difference was found in the cell viability (the ratio of the CFU to the cell number) between WT and the *nurA* and/or *herA* disruptants (Fig. 9B). Similarly, no significant differences were observed for cell lengths in log phase and colony sizes (data not shown). In contrast, Δ*recJ* showed a lower maximum cell density in the stationary phase, a lower cell viability (Fig. 9), and the longer cell shape than WT (data not shown) as previously reported (51). These results suggest that NurA and HerA have no effects on cell growth and viability.

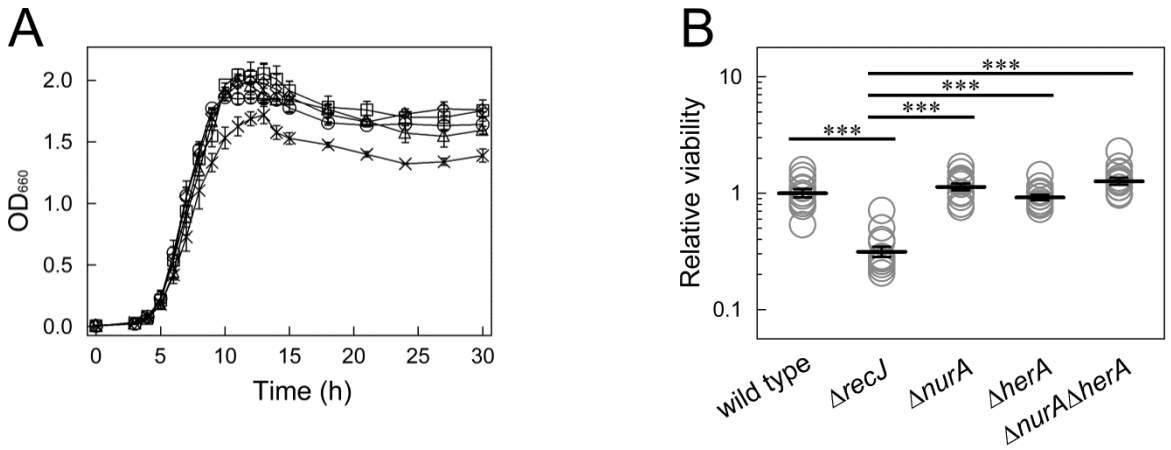

Fig. 9 Cell growth and cell viability. (A) Growth curves. Cell growth was monitored by OD_{660}. Symbols are as follows: circles, WT; crosses, Δ*recJ*; triangles, Δ*nurA*; diamonds, Δ*herA*; and squares, Δ*nurA*Δ*herA*. Bars indicate the standard error of the means from four independent experiments (n = 4). (B) Cell viability. Cell viability is expressed as relative to geometrical means of WT. Circles indicate individual measurements. Cross bars and vertical bars indicate geometric means (n = 12) and standard error of geometric means, respectively. Three asterisks (***) indicate *p* values less than 0.001 for respective strains. All other comparisons that did not show statistically significant differences are not indicated.

To further examine the effect of the gene disruption on genome integrity, the spontaneous mutation frequency was measured as the frequency of streptomycin-resistant mutants by a modified Luria-Delbrück fluctuation test (64). Measuring resistance to streptomycin is a classical way of determining the spontaneous mutation frequency: the streptomycin resistance is conferred by mutations in the genes of the ribosomal protein S12 and 16S rRNA (73, 74). Especially in *T. thermophilus*, the resistance and pseudo-dependence to streptomycin is conferred by mutations of ribosomal protein S12 (75–77). Thus, these mutation frequencies are considered an index of DNA repair capability. No difference was detected between WT and Δ*nurA*, Δ*herA*, and Δ*nurA*Δ*herA* (Fig. 10). In contrast, Δ*recJ* showed a higher mutation frequency than WT (Fig. 10), as previously reported (51). These results suggest that NurA and HerA have no effect on prevention of mutations that could be detected in this assay.

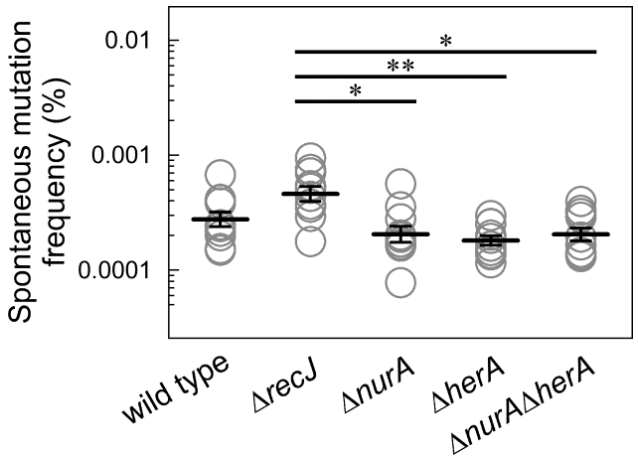

Fig. 10 Spontaneous mutation frequency. Circles indicate individual measurements. Cross bars and vertical bars indicate geometric means (n = 10) and standard error of geometric means, respectively. *, $0.01 \leq p < 0.05$; **, $0.001 \leq p < 0.01$.

Involvement of NurA and HerA in homologous recombination

To investigate the possibility that NurA and HerA carry out DNA end processing in *T. thermophilus* HB8, I measured the efficiency of HR between the genomic DNA and the plasmid DNA. In many archaea, NurA and HerA are thought to be involved in end resection in HR repair (4). In general, recombination repair-related enzymes are also involved in genetic recombination. In this assay, the frequency of DNA uptake (F_D) and the apparent frequency of HR (F_H) were measured by using pMK18HK and pGEM-T Easy/Δ*csp2*::*Hyg*^{R}, respectively. Wild-type and gene-disruptant strains showed that an increase in the F_D and F_H depended on the concentration of each DNA (Figs. 11A and B). However, the difference in F_D value was not significant between WT and each disruptant, although all of the disruptants seemed to show higher values than WT (Fig. 11A). Similarly, no significant difference in F_H was found between WT and the disruptants (Fig. 11B). In this assay, F_H contains the contribution from F_D because the recombination event between genomic DNA and plasmid DNA inevitably occurs after DNA uptake. Therefore, I calculated a fraction of F_H to F_D, which could be the index for the efficiency of HR (F_H/F_D). The differences of the F_D and F_H values (Figs. 11A and B) were not statistically significant between WT and each disrupt ant. However, the F_H/F_D values of the disruptants tended to be lower than those of WT (Fig. 11C). It was difficult to argue that NurA and HerA are not associated with HR under the conditions without DNA damages.

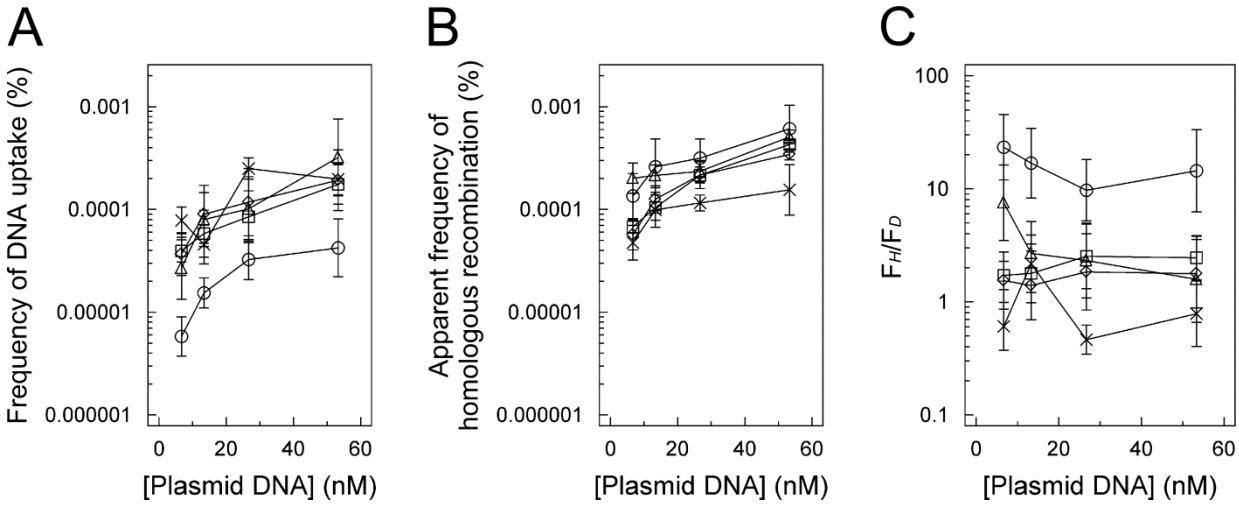

Fig. 11 Frequency of DNA uptake and homologous recombination. (A) Frequency of DNA uptake (F_D). (B) Apparent frequency of HR (F_H). (C) Relative efficiency of HR (the ratio of F_H to F_D). Symbols are as follows: circles, WT; crosses, Δ*recJ*; triangles, Δ*nurA*; diamonds, Δ*herA*; and squares, Δ*nurA*Δ*herA*. Bars indicate the standard error of the means (n = 4).

Δ*nurA*, Δ*herA*, and Δ*nurA*Δ*herA* show resistance to UV irradiation and MMC

To examine the involvement of NurA and HerA in DNA repair, I compared the sensitivities to several kinds of DNA damage between WT and various disruptants. First, I analyzed the sensitivity to UV irradiation at 254 nm (UV-C), which leads to the formation of DNA photoproducts including cyclobutane pyrimidine dimers and 6-4 photoproducts. The gene disruption of some DNA repair proteins are known to increase sensitivity to UV irradiation: Δ*recJ* was more sensitive to UV than WT (Fig. 12A) (51). It should be mentioned that the survival percentage of Δ*recJ* was nearly unchanged at higher dose levels (60 to 96 Jm^{-2}). Similar phenomenon in the slope of survival curves was observed with *uvrA* and *recA* mutants (78). Unexpectedly, however, Δ*nurA*, Δ*herA*, and Δ*nurA*Δ*herA* showed extremely higher resistance to UV than WT (Fig. 12A). Both Δ*herA* and Δ*nurA*Δ*herA* showed greater resistance than Δ*nurA*, whereas no difference was found in the resistance of Δ*herA* and Δ*nurA*Δ*herA*. This suggests that the deletion of *herA* is responsible for these phenotypes. These three disruptants were also more resistant to UV irradiation at 312 nm (UV-B) than WT (Fig. 12B). UV-B is considered a major component of solar radiation that can lead to the formation of photoproducts because UV-C (200–280 nm) is quantitatively absorbed by oxygen and ozone in the earth's atmosphere (79). These results at least suggest that NurA and HerA are involved in the impairment, but not the promotion, of the repair of UV-induced DNA damage.

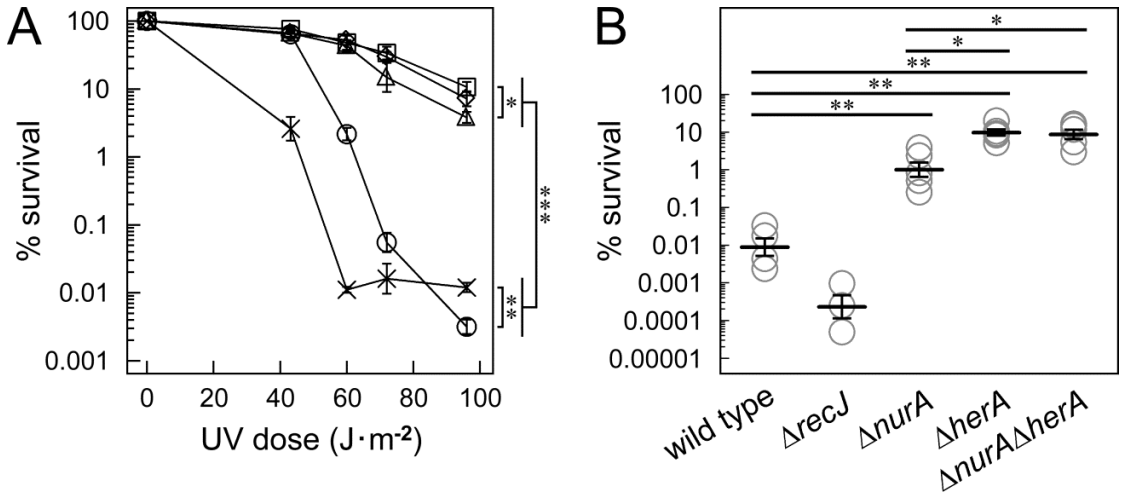

Fig. 12 UV sensitivity. (A) Comparing the sensitivity to UV irradiation at 254 nm (UV-C) among strains under different doses. Symbols indicate the following: circles, WT; crosses, Δ*recJ*; triangles, Δ*nurA*; diamonds, Δ*herA*; and squares, Δ*nurA*Δ*herA*. Bars indicate the standard error of geometric means ($n \geq 5$). In this figure, asterisks indicate *p* values between WT and each disruptant strain at 96 Jm^{-2}. (B) The sensitivity to UV irradiation of 312 nm at 224 Jm^{-2}. Circles indicate individual measurements. Cross bars and vertical bars indicate geometric means ($n \geq 3$) and standard error of geometric means, respectively. *, $0.01 \leq p < 0.05$; **, $0.001 \leq p < 0.01$; ***, $p < 0.001$.

The disruptants of *nurA* and *herA* also showed higher resistance to MMC than WT (Fig. 13). MMC induces the monoadducts, as well as the interstrand- and intrastrand-crosslink structures of DNA (80). This result suggests that NurA and HerA proteins are also involved in the impairment of the repair of DNA damage induced by MMC treatment. It should be noted that over 43.2 Jm^{-2} of UV and 1 μg/ml MMC clear differences were observed in the survival rate between WT and disruptants of *nurA* and/or *herA* (Figs. 12A and 13). These dose levels seem to be boundaries at which DNA repair systems can cope with UV- and MMC-induced lesions in the presence of NurA and/or HerA. Additionally, under the conditions that the survival rates of WT were 0.1%, the resistances of the disruptants to MMC treatment were significantly lower than those to UV irradiation (Figs. 12A and 13). Furthermore, all of the disruptant mutants had no difference in the resistance to MMC treatment, whereas Δ*herA* and Δ*nurA*Δ*herA* showed higher resistance than Δ*nurA* to UV irradiation (Figs. 12A and B).

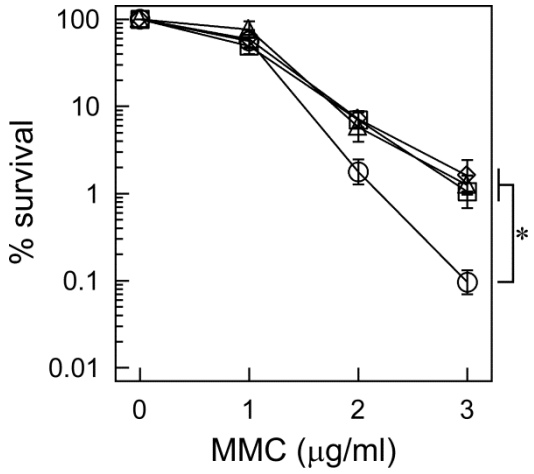

Fig. 13 Comparing the sensitivity to MMC treatment among strains under different doses. Symbols indicate the following: circles, WT; triangles, Δ*nurA*; diamonds, Δ*herA*; and squares, Δ*nurA*Δ*herA*. Bars indicate the standard error of the means (n = 4). The asterisk indicates *p* value in the presence of 3 μg/mL MMC. *, $0.01 \leq p < 0.05$.

To investigate whether the observed high resistance was ascribed to the loss of NurA or HerA protein or indirect effects by the gene disruption, I complemented Δ*nurA* and Δ*herA* strains by the overexpression of *nurA* and *herA*, respectively. The protein expression of NurA in Δ*nurA* and HerA in Δ*herA* was confirmed by affinity purification and Western blotting, respectively (Figs. 14A and B). I then measured their sensitivities to UV-C irradiation at a high dose. Complementation of *nurA* and *herA* in Δ*nurA* and Δ*herA*, respectively, led to a decrease in the UV resistance to the levels equivalent to the resistance of WT (Figs. 14C and D). In contrast, the overexpression of NurA or HerA in WT had no effect on the UV sensitivity. These results confirm that the deletion of *nurA* or *herA* increased the UV resistance of *T. thermophilus* HB8.

In addition, to investigate whether enzymatic activities of NurA and HerA contributed to the UV resistance, I constructed the two strains overexpressing function-deficient mutants of NurA and HerA. Asp51 of *T. thermophilus* HB8 NurA is one of the residues that is responsible for metal binding; that is, for the nucleolytic activity (Fig. 5A). Lys168 of *T. thermophilus* HB8 HerA is an important residue for ATP binding in the Walker A motif; that is, for the ATPase activity (Fig. 5B). Expression of $NurA_{D51A}$ and $HerA_{K168A}$ proteins in Δ*nurA* and Δ*herA* cells were confirmed by affinity purification and Western blotting, respectively; the mutant and WT proteins were expressed at comparable levels (Figs. 15A and B). The strains overexpressing $NurA_{D51A}$ in Δ*nurA* showed the level of UV-C resistance comparable to that of Δ*nurA* with an empty vector (Fig. 15C). Also, no difference was observed between the Δ*herA* strains with $HerA_{K168A}$ overexpression plasmid and empty vector (Fig. 15D). These results suggest that the enzymatic activities of NurA and HerA were involved in the UV sensitivity of *T. thermophilus* HB8.

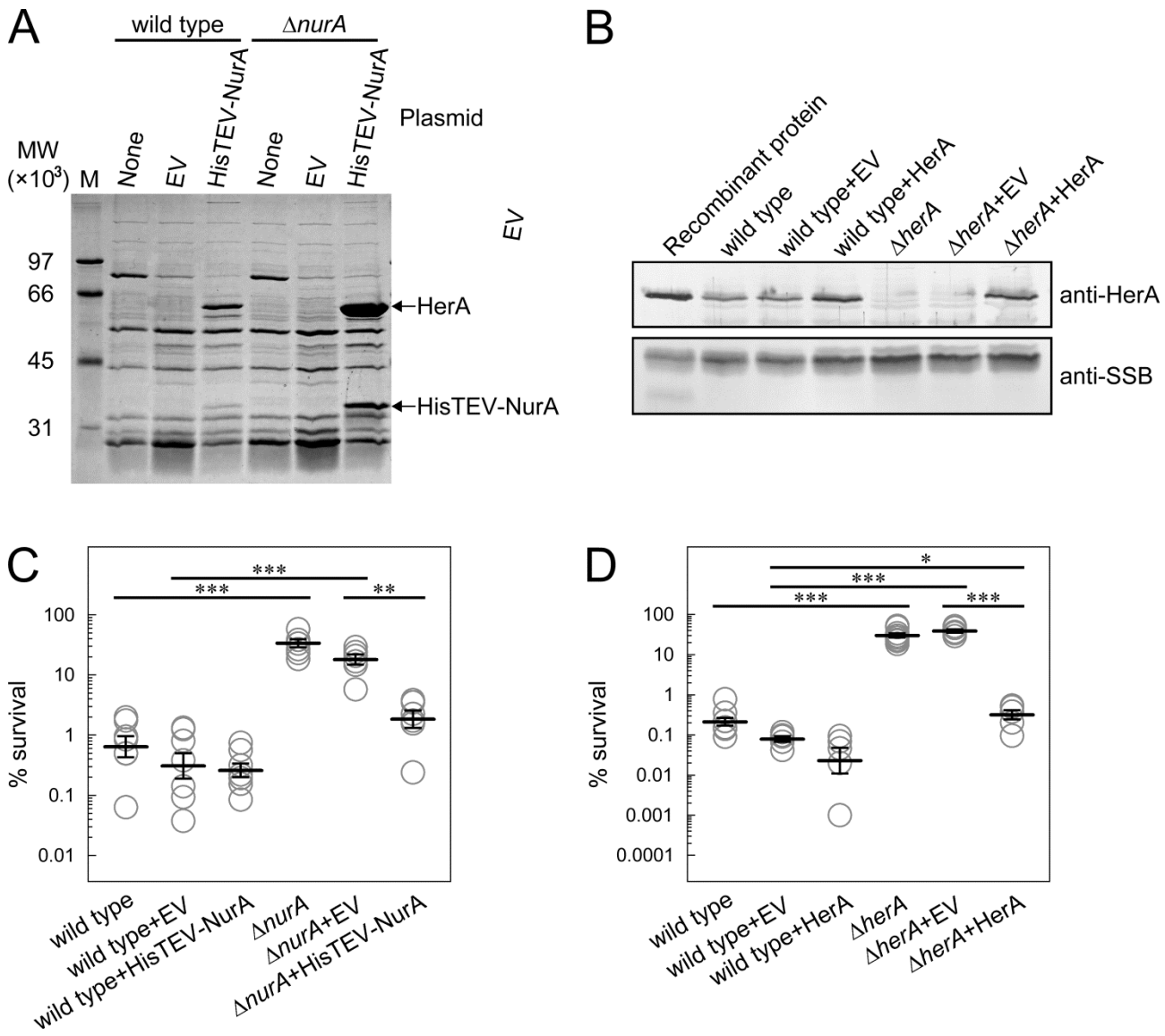

Fig. 14 UV sensitivity of the complemented strains. (A) Expression of His-tagged NurA in WT and Δ*nurA*. The expression was confirmed by SDS-PAGE after affinity purification with TALON resin. (B) Expression of HerA in WT and Δ*herA*. The expression was confirmed by Western blotting with anti-HerA antiserum. SSB serves as an internal loading control. As controls for the mobility of HerA and SSB proteins, 50 ng of recombinant HerA and SSB were also applied. (C) Sensitivity of *nurA*-overexpressing strains to UV light of 254 nm at 72 Jm^{-2}. (D) Sensitivity of *herA*-overexpressing strains to UV light of 254 nm at 96 Jm^{-2}. EV indicates an empty vector. In (C) and (D), circles indicate individual measurements. Cross bars and vertical bars indicate geometric means (n = 7 for (C) and n ≥ 5 for (D)) and standard error of geometric means, respectively. *, $0.01 \leq p < 0.05$; **, $0.001 \leq p < 0.01$; ***, $p < 0.001$.

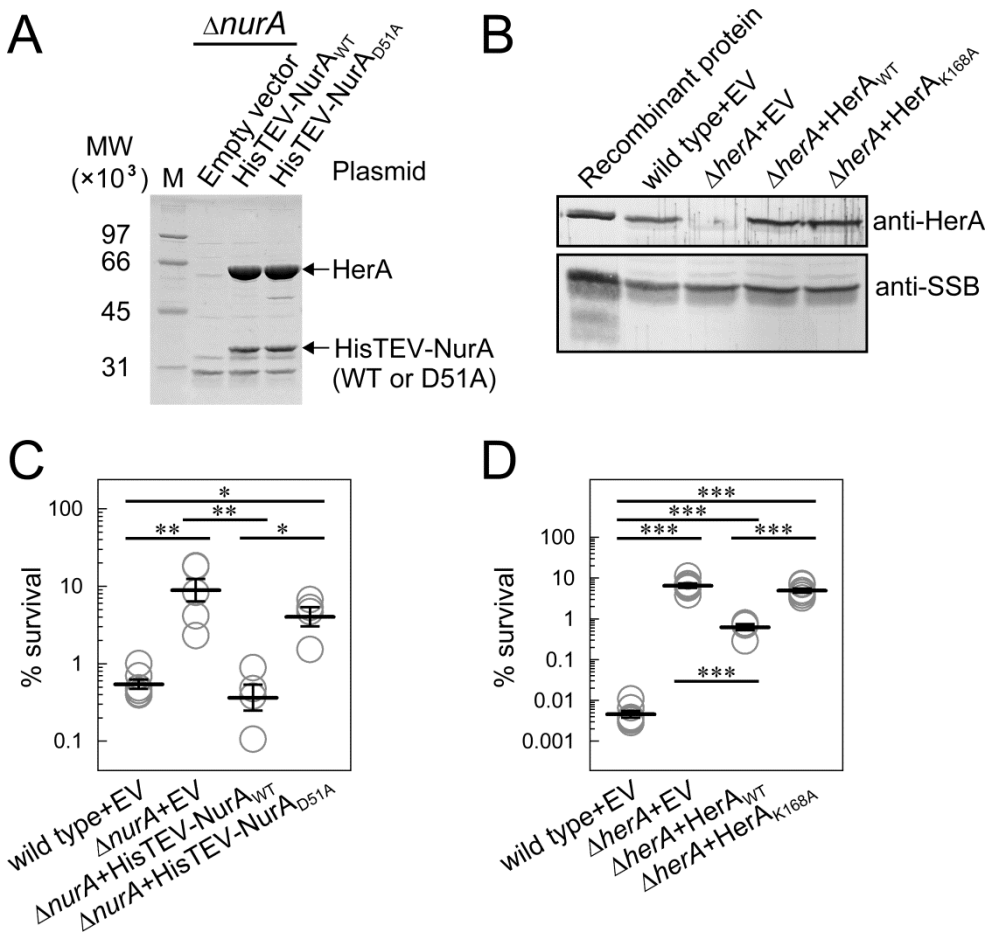

Fig. 15 UV sensitivity of the strains overexpressing function-deficient mutants of NurA and HerA. (A) Expression of His-tagged NurA (WT and D51A) in Δ*nurA*. The expression was confirmed by SDS-PAGE after affinity purification with TALON resin. (B) Expression of HerA (WT and K168A) in Δ*herA*. The expression was confirmed by Western blotting with anti-HerA antiserum. SSB serves as an internal loading control. As controls for the mobility of HerA and SSB proteins, 50 ng of recombinant HerA and SSB were also applied. (C) Sensitivity of *nurA*-overexpressing strains to UV light of 254 nm at 72 Jm^{-2}. (D) Sensitivity of *herA*-overexpressing strains to UV light of 254 nm at 96 Jm^{-2}. In (C) and (D), circles indicate individual measurements. Cross bars and vertical bars indicate geometric means ($n \geq 4$ for (C) and $n = 6$ for (D)) and standard error of geometric means, respectively. *, $0.01 \leq p < 0.05$; **, $0.001 \leq p < 0.01$; ***, $p < 0.001$.

To further investigate whether these resistances were attributed to repairing DNA lesions in an error-free manner or to overcoming them via the error-prone process, that is, translesion DNA synthesis (TLS), the frequency of mutations induced by UV irradiation was measured (Fig. 16). This assay was carried out under the condition that all of the strains showed approximately 10% viability by UV irradiation (Fig. 16A; also see Fig. 12A). In the WT strain, no mutagenesis by UV irradiation was observed (Fig. 16B; also see Fig. 10). Also, no UV mutagenesis was observed in any of the disruptant strains (Fig. 16B; also see Fig. 10). These results imply that TLS in an error-prone manner was not affected by the disruption of *nurA* and/or *herA* in the process of repairing UV-induced damages.

Furthermore, no differences were found in the growth rate between WT and all disruptant strains, even after UV irradiation (Fig. 16C). It should be noted that all of the strains were exposed to different doses of UV radiation to adjust their viability. This result suggests that UV irradiation has no effect on the cell growth of survivors.

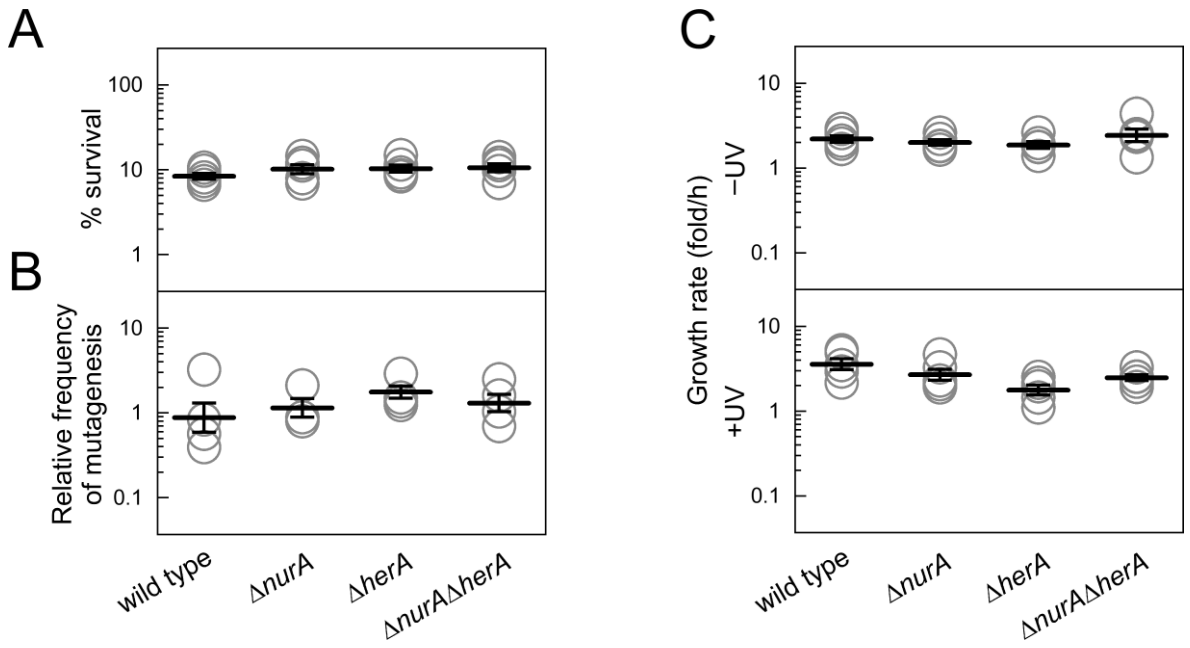

Fig. 16 UV-induced mutagenesis. (A) The survival rate at the time point of UV irradiation. (B) The relative frequency of mutagenesis by UV irradiation. This was measured as the frequency of streptomycin-resistant cells under the condition that all strains showed 10% survival by UV irradiation, as shown in (A). Circles indicate individual measurements. Cross bars and vertical bars indicate geometric means (n = 5) and standard error of geometric means, respectively. (C) The relative growth rate. These were calculated from the numbers of the living cells at 0 h and 3 h after UV irradiation and no irradiation.

UV irradiation assay with multiple gene disruptants

To address cellular function of NurA and HerA in more detail, I analyzed the UV sensitivity of Δ*nurA*Δ*herA* strain with an additional disruption of a repair-related gene UV-induced lesions, such as cyclobutane pyrimidine dimer (CPD), are known to be mainly repaired by nucleotide excision repair (NER) and by HR (also described in Discussion section) (1). Therefore, as targets for additional gene disruption, I selected *uvrA* and *trcf* genes for NER-related genes, and *recJ* and *recR* genes for HR-related genes. UvrA is the first NER component to detect DNA lesions. TRCF, transcription-repair coupling factor, dissociates RNA polymerase stalled at a template strand lesion and recruits NER machinery. RecJ, a 5'→3' exonuclease, initiates DSB end resection in the RecFOR pathway of HR. RecR stabilizes the assembly of a RecFOR complex, which functions as a mediator that loads RecA on ssDNA. Single and multiple disruptions of these genes were successfully achieved, that is, Δ*uvrA*::Hyg^R (Δ*uvrA*), Δ*trcf*::Hyg^R (Δ*trcf*), Δ*recJ*::Hyg^R (Δ*recJ*), Δ*recR*::Hyg^R (Δ*recR*), Δ*nurA*Δ*herA*::*HTK*Δ*uvrA*::Hyg^R (Δ*nurA*Δ*herA*Δ*uvrA*), Δ*nurA*Δ*herA*::*HTK*Δ*trcf*::Hyg^R (Δ*nurA*Δ*herA*Δ*trcf*), Δ*nurA*Δ*herA*::*HTK*Δ*recJ*::Hyg^R (Δ*nurA*Δ*herA*Δ*recJ*), Δ*nurA*Δ*herA*::*HTK*Δ*recR*::Hyg^R (Δ*nurA*Δ*herA*Δ*recR*) (Fig. 17).

Fig. 17 (next page) PCR verification of gene disruption. (A) Disruption of *uvrA* in WT (left) and Δ*nurA*Δ*herA*::*HTK* strain (right). (B) Disruption of *trcf* in WT (left) and Δ*nurA*Δ*herA*::*HTK* strain (right). (C) Disruption of *recJ* in WT (left), and of *nurA-herA* in Δ*recJ*::Hyg^R strain (right). (D) Disruption of *recR* in WT (left), and of *nurA-herA* in Δ*recR*::Hyg^R strain (right). (E) Disruption of *recR* in Δ*uvrA*::*HTK* strain. The external (e) and internal (i1 and i2) primer pairs are as follows: e, primers complementary to upstream and downstream regions of target genes; i1, primers complementary to targeted genes and upstream or downstream regions; i2, primers complementary to the Hyg^R or *HTK* region, and upstream or downstream region. The genomic DNAs or cells as templates for PCR are as follows: NH, Δ*nurA*Δ*herA*::*HTK*; NHA, Δ*nurA*Δ*herA*::*HTK*Δ*uvrA*::Hyg^R; NHT, Δ*nurA*Δ*herA*::*HTK*Δ*trcf*::Hyg^R; NHJ, Δ*nurA*Δ*herA*::*HTK*Δ*recJ*::Hyg^R; NHR, Δ*nurA*Δ*herA*::*HTK*Δ*recR*::Hyg^R; and AR, Δ*uvrA*::Hyg^RΔ*recR*::*HTK*. M_H indicates a λ-HindIII DNA size marker and M_B indicates a λ-BstPI DNA size marker.

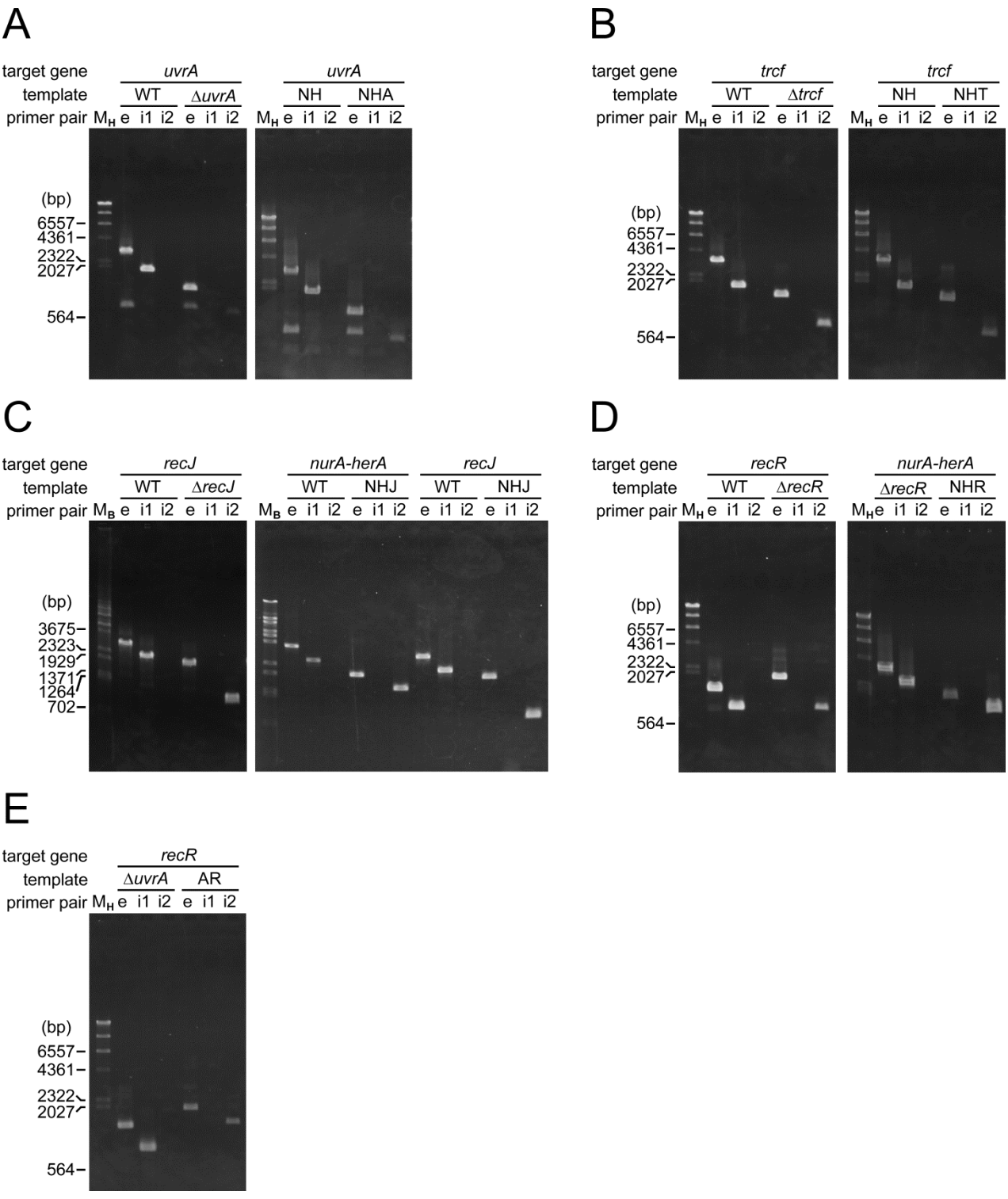

Fig. 17 (continued)

As expected, Δ*uvrA* showed significantly higher UV sensitivity than WT. If NurA-HerA impairs HR pathway, but not NER pathway, Δ*nurA*Δ*herA*Δ*uvrA* would show the decreased UV sensitivity compared to Δ*uvrA*. Interestingly, the disruption of *nurA-herA* in Δ*urvA* did not decrease UV sensitivity compared to Δ*uvrA*, which was distinctly different from the case for WT (Fig. 18A). These results seem to support the notion that NurA-HerA does not impair other repair processes than NER pathway. Furthermore, the sensitivity of Δ*nurA*Δ*herA*Δ*uvrA* was slightly higher than that of Δ*uvrA* (Fig. 18A). This result suggests that NurA-HerA seems to contribute positively, not inhibitingly, to other repair processes than NER. In addition, a part of Δ*nurA*Δ*herA* cells, as well as Δ*uvrA* cells, formed smaller colonies with UV irradiation compared to non-irradiated cells (Fig. 19). WT cells had no difference in colony size between with and without UV irradiation (Fig. 19). This phenotype was observed at 43.2 Jm^{-2} of UV irradiation, at which WT and Δ*nurA*Δ*herA* showed UV sensitivity at the same level. Such a phenotype was also observed under higher dose of UV irradiation (98 Jm^{-2}; data not shown). This supports the notion that NurA-HerA positively contribute to the repair of UV-induced lesions. It should be noted here that growth defect of Δ*nurA*Δ*herA* after UV irradiation was not observed in the experiment for estimating the UV-induced mutagenesis (Fig. 16C). This may be because the length of time for culturing cells after UV irradiation was too short to detect the growth defect, or because the number of cells showing slow growth was too low to be observed as the growth defects in cell population. Δ*trcf* also showed higher sensitivity than WT, but the disruption of *nurA-herA* in Δ*trcf* decreased the UV sensitivity to the same level as in WT (Fig. 18A). These results suggest that NurA-HerA does not impair the repair process in which TRCF is involved.

The disruption of *nurA-herA* in Δ*recJ* slightly but significantly restored the UV resistance compared to Δ*recJ*, suggesting that NurA-HerA impair other repair processes than RecJ-dependent pathway. In contrast, Δ*recR* and Δ*nurA*Δ*herA*Δ*recR* showed quite similar UV sensitivity, which was higher than WT (Fig. 18B). These results suggest that NurA-HerA does not impair other repair processes than RecR-dependent HR pathway. This may further suggest that NurA-HerA is positively or negatively associated with RecR-dependent HR pathway.

Further, I compared the UV sensitivity between the single-gene disruptants, Δ*uvrA* and Δ*recR*, and double-gene disruptant Δ*uvr*AΔ*recR*. The survival curves of the two single-gene disruptants were similar, while Δ*recR* showed slightly higher sensitivity than Δ*uvrA* (Fig. 18C, also see 18A

and 18B). The sensitivity of Δ*uvr*AΔ*recR* was significantly higher than those of Δ*uvrA* and Δ*recR* (Fig. 18C). Apparent additive effects of UvrA and RecR deficiencies in the repair of UV-induced lesions suggest no interdependence of NER and HR in this process.

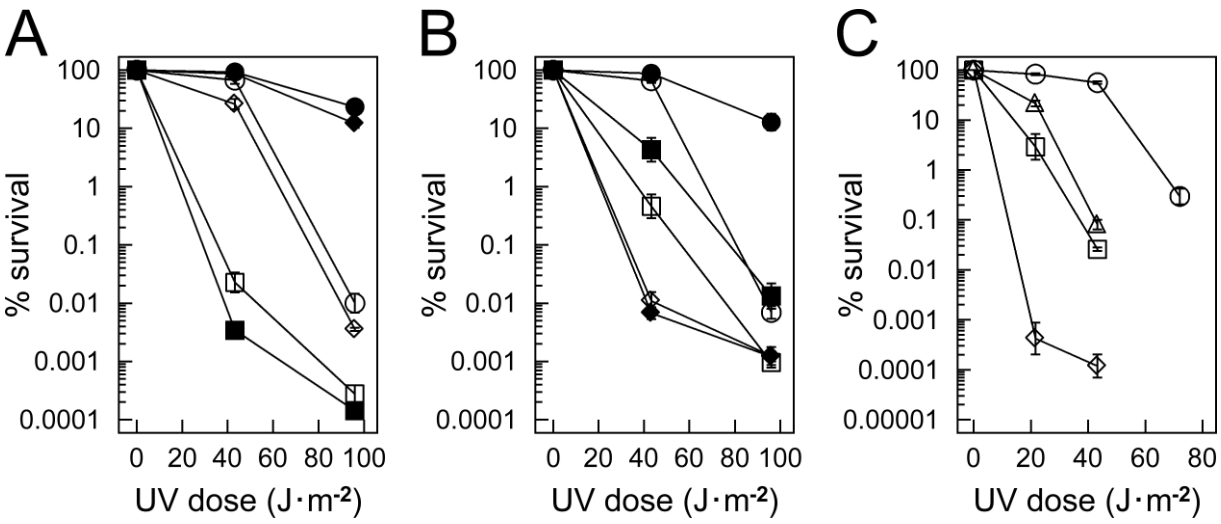

Fig. 18 Comparing UV sensitivities among strains under different doses. (A) The targets of gene disruption are *nurA-herA* and NER-related genes. Symbols indicate the following: open circles, WT; closed circles, Δ*nurA*Δ*herA*; open squares, Δ*uvrA*; closed squares, Δ*nurA*Δ*herA*Δ*uvrA*; open diamonds, Δ*trcf*; and closed diamonds, Δ*nurA*Δ*herA*Δ*trcf*. (B) The targets of gene disruption are *nurA-herA* and HR-related genes. Symbols indicate the following: open circles, WT; closed circles, Δ*nurA*Δ*herA*; open squares, Δ*recJ*; closed squares, Δ*nurA*Δ*herA*Δ*recJ*; open diamonds, Δ*recR*; and closed diamonds, Δ*nurA*Δ*herA*Δ*recR*. (C) The targets of gene disruption are *uvrA* and *recR*. Symbols indicate the following: open circles, WT; triangles, Δ*uvrA*, open squares, Δ*recR*; and diamonds, Δ*uvrA*Δ*recR*. Bars indicate the standard error of geometric means (n ≥ 3 for (A), n ≥ 4 for (B) and (C)).

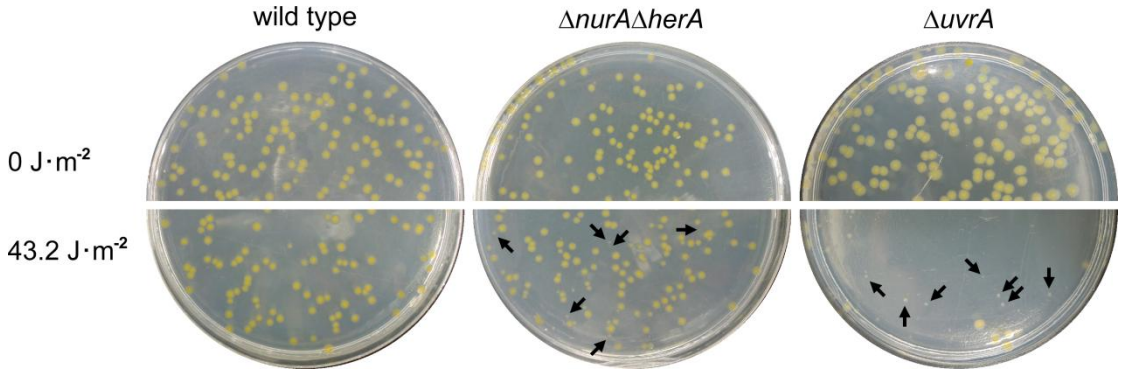

Fig. 19 Colony size after UV irradiation. Top and bottom of figures indicate emerging colonies after no irradiation (0 Jm^{-2}) and irradiation (43.2 Jm^{-2}) of UV, respectively. Black arrows indicate small colonies formed after UV irradiation.

Deletion of *nurA* and *herA* has no effects on sensitivities to oxidative stress and a replication inhibitor

It was possible that the different kinds of DNA lesions resulted in the differences in the disruptants' sensitivities to UV irradiation and MMC treatment. I then examined the sensitivity of Δ*nurA*, Δ*herA*, and Δ*nurA*Δ*herA* strains to oxidative stress and treatment with a DNA replication inhibitor. First, I analyzed the sensitivity to hydrogen peroxide (H_2O_2), which causes oxidative lesions on DNA (81). As shown in Fig. 20A, the WT and disruptants showed no significant difference in viability. This result indicates that NurA and HerA had no effect on the repair of oxidative lesions. Second, I measured the sensitivity to nalidixic acid (NA), which is known to induce DSBs by inhibiting subunit A of DNA gyrase (82). The antibacterial activity of NA has also been known in many bacteria (83, 84), and it has already been reported that the supercoiling activity of recombinant *T. thermophilus* GyrA is inhibited by NA (85). In this experiment, NA treatment was performed at 60°C because no NA sensitivity was observed at 70°C, the optimal growth temperature for *T. thermophilus* (data not shown). The disruptants of *nurA* and *herA* showed similar NA sensitivity to WT (Fig. 20B). This result indicates that NurA and HerA had no effect on the repair of lesions caused via inhibition of DNA gyrase by NA. In contrast, Δ*recJ* showed higher NA sensitivity than WT (Fig. 20B). It should be noted that under the mock condition (10 mM NaOH), WT and disruptants of *nurA* and/or *herA* showed cell growth, but Δ*recJ* did not (Fig. 20B). However, the survival fraction of Δ*recJ*, the survival rate with NA to those with the mock, was 10 times lower than that of WT at 6 h after NA addition, indicating the involvement of RecJ in the repair of lesions caused via NA treatment.

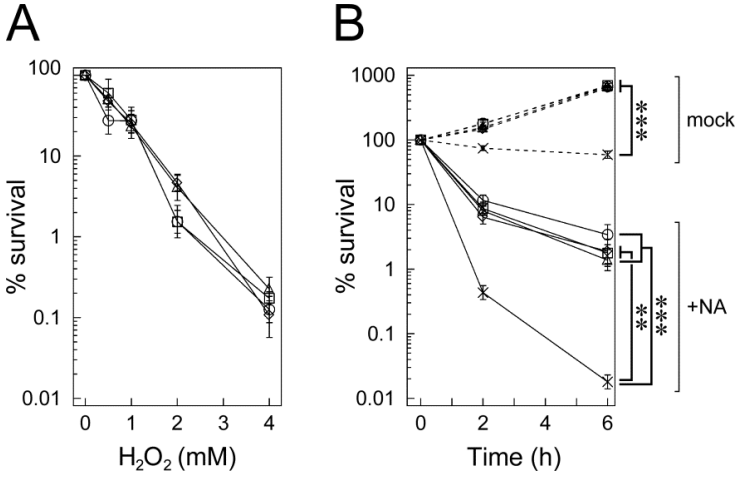

Fig. 20 (A) Sensitivity to H_2O_2 treatment. (B) Sensitivity to acute treatment of NA. Bars indicate the standard error of the means (n = 5 for (A) and (B)). Dashed and solid lines indicate the results in the absence (mock, 10 mM NaOH) and presence of NA, respectively. Asterisks indicate *p* values for respective strains under the condition with mock or NA at 6 h after addition. Symbols are as follows: circles, WT; crosses, Δ*recJ*; triangles, Δ*nurA*; diamonds, Δ*herA*; and squares, Δ*nurA*Δ*herA*. Bars indicate the standard error of geometric means. **, $0.001 \leq p < 0.01$; ***, $p < 0.001$.

NurA and HerA interact with each other *in vitro* and *in vivo*

In addition to genetic studies, I investigated the physical interaction between NurA and HerA proteins. Each recombinant protein was overexpressed in *E. coli* and was purified through several steps of chromatography (Fig. 21). Analysis by a Fourier transform ion cyclotron resonance mass spectrometer revealed that the molecular masses of the recombinant NurA and HerA were 31,640 Da and 63,972 Da, respectively (data not shown). The value of the recombinant HerA was in agreement with that calculated from the full-length sequence (63,974 Da), whereas the value of the recombinant NurA was lower than that of the full-length NurA (31,771 Da), indicating the loss of the N-terminal first methionine.

The association states of NurA and HerA were analyzed by size-exclusion chromatography (Fig. 22A). The results showed the apparent molecular weight of NurA alone was 28,000, indicating its monomeric state in solution, whereas that of HerA was 324,000, indicating its pentameric or hexameric state (Fig. 22A). When the mixture of NurA and HerA at a molar ration of 3:5 (as the monomers) was analyzed, two peaks were observed (Fig. 22A). One peak with an apparent molecular weight of 28,000 corresponded to the monomeric NurA. The other peak (376,000) was obviously larger than that of the pentameric/hexameric HerA and contained both HerA and NurA (Fig. 22B), indicating that HerA interacts with NurA in solution. The difference in the apparent molecular weights between HerA-NurA complex and HerA alone was approximately 52,000, which was apparently close to the value of the two NurA molecules. Therefore, it was supposed that NurA and HerA form a complex with 2:5 or 2:6 as the stoichiometry. This stoichiometry is similar to those of archaeal and *Deinococcus* homologs (34–36, 40).

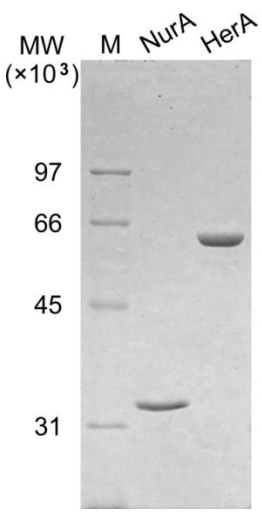

Fig. 21 Recombinant NurA and HerA. Purified NurA and HerA were analyzed by SDS-PAGE.

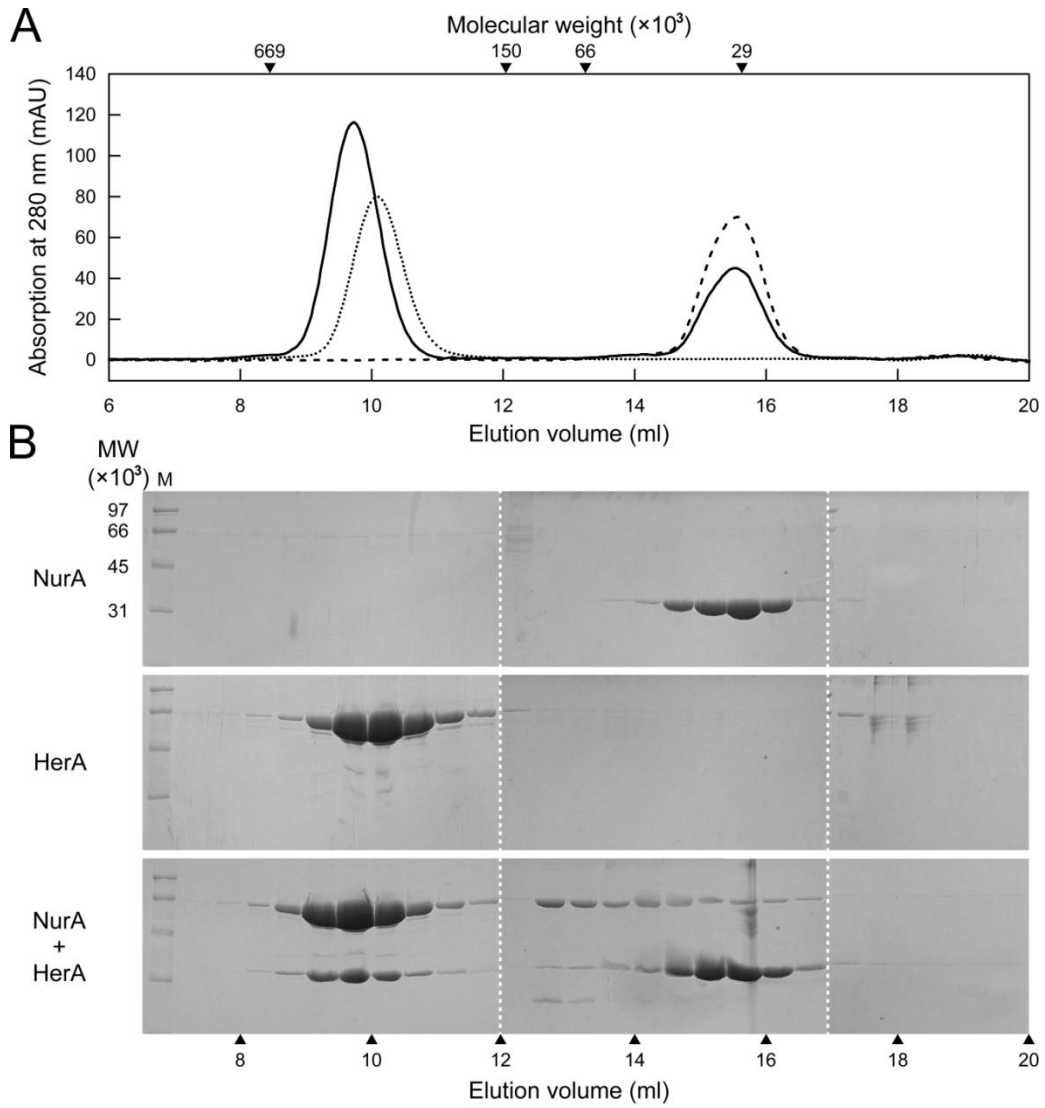

Fig. 22 Physical interaction analysis between NurA and HerA by size-exclusion chromatography. (A) The chromatograms of NurA and/or HerA. Dashed, dotted, and solid lines indicate NurA, HerA, and NurA and HerA, respectively. (B) Separation of the eluted NurA and/or HerA by SDS-PAGE. Horizontal bars indicating the elution volume are adjusted between (A) and (B).

This hypothesis was verified by native PAGE (Fig. 23). When the molar ratios of HerA to NurA were changed by varying the NurA concentrations, the bands corresponding to HerA became decreased. Concomitantly, the bands with lower mobility appeared, which likely corresponded to the NurA-HerA complex (Fig. 23). It should be mentioned that the NurA protein could not enter the gel in this assay condition as shown in Fig. 23 because the isoelectric point of NurA (9.1, calculated by Compute pI/Mw (http://web.expasy.org/compute_pi/)) is higher than the pH of buffers for native PAGE (6.8 for the sample and concentration buffers; 8.3 for the running buffer). The band of HerA

disappeared when HerA and NurA were applied at the molar ratio of 6:2. These results strongly support the above suggestion that NurA and HerA form the complex with a molar ratio of 2:6. In addition, HerA and the NurA-HerA complex showed discrete bands in all ranges of NurA concentration. This suggests that the equilibrium between association and dissociation states of NurA-HerA complex is slow.

Furthermore, I analyzed the intermolecular region of the NurA-HerA complex. By limited digestion of HerA with trypsin, I obtained the truncated HerA that lacked the N-terminal HAS domain (ΔN-HerA) (Fig. 24A). This ΔN-HerA did not interact with NurA in native PAGE (Fig. 24B). These results suggest that the HAS domain of HerA is necessary for interaction with NurA.

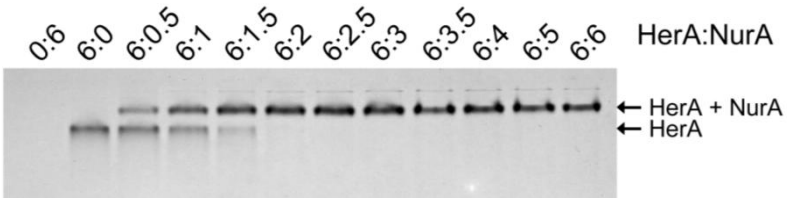

Fig. 23 Interaction analysis between NurA and HerA by native PAGE. The mole ratio of HerA to NurA in each lane is indicated above the figure.

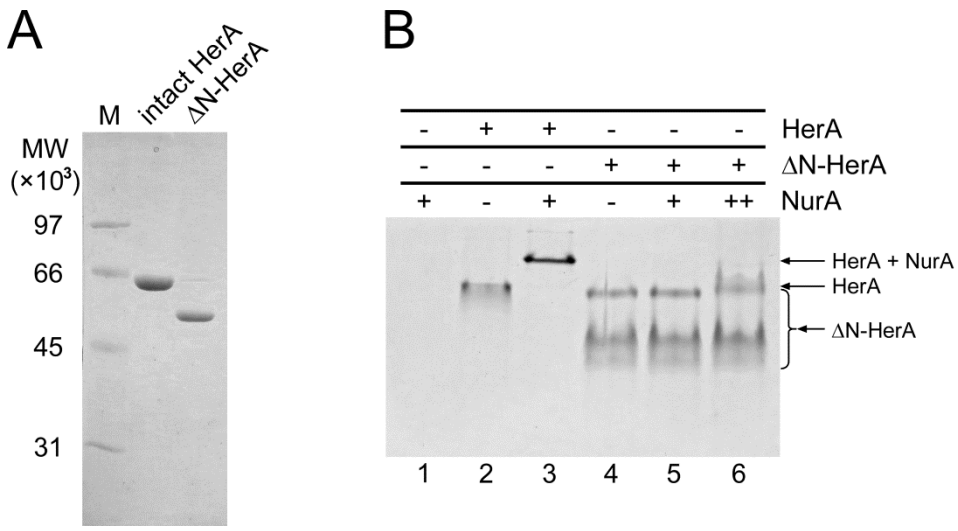

Fig. 24 Interaction analysis between NurA and ΔN-HerA. (A) Purified ΔN-HerA on SDS-PAGE. (B) Interaction analysis by native PAGE. NurA and intact HerA were applied in lane 3 as the positive control. Concentrations of proteins are as follows: −, 0 μM; + of HerA and ΔN-HerA, 2.5 μM; + of NurA, 0.83 μM; and ++, 12.5 μM.

To examine that NurA and HerA form the complex in *T. thermophilus* HB8 cells, the Δ*nurA* and Δ*herA* strains were complemented with HisTEV-NurA and HerA-His_6 plasmids, respectively, and proteins interacting with each His-tagged protein were probed by affinity purification and mass spectrometry. In each complemented strain, endogenous HerA and NurA were identified as the interacting proteins for HisTEV-NurA and HerA-His_6, respectively (Fig. 25). In the case of Δ*nurA*, the band of approximately 64,000 Da was detected only in the strain complemented with the HisTEV-NurA plasmid. This band was identified as HerA by peptide mass fingerprinting. Similarly, in the case of Δ*herA*, NurA was identified as an interactor protein of the HerA-His_6 protein. The interaction of HisTEV-NurA with HerA in the Δ*nurA* strain was also confirmed by Western blotting with the anti-HerA antiserum (Fig. 26). These results suggest that NurA and HerA interact with each other *in vivo*.

In addition, Figure 26 shows that NurA does not interact with several other proteins involved in DNA repair and HR, such as RecA. In a previous report, NurA physically interacted with SSB in *Sulfolobus tokodaii* (86), and HerA interacted with RecJ in *D. radiodurans* (48). However, SSB and RecJ were not detected as interactors with NurA in *T. thermophilus* HB8 cells (Fig. 26). Native PAGE also indicated no interaction of SSB and RecJ with HerA, as well as NurA (Fig. 27). These results suggest that NurA and HerA in *T. thermophilus* HB8 have properties that differ from those of *Sulfolobus* NurA and *Deinococcus* HerA in protein-protein interactions.

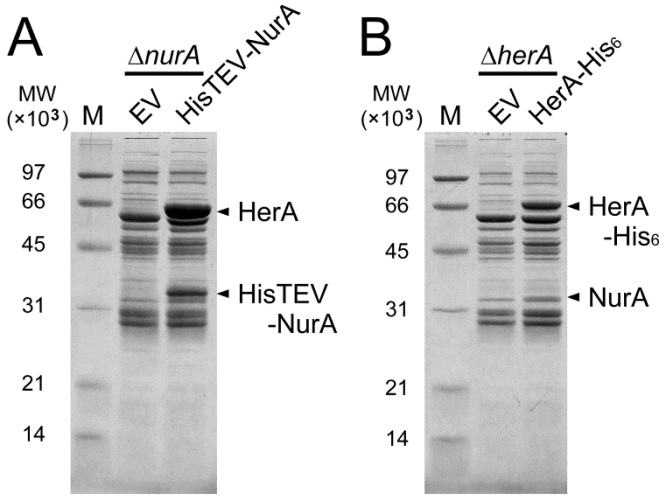

Fig. 25 *In vivo* interaction between NurA and HerA. (A) Interactor proteins of HisTEV-NurA in Δ*nurA*. (B) Interactor proteins of HerA-His_6 in Δ*herA*. EV indicates an empty vector, which is the negative control for protein-protein interaction: proteins observed in the "EV" lane were nonspecifically bound to the TALON resin.

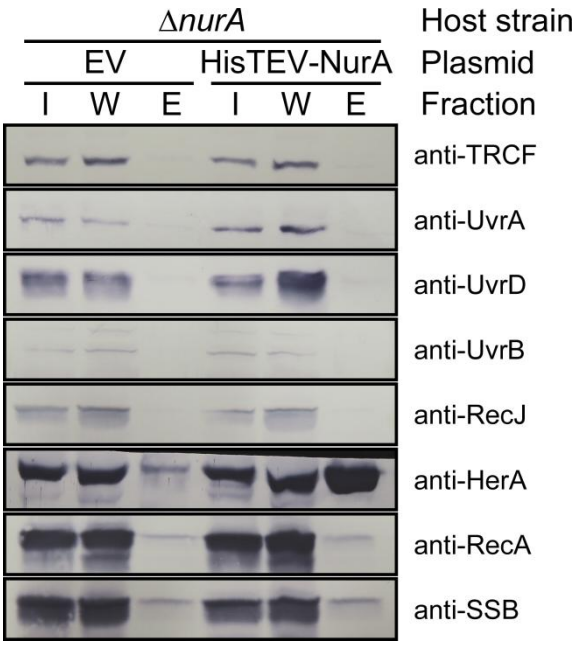

Fig. 26 *In vivo* search for proteins interacting with HisTEV-NurA. Interactors were purified by affinity purification with TALON resin and probed by Western blotting with the indicated antisera. EV indicates an empty vector for negative control of protein-protein interaction. Fractions are indicated as follows: I, input; W, the first fraction of three-times washing procedures; and E, eluate.

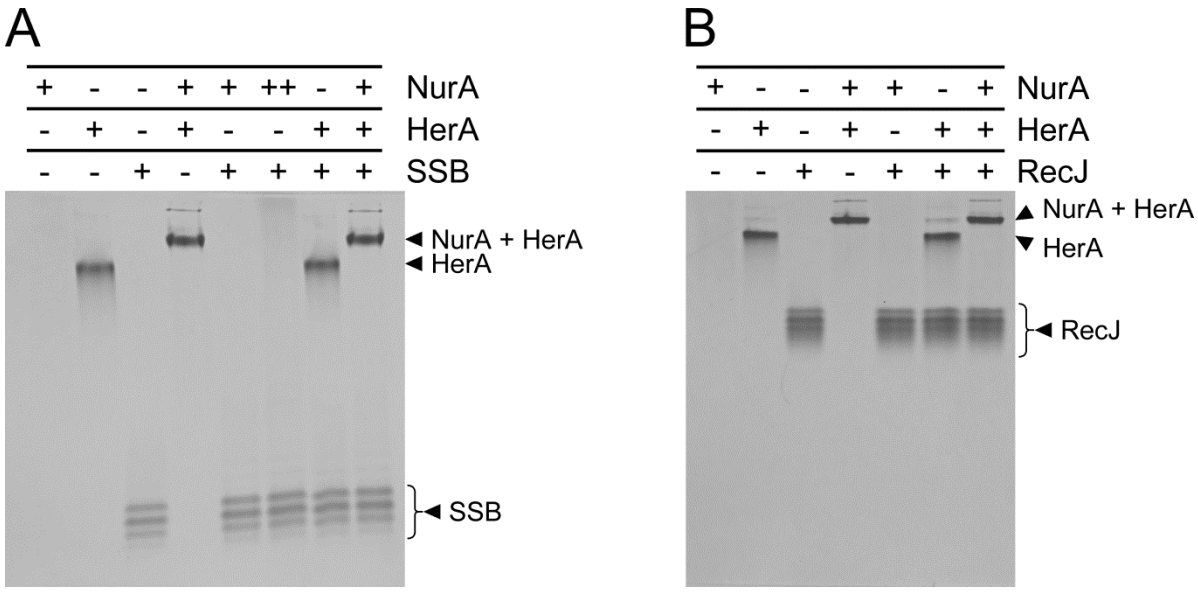

Fig. 27 Interaction analysis of NurA and HerA with SSB (A) and RecJ (B) by native PAGE. Concentrations of each protein are shown as follows: –, 0 μM; +, 4 μM; and ++, 40 μM.

I also analyzed secondary structures of NurA and HerA by CD spectrometry. The observed spectrum of NurA-HerA complex (0.6 μM NurA plus 1.8 μM HerA; $NurA_2$-$HerA_6$) was almost the same as the calculated sum of those of the individual proteins at the same concentrations (Fig. 28A). This indicated that the formation of NurA-HerA complex had no significant effect on the secondary structures of NurA and HerA. It should be noted here that formation of NurA-HerA complex increased their thermostability. From the thermal denaturation curves, the transition temperatures (T_m) of NurA-HerA complex was higher than those of NurA and HerA (Fig. 28B). Such stabilization may be due to the intermolecular interaction and/or conformational changes.

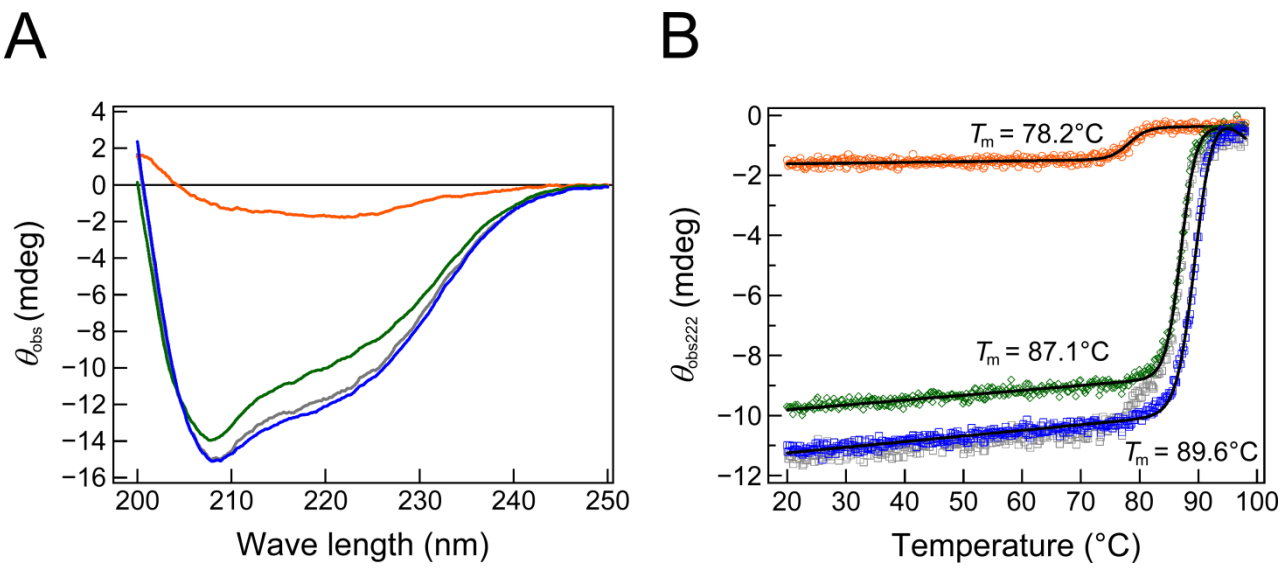

Fig. 28 CD spectra (A) and thermostability (B) of NurA and HerA. Colors are as follows: orange, NurA; green, HerA; blue, $NurA_2$-$HerA_6$ complex; and gray, the calculated sum of individual signals of NurA and HerA. In (B), black lines on each plot indicate the theoretical curves fitted to experimental data according to Equation 1.

NurA has nuclease activity to ssDNA and dsDNA.

To verify that *T. thermophilus* HB8 NurA retains the enzymatic activities, I investigated the nuclease activity of recombinant NurA with 5′-end labeled oligonucleotide as substrates. *T. thermophilus* HB8 NurA showed nuclease activity in the presence of Mn^{2+} or Mg^{2+} (Fig. 29A), and preferred Mn^{2+} to Mg^{2+} as a co-factor (Fig. 29A). The highest activity was observed with 1 mM Mn^{2+} (Fig. 29B). For a 21-mer ssDNA substrate, an exonucleolytic product (1-mer) in the 5′ to 3′ direction was mainly observed (Fig. 29C). On the other hand, in a 21 bp dsDNA substrate, endonucleolytic products were mainly observed (Fig. 29C). These suggest that *T. thermophilus* HB8 NurA retains the nuclease activity to both ssDNA and dsDNA. Although an exonucleolytic product was also observed for a dsDNA substrate, the amount was smaller than that for ssDNA, implying the importance of a 5′ single-stranded region for the exonuclease activity.

Endonucleolytic products were also observed with ssDNA (Fig. 29C). These products might be generated by the nicking activity (described later) on partially and transiently formed duplex regions as homodimers or hairpin structures. Indeed, when using $(dT)_{30}$ substrate, which hardly has the higher order structures, endonucleolytic products was not observed, and only 5′→3′ exonucleolytic product was generated (Fig. 29D, left). The specificity constant (k_{cat}/K_M) of 5′→3′ exonuclease activity for $(dT)_{30}$ was approximately 70 $M^{-1}s^{-1}$ (Fig. 29D, right). This result supports the notion that endonucleolytic products from a 21-mer ssDNA substrate was generated by the nicking activity, which is mentioned below.

It is probable that *T. thermophilus* HB8 NurA does not simultaneously digest two strands of dsDNA, but digests only one strand such as a nickase, because the size-exclusion chromatography demonstrated that this protein was monomeric form (Figs. 22A and B). To verify this hypothesis, I analyzed the nucleolytic activity to covalently closed circular (ccc) plasmid dsDNA. If only one strand of substrate is digested in one reaction event, open circular (oc) DNA would be observed as an intermediate. On the other hand, if both strands are digested, then linear DNA would be generated immediately. As shown in Fig. 29E, while the cccDNA substrate decreased, ocDNA was generated first and subsequently linear DNA was observed. These suggest that *T. thermophilus* HB8 NurA showed nicking activity with respect to dsDNA, rather than simultaneous double-strand digestion activity. It should be mentioned that exonucleolytic products were observed with dsDNA after longer incubation times (Fig. 29C). This is likely because short nicking products were

dissociated into ssDNA, which were digested by 5′→3′ exonuclease activity. In the case of *T. thermophilus* HB8, the NurA-HerA interaction had no effect on the exo- and endonuclease activities of NurA on both ssDNA and dsDNA (Fig. 29F). It is quite different from archaeal and *Deinococcus* NurA: their activities are stimulated by interaction with HerA (34, 37, 40). Furthermore, on ccc plasmid dsDNA, the nicking activity of *T. thermophilus* HB8 NurA did not change by interaction with HerA (Fig. 29G). This is similar to the activity of archaeal and *Deinococcus* NurA (32, 40).

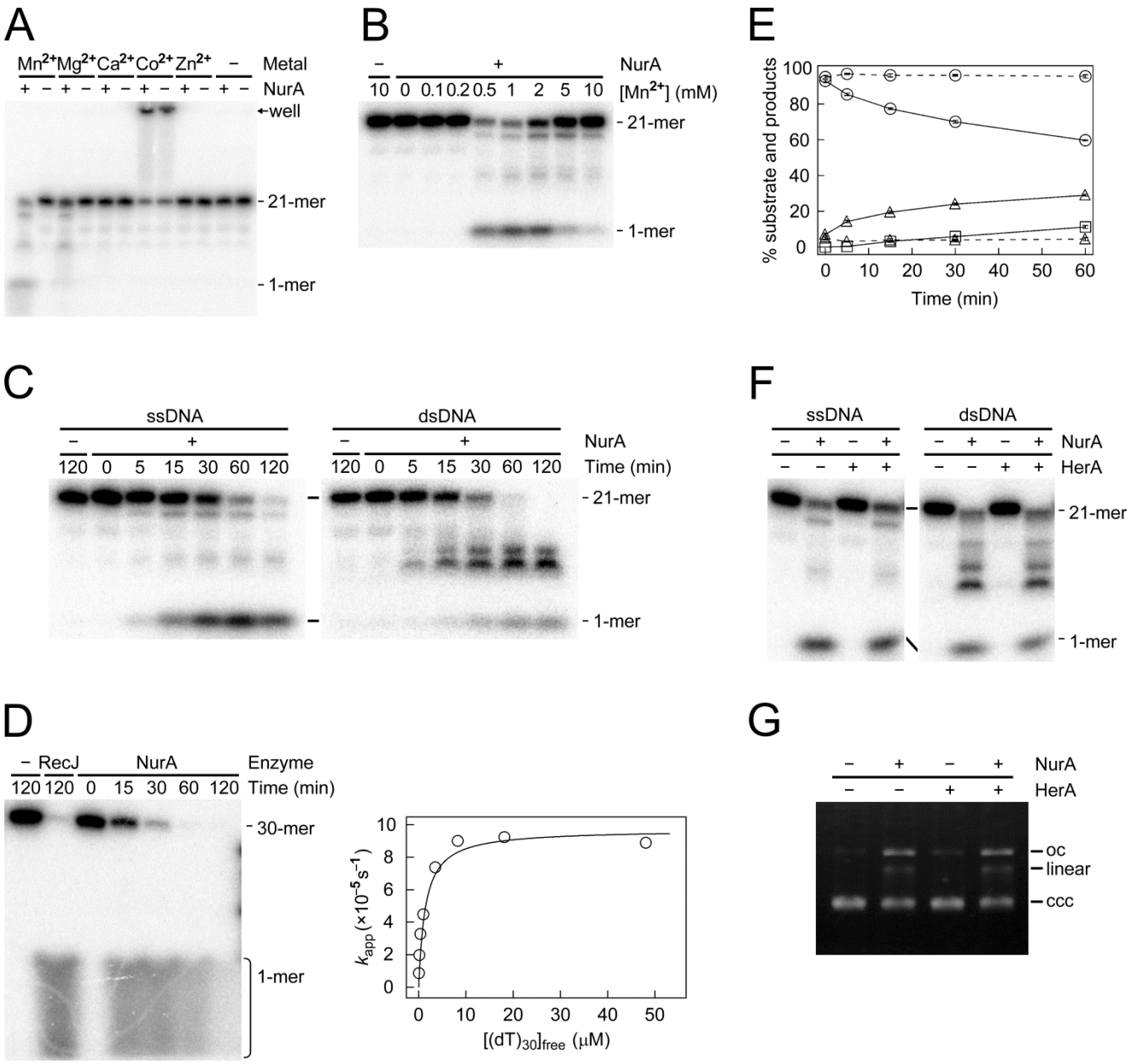

Fig. 29 Nuclease activity of NurA. (A) Metal-ion dependency of nuclease activity. (B) Dependency on the concentration of Mn^{2+}. (C) The time-course analysis of the nuclease activities to ssDNA (21-mer, 1T21) and dsDNA (21 bp). (D) The time-course analysis (left) and the kinetic analysis of 5′→3′ exonuclease activity (right) using $(dT)_{30}$. RecJ was used as the positive control of 5′→3′ exonuclease activity. Circles are the experimental data, and a solid line is the theoretical curve based on Equation 3. The k_{cat} and K_M values were calculated to be 9.7×10^{-5} s^{-1} and 1.4 μM, respectively. (E) The time-course analysis of nicking activity of NurA with covalently closed circular (ccc) plasmid. Symbols are as follows: circles, ccc; triangles, open circular (oc); squares, linear. Solid and dashed lines indicate the presence and absence of NurA, respectively. Bars indicate the standard error of means (n = 3). (F) NurA nuclease activity on DNA in the absence and presence of HerA. (G) Nicking activity in the absence and presence of HerA.

HerA has ATPase activity.

I also investigated ATPase activity of *T. thermophilus* HB8 HerA, which is supposed to drive its helicase activity. By an assay using [γ-^{32}P]ATP, the hydrolytic product, P_i, was detected in the presence of Mg^{2+}, Mn^{2+}, and Co^{2+} (Fig. 30A). The ATPase activity was very low (k_{cat}/K_M = 2.8 × 10^2 ($M^{-1}s^{-1}$)), and no significant difference of the activity was observed between with and without DNA (Fig. 30B). Surprisingly, the HerA ATPase activity decreased in the presence of NurA (Fig. 30C). This decrease depended on the concentration of NurA. Based on this dependence, the K_d value between a hexameric HerA and monomeric NurAs was calculated to be approximately 8.8 × 10^{-3} $\mu M^{2.6}$ (Fig. 30C). The number of NurA molecules that interact with one HerA hexamer (*n* in Equations 7 to 12) was calculated to be approximately 2.6. I was not able to detect any helicase activity of *T. thermophilus* HB8 HerA (data not shown), although more detailed analysis is needed.

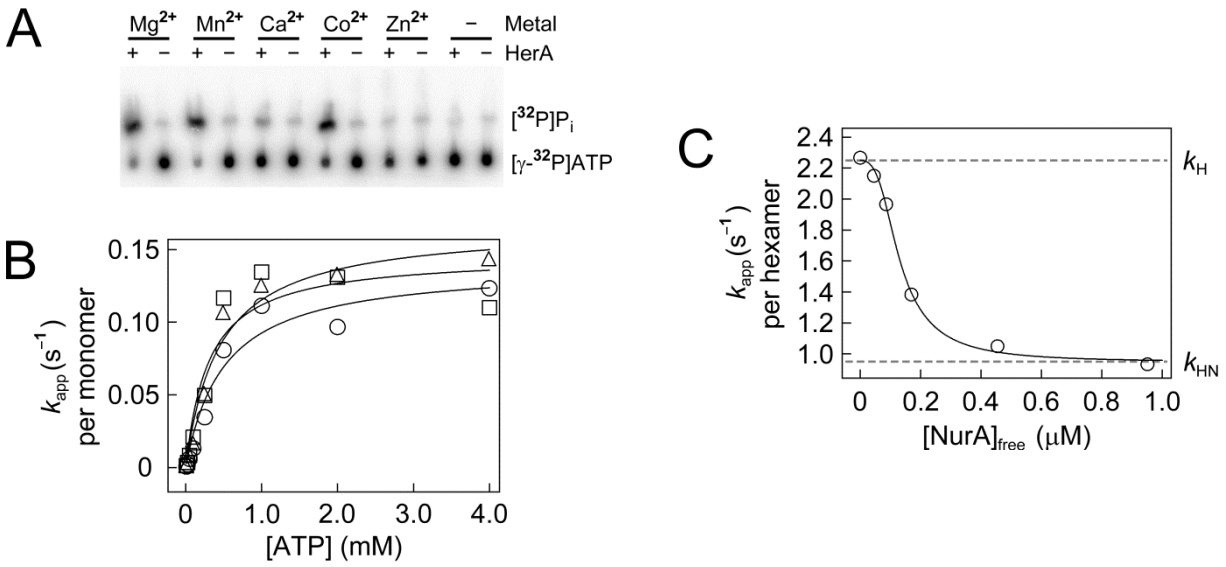

Fig. 30 ATPase activity of HerA. (A) Metal-ion dependency of ATPase activity. (B) The kinetic analysis of ATPase activity in the absence or presence of DNA. Symbols are as follows: circles, DNA free; triangles, ssDNA; squares, dsDNA. Solid lines are theoretical curves. (C) The variation of ATPase activity by the interaction between HerA and NurA. Circles are observed values, and the solid line is a theoretical curve calculated from Equation 12 (see Materials and Methods). Dashed gray lines are k_H (up) and k_{HN} (bottom), respectively. Kinetic parameters k_H, k_{HN}, and K_d are apparent rate constant of hexameric HerA without or with two NurAs (as the monomer) and dissociation constant between hexameric HerA and two NurAs (as the monomer), respectively. The k_H, k_{HN}, and K_d values were calculated to be 2.2 s^{-1}, 0.95 s^{-1} and 8.8 × 10^{-3} $\mu M^{2.6}$, respectively.

Discussion

Nonessentiality of *nurA* and *herA* for survival in *T. thermophilus* HB8 (Fig. 8A) is basically similar to those in *D. radiodurans* (40). This is in contrast to archaeal *nurA* and *herA*, which are essential for survival (41–43). In addition, disruption of *nurA* and *herA* had no influence on cell growth and viability in *T. thermophilus* HB8. This is in contrast to *D. radiodurans* Δ*nurA*, Δ*herA*, and Δ*nurA*Δ*herA*, which showed shorter lag and shorter logarithmic growth phases compared to WT (40). In *T. thermophilus* HB8, the double-gene disruptants, Δ*recJ*Δ*nurA* and Δ*recJ*Δ*herA* (data not shown), and triple-gene disruptant Δ*recJ*Δ*nurA*Δ*herA* were able to be generated. These findings suggest two possibilities: in *T. thermophilus* HB8 cells nuclease activity might have been not essential for end resection, and another nuclease and/or helicase would have functioned in end resection. In the case of *Acinetobacter baylyi*, the double null mutants *recJ recD* and *recJ recBCD* cannot survive; this bacterium has no other 5′-end processing enzyme (54). In contrast, in *Mycobacterium smegmatis*, an end resection enzyme AdnAB (a functional homolog of RecBCD) can be disrupted and that nuclease activity is not essential for DSB repair though this bacterium has no other 5′-to-3′ exonuclease, such as RecJ (87).

The nuclease activity of *T. thermophilus* HB8 NurA in the absence of HerA is similar to *S. acidocaldarius* NurA (27), but is in contrast to *P. furiosus*, *S. solfataricus*, and *D. radiodurans* NurAs, which show nuclease activity only in the presence of HerA (34, 37, 40). *T. thermophilus* HB8 NurA also had nicking activity to circular dsDNA in an HerA-independent manner (Figs. 29E and G), and this characteristic is in agreement with that of *D. radiodurans* and *S. solfataricus* NurA (32, 40). Similarly, *T. thermophilus* HB8 HerA retained ATPase activity. These nuclease and ATPase activities were required for restoring UV sensitivity of *nurA* and *herA* disruptants, respectively, to WT level. These suggest that the activities of NurA and HerA are essential for their cellular functions, which are likely to be different from those of their orthologues of other species.

Even though *T. thermophilus* HB8 NurA alone did not form a dimer, *T. thermophilus* HB8 NurA and HerA were likely to form a complex mediated by the HAS domain of HerA with a stoichiometry of 2:6 (Figs. 23 and 24). This is essentially similar to archaeal and *Deinococcus* homologs. Furthermore, NurA and HerA were detected as the interactor proteins *in vivo* (Fig. 25). These findings may imply that the coexistence of NurA and HerA is necessary for their cellular functions in *T. thermophilus* HB8.

The most interesting and unexpected findings were that disruption of *nurA* and/or *herA* in *T. thermophilus* HB8 increased resistance to UV irradiation and MMC treatment compared to WT. Moreover, it appears that the enzymatic activities of NurA and HerA in *T. thermophilus* HB8 cells are involved in impairment of or competition with the repair of UV- and MMC-induced damages to DNA. By contrast, in *D. radiodurans*, Δ*nurA*, Δ*herA*, and Δ*nurA*Δ*herA* show no difference in the resistance to UV and γ-ray irradiation compared to WT (40), although Δ*nurA* shows higher resistance to MMC treatment than WT (48). These differences suggest that NurA and HerA have different functions in the response to UV- and MMC-induced DNA damages between *T. thermophilus* HB8 and *D. radiodurans*.

UV irradiation and MMC treatment can cause similar but different types of lesions. UV irradiation induces cyclobutane pyrimidine dimers and 6-4 photoproducts, whereas MMC causes monoadducts and intra- and inter-strand crosslinks in DNA (80). This difference might be reflected in the difference in the observed resistance: the resistance to UV irradiation was significantly higher than resistance to MMC treatment under the condition that WT showed 0.1% survival (Figs. 12A and 13). This may indicate that NurA and HerA impair the repair system for UV-induced damages more strongly than that for MMC-induced damages.

In contrast to the sensitivity to UV irradiation and MMC treatment, WT and disruptant mutants of *nurA* and/or *herA* had no differences in sensitivity to H_2O_2 or NA treatment (Fig. 20). Oxidative lesions induced by H_2O_2 and lesions induced via inhibition of replication by NA are repaired mainly by base excision repair and HR repair, respectively (88, 89). These suggest that NurA and HerA have a specific influence on the repair system for photoproducts and DNA-crosslink lesions. In addition, it seems likely that there was no significant difference in the relative efficiency of HR (F_H/F_D) between WT and disruptants (Fig. 11C). This may also support no association of NurA and HerA with HR, although complementary experiments are required.

It should be mentioned here that F_H was higher than F_D (Figs. 11A and B). One possible explanation might be the different events necessary for acquisition of antibiotics resistance between the two plasmids, pMK18HK (for F_D) and pGEM-T Easy/Δ*csp2*::*Hyg*^{R} (for F_H). The process of transformation comprises three main stages: DNA uptake, reconstitution of plasmid DNA or recombination of homologous DNA into the chromosome, and phenotypic expression of acquired genetic element (90). The DNA uptake system of *T. thermophilus* displays no sequence specificity

(91). The incorporated DNAs originated from the respective plasmids would be cut at a similar number of sites by restriction enzymes inherent to *T. thermophilus*. *Hyg*^{R} should be expressed under the control of the same promoter in both cases. However, ssDNAs originated from the uptaken plasmids are processed differently. In the case of pMK18HK (4.2 kbp), the plasmid dsDNA is degraded into ssDNA, and then the replicable plasmid must be reconstituted from the ssDNA to contain at least 2.8 kbp including *Hyg*^{R} gene and *ori* region to acquire resistance to hygromycin B. In contrast, in the case of pGEM-T Easy/ Δ*csp2*::*Hyg*^{R} (5.1 kbp), at least 2 kbp including *Hyg*^{R} gene and the flanking regions must be incorporated into the chromosome via HR to acquire resistance to hygromycin B. The difference in efficiency between reconstitution and recombination may account for why F_H was greater than F_D.

UV-induced photoproducts or MMC-induced DNA-crosslink lesions are repaired via several repair pathways. In bacteria, UV-induced photoproducts are repaired via NER, direct repair, and/or HR repair (1). In this study, cells were cultured in a dark condition after UV irradiation. Therefore, the cyclobutane pyrimidine dimers and 6-4 photoproducts would be repaired via NER or HR repair. On the other hand, MMC-induced lesions are repaired as follows: the monoadducts and intrastrand crosslinks are repaired via NER, and the interstrand crosslinks are repaired via double-step NER mediated by HR repair (92). Further, UV-induced photoproducts, chemical adducts, and DNA crosslinks can be bypassed by TLS polymerases (93, 94). *T. thermophilus* HB8 has no gene for Y-family DNA polymerases for TLS (1). However, it is possible to suppose that DNA polymerase I (PolI) and DNA polymerase III (PolIII) holoenzyme function as TLS polymerases like in *E. coli* (95, 96). It was also reported that PolI from *Thermus aquaticus* performs TLS (97). Taken together, it can be considered that NurA and HerA impair or compete with NER, HR and/or TLS repair processes. It should be mentioned here that Δ*nurA* showed lower resistance to UV irradiation than Δ*herA* and Δ*nurA*Δ*herA*, but not to MMC treatment (Figs. 12A and 13). This may suggest that HerA and NurA do not equally contribute to the apparent suppression of DNA repair systems and that HerA apparently impairs the repair pathway for UV-induced DNA lesions more significantly than NurA.

The accumulation of DNA damage can lead to an increase in the mutation frequency. In fact, in *E. coli*, the mutation frequency increases in response to UV irradiation (98). The frequency of UV-induced mutations was about 300 times higher than that of spontaneous mutations at the UV

dose at which 45% of cells can survive (99). However, in this study, no increase in the mutation frequency by UV irradiation was detected in both WT and the disruptant mutants of *nurA* and/or *herA* at least in the analysis using streptomycin (Fig. 16B). In *T. thermophilus*, the resistance and pseudo-dependence to streptomycin is conferred by mutations of ribosomal protein S12 due to C→T and A→G base substitutions (77), and these substitutions were common to most of those in *E. coli* (77, 99). Furthermore, *T. thermophilus* ribosomal protein S12 contains the 5′-CCCCA-3′ (the underline indicates a triplet coding for Pro41), which potentially mutable sequence necessary for UV mutagenesis through cytosine–cytosine photoproducts leading to 5′-CCTCA-3′ (Leu) and 5′-CTCCA-3′ (Ser). In addition, there were no differences in UV mutagenesis among all of the strains, even when the disruptants of *nurA* and/or *herA* were subjected to a higher dose of UV than WT (Fig. 16B; also see Fig. 12A). Ohta *et al.* also previously reported that no obvious UV-induced mutations were observed in *T. thermophilus* when it was assayed by reversion at 5′-CTC-3′ in *hisD* mutant (100). These suggest that UV damage in the *nurA* and/or *herA* disruptants is correctly repaired or overcome, as well as the damage in WT is, at least at 5′-TC-3′ and 5′-CC-3′.

The additive gene disruption in Δ*nurA*Δ*herA* cells provided insight into the cellular function of NurA and HerA. The results shown in Fig. 18A suggest that NurA and HerA positively contributes to other DNA repair processes than NER pathway. This suggestion was supported by the growth defect of *nurA*-*herA* disruptant after UV irradiation (Fig. 19). These seem to be in contrast to that NurA and HerA seem to impair the repair of UV-induced lesions at high doses of UV irradiation (Fig. 12) However, at low doses of UV irradiation (43.2 Jm^{-2} or less), *T. thermophilus* HB8 cells showed the similar resistance to UV-induced lesions regardless of the presence or absence of NurA and HerA. (Fig. 12A). This apparent discrepancy may be associated with different density of UV-induced lesions on DNA. There is the possibility that action of NurA and HerA on non-NER pathway generates some DNA structures which induce toxicity at high doses of UV irradiation. This hypothesis may be consistent with the results that NurA and HerA seem to impair other repair processes than RecJ-dependent steps and that they do not impair other repair pathways than RecR-dependent repair process (Fig. 18B). A candidate for a non-NER and RecR-dependent pathway is an NER-bypass pathway in which DNA repair can be achieved through HR via replication. Furthermore, considering the similar NA sensitivities between WT and disruptants of *nurA* and/or *herA* (Fig. 20B), NurA and HerA would be involved in a prior step to recombination

process. In addition, there was no interdependency between HR and NER pathways (Fig. 18C).

Possible toxic action of NurA and HerA on UV-irradiated DNA may be through the nuclease activity of NurA. I only detected weak nuclease activity of NurA on undamaged DNA (Fig. 29). Lesion-specific differences in the DNA damage response of *nurA* and *herA* disruptants might also provide some insights into molecular mechanism of action of NurA and HerA. As discussed above, NurA and HerA are thought to have a specific influence on the repair for photoproducts and DNA-crosslink lesions. This may suggest that NurA (and HerA) has a preference for these lesions. In NER, UvrAB complex recognizes the bending of DNA caused by photoproducts and DNA cross-links (2). Although NurA and HerA are unlikely to be not involved in repair of DNA damages, this complex may directly recognize bulky photoproducts and DNA-crosslinks or the bending of DNA induced by these lesions.

Taken together, we propose a model for the cellular functions of NurA and HerA in *T. thermophilus* HB8 as follows (Fig. 31). UV-induced lesions are mainly repaired via NER and HR pathways, and HR pathway would progress through replication processes. NurA and HerA direct the repair pathway to RecR-dependent HR at the step where RecJ is not involved. Depending on the density of UV-induced lesions on DNA, NurA and HerA induce a nick near the site of a DNA lesion (Fig. 32A, step I), such as a photoproduct and a bulky adduct (red ovals). Progression of the replication fork leads to DSB on a nicked strand. RecJ generates 3′ overhang at the DSB end, and concomitantly removes the DNA lesion by its exonuclease activity (step II-a). Then replication fork can be restarted through strand exchange between sister chromatids (step III), and resolution of Holliday junction (open triangles) (step IV-a). In the absence of RecJ, the DSB end is unwound by some helicase (step II-b), and the replication fork is reformed via HR (step IV-b). In this pathway, the remaining DNA lesion is repaired in NER (step V). In the absence of NurA and HerA (Fig. 31B), the replication fork is arrested at the site of a DNA lesion (step i). The arrested folk is overcome via extension of the leading strand after template switch between sister chromatids (step ii). Using the rewound template, the lesion can be repaired in NER (step iii-a). After the replication fork is reformed (step iii-b), the remaining lesion is repaired in NER (step iv).

In this process, NurA and HerA generate some DNA structures, including nicks leading to DSB, depending on the density of UV-induced lesions on DNA. Such a structure would be properly processed in RecR-dependent pathway under low dose of UV irradiation. However, under high dose

of UV irradiation, such structures would be generated too much to handle and thus become toxic. Different levels of toxicity depending on the density of UV-induced lesions might function as a sensor to detect the capacity of UV-induced stress. When multiple UV-induced lesions are clustered in close proximity to one another, toxic structures may be generated by enzymatic activities of NurA and HerA. It should be noted that in nature, bacterial cells are unlikely to be subjected to such high doses of UV irradiation.

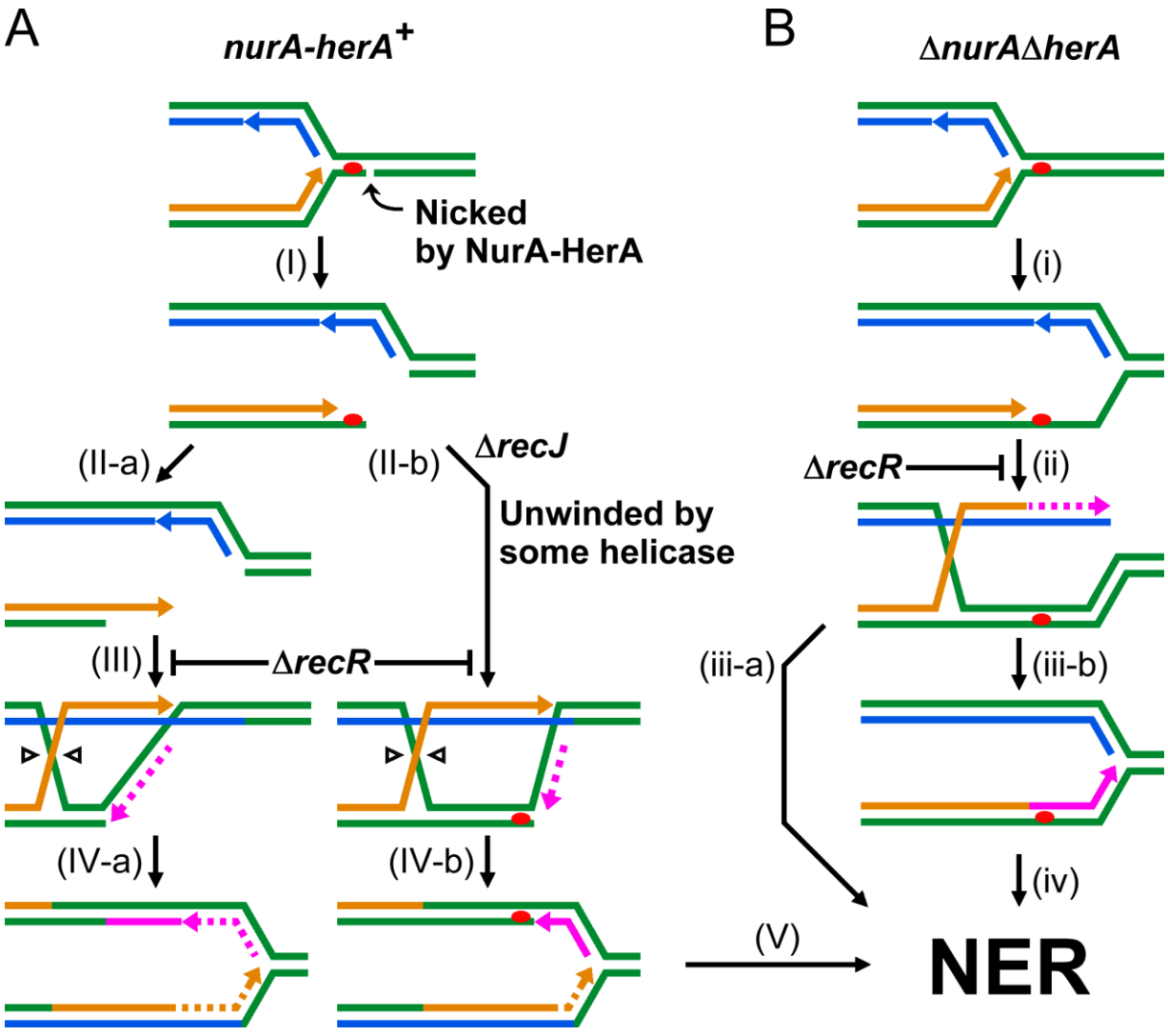

Fig. 31 A model for the function of NurA and HerA in *T. thermophilus* HB8. A photoproduct and a bulky adduct (red ovals) are repaired via HR and NER in the presence (A) or absence (B) of NurA-HerA. The details are described in the text.

I explore other possibilities for the function of NurA and HerA in *T. thermophilus* HB8 from different viewpoints. HerA protein belongs to the same protein superfamily as FtsK (FtsK-HerA superfamily) (101). This has raised the possibility that aside from its role in DNA repair HerA functions in chromosome segregation in archaea, in which *nurA* and *herA* are essential (101, 102). FtsK is a multifunctional protein that coordinates chromosome segregation and cell division in bacteria. No true structural homolog of FtsK has been reported in archaea. On the other hand, *T. thermophilus* has an FtsK protein. One of *Thermus* species, *T. thermophilus* HB27, has three FtsK-HerA family protein other than FtsK (TT_C0474) (described later), however, the gene coding for FtsK cannot be disrupted, indicating that others cannot substitute for FtsK (103). Therefore, it is unlikely that *T. thermophilus* HB8 HerA contributes to the cell division as a functional homolog of FtsK.

The relationship of NurA and HerA to CRISPR-Cas system has been proposed. In many *Pyrobaculum* species, *nurA*- and *herA*-like genes are clustered the CRISPR-associated gene *csm6*, and they are co-transcribed (46). In addition, the expression levels of *Sulfolobus islandicus nurA*-like (*sire_0014*), *herA* (*sire_0064*) and *herA*-like genes (*sire_0095* and *sire_1857*) are up-regulated by CRISPR activator Csa3a (47). In contrast, the transcription level of *nurA* and *herA* in *T. thermophilus* HB8 does not clearly respond to growth phase and or phage infection (Figs. 6 and 7). Nevertheless, the increase in the DNA uptake frequency by disruption of *nurA* and *herA* (Fig. 11A) may suggest the possible involvement of *T. thermophilus* HB8 NurA and HerA in CRISPR systems. In addition, the expression response may be merely unnecessary due to higher cellular concentration of HerA (and maybe NurA) than general DNA repair proteins.

The *nurA* and *herA* genes were constitutively transcribed (Fig. 6). Based on the volume of a *T. thermophilus* HB8 cell estimated by Kondo *et al.* (~ 2×10^{-15} L/cell) (104), the intracellular concentration of hexameric HerA was calculated to be 2–3 μM from the Western blots (Figs. 8C, 14B, and 15B). The intracellular concentration of NurA could not be calculated quantitatively because NurA proteins were collected from *T. thermophilus* HB8 cells by enrichment via affinity purification. However, cotranscription of *nurA* and *herA* from the operon-like gene cluster implies that NurA is also present at the micromolar level. These concentrations are quite higher than those of general DNA repair proteins in bacteria (10–500 nM) (105–108). Such relatively high concentration of *T. thermophilus* HB8 HerA (and NurA) may be required for continuous monitoring

of intracellular environment in all growth phases. It should be noted that such high concentrations appear to be similar to or higher than those in archaea. The amounts of HerA and NurA are estimated to be about 960 and 850 molecules in *Sulfolobus islandicus* cells (41), and the cell size of *Sulfolobus* sp. is about 1 μm (109). Assuming spherical cell shape, the intracellular concentrations of *S. islandicus* HerA (as the hexamer) and NurA (as the dimer) can be calculated to be about 500 nM and 1.4 μM, respectively.

The apparent difference in NurA-HerA functions between *T. thermophilus* and other species may be partly ascribed to differences in their quaternary structures. Recombinant *T. thermophilus* HB8 HerA showed a hexameric state (Fig. 23) such as archaeal and *Deinococcus* HerAs (34, 35, 40). On the other hand, *T. thermophilus* HB8 NurA showed only a monomeric state. This is in contrast to the known archaeal NurAs, which form homodimers (33, 34, 86), and *Deinococcus* NurA, which shows monomer-dimer equilibration (40). In addition, the crystal structure of *Thermotoga maritima* NurA shows dimeric form, although it remains unclear whether or not *Thermotoga* NurA forms a dimer in solution. Therefore, *T. thermophilus* HB8 NurA may exist in solution in monomer-dimer equilibrium or mainly in a monomeric state.

The difference of the putative cellular function of HerA and NurA between *T. thermophilus* and other species may be related to those in the molecular structures and functions. The nuclease activity of *T. thermophilus* HB8 NurA was not influenced by interaction with HerA (Fig. 29F), whereas the nuclease activities of *D. radiodurans* and archaeal NurAs are enhanced by HerAs (34, 37, 40). This may imply the possibility that the HerA binding to NurA have a certain effect on other function of NurA, which was not found in this work, or that some kind of protein is required for affecting the nuclease activity of NurA. The ATPase activity of *T. thermophilus* HB8 HerA decreased by interaction with NurA (Fig. 30C), but was not affected by DNA (Fig. 30B). These are in contrast to the activity of *D. radiodurans* and archaeal HerAs, which are enhanced by DNA and by interaction with NurA (28, 29, 34, 38, 40). These differences might be related to the difference of the function of HerA (and NurA) between *T. thermophilus* and other species.

During my study, Blesa *et al.* reported that HerA (TT_C0147; designated as HepA) of *Thermus thermophilus* HB27 is involved in gene exchange between *T. thermophilus* HB27 cells called “transjugation” (transformation-dependent conjugation) in donor cells and has the possibility of association with some DNA repair (110). This was unexpected because *T. thermophilus* HB27 is a

very closely related species of *T. thermophilus* HB8. Phylogenetic trees of bacterial NurA and HerA (Figs. 4A and B) suggest that *Thermus* species were speciated after acquisition of *nurA* and *herA* genes. Gene arrangements around *nurA* and *herA* are quite similar in the genomes of *Thermus* species (110). HepA has the same amino acid sequence as *T. thermophilus* HB8 HerA except for Trp126. Disruption of *hepA* led to the decrease in the transformation frequency (equivalent to DNA uptake frequency in this study) and the increase in the UV sensitivity (110). These phenotypes are opposite to those of Δ*herA* in *T. thermophilus* HB8. This discrepancy might possibly result from the differences in genetic background between these two strains. *Thermus thermophilus* HB27 has two types of NurA- and HerA-like proteins besides NurA (TT_C0145) and HepA, and has UV-dependent endonuclease (UvdE; TT_P0052), whereas *T. thermophilus* HB8 does not have paralogs of NurA and HerA and UvdE ortholog. One of the HerA-like proteins (TT_C1430) is thought to be involved in DNA repair because the disruption of this gene led to an increase in the UV sensitivity (103). The other HerA-like protein (TT_C1879) is involved in transjugation in the different manner from HepA (103, 110). In addition, UvdE functions in the repair of UV-induced lesions in an alternative pathway for NER (111). These imply that *T. thermophilus* HB27 has diverse pathways for repairing UV-induced lesions compared to *T. thermophilus* HB8. Furthermore, *T. thermophilus* HB27 NurA lacks about 40 C-terminal residues compared to *T. thermophilus* HB8 NurA. This C-terminal region of *T. thermophilus* HB8 NurA contains the metal-binding residue Glu268 for nuclease activity and the hydrophobic residue Val252 for interaction with HerA (Fig. 32). This strongly suggests that *T. thermophilus* HB27 NurA has no or different nuclease activity and inability to interact with HerA, although NurA and one of NurA-like proteins (TT_C1429) in *T. thermophilus* HB27 have not been studied at all. Another NurA-like protein (TT_C1878) is thought to be involved in transjugation with TT_C1879 (103). These might lead to the difference of cellular functions between HepA (HB27) and HerA (HB8).

Comparing the NurA-HerA proteins among *T. thermophilus*, *D. radiodurans*, and archaea, their cellular functions seem to be different. As previously reported by Nelson-Sathi *et al.* (112), *nurA* (and maybe also *herA*) is thought to be exported from archaea and to be acquired by bacteria via horizontal gene transfer between species or domains. In addition, *nurA* and *herA* genes may have been diversified via gene duplication. For example, *Sulfolobus islandicus* REY15A has five *nurA*-like genes and seven *herA*-like genes in addition to *sire_0061* and *sire_0064* (*nurA* and *herA*

orthologs, respectively). The molecular phylogenetic trees of NurA- and HerA-like proteins suggest that these genes would have been duplicated in the ancestral strain of *Sulfolobus* species before speciation (Fig. 33A and B). There are also bacteria harboring several kinds of *nurA* and *herA*(-like) genes, such as *T. thermophilus* HB27 (Fig. 4A and B): *tt_c0145* (*nurA*), *tt_c1429*, and *tt_c1878* for *nurA*(-like) genes; and *tt_c0147* (*hepA*), *tt_c1430*, and *tt_c1879* for *herA*(-like) genes. However, *tt_c1878* and *tt_c1879* are placed in different clades from *nurA* and *hepA*, respectively, implying that they seem not to be the paralogous genes of *nurA* and *hepA* (Figs. 4A and B). The same seems to be applied to *tt_c1429* and *tt_c1430* genes, although they are not included in Fig. 4. These may suggest that *T. thermophilus* HB27 has acquired *nurA*(-like) and *herA*(-like) genes more than once via horizontal gene transfer. It should be noted here that *T. thermophilus* HB8, used in this study, has no other *nurA*- and *herA*-like genes. Through the combination of gene transfer and gene duplication, NurA and HerA may have gained novel cellular functions.

In conclusion, I have presented interesting phenotypes of the *nurA* and *herA* disruptants in *T. thermophilus* HB8 and proposed a novel role of these gene products in the repair of photoproducts and DNA crosslinks. It is still difficult to explain how activities of *T. thermophilus* HB8 NurA and HerA contribute to their cellular functions. To clarify this point, it is necessary for the molecular functions of NurA and HerA to be analyzed in more details.

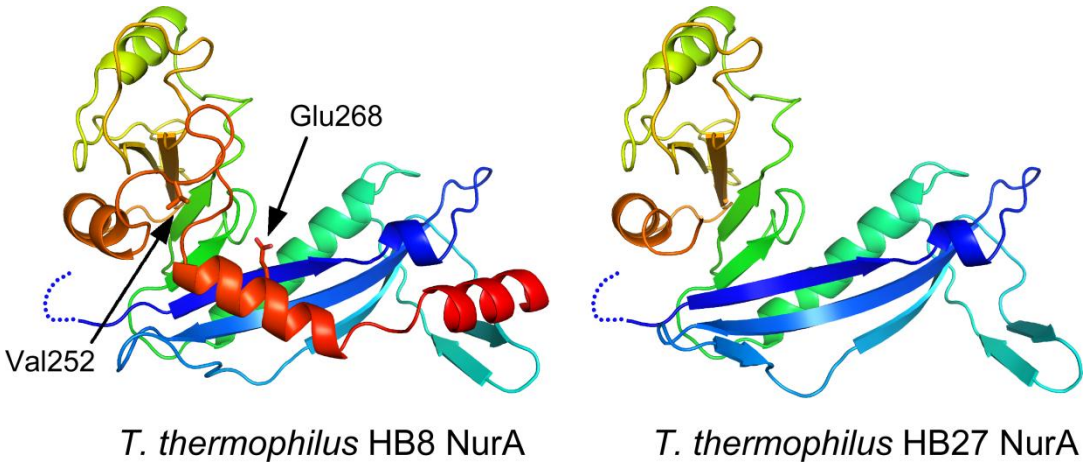

Fig. 32 Comparison of structures of NurA between *T. thermophilus* HB8 (left) and *T. thermophilus* HB27 (right). Each protein is rainbow-colored from N- (blue) to C-termini (red). These structures were predicted by the SWISS-MODEL (https://swissmodel.expasy.org/) based on the Thermotoga maritima NurA (PDB ID, 1ZUP). The figures were generated using PyMOL (The PyMOL Molecular Graphics System, Version 1.5 Schrödinger, LLC; (https://www.pymol.org/))

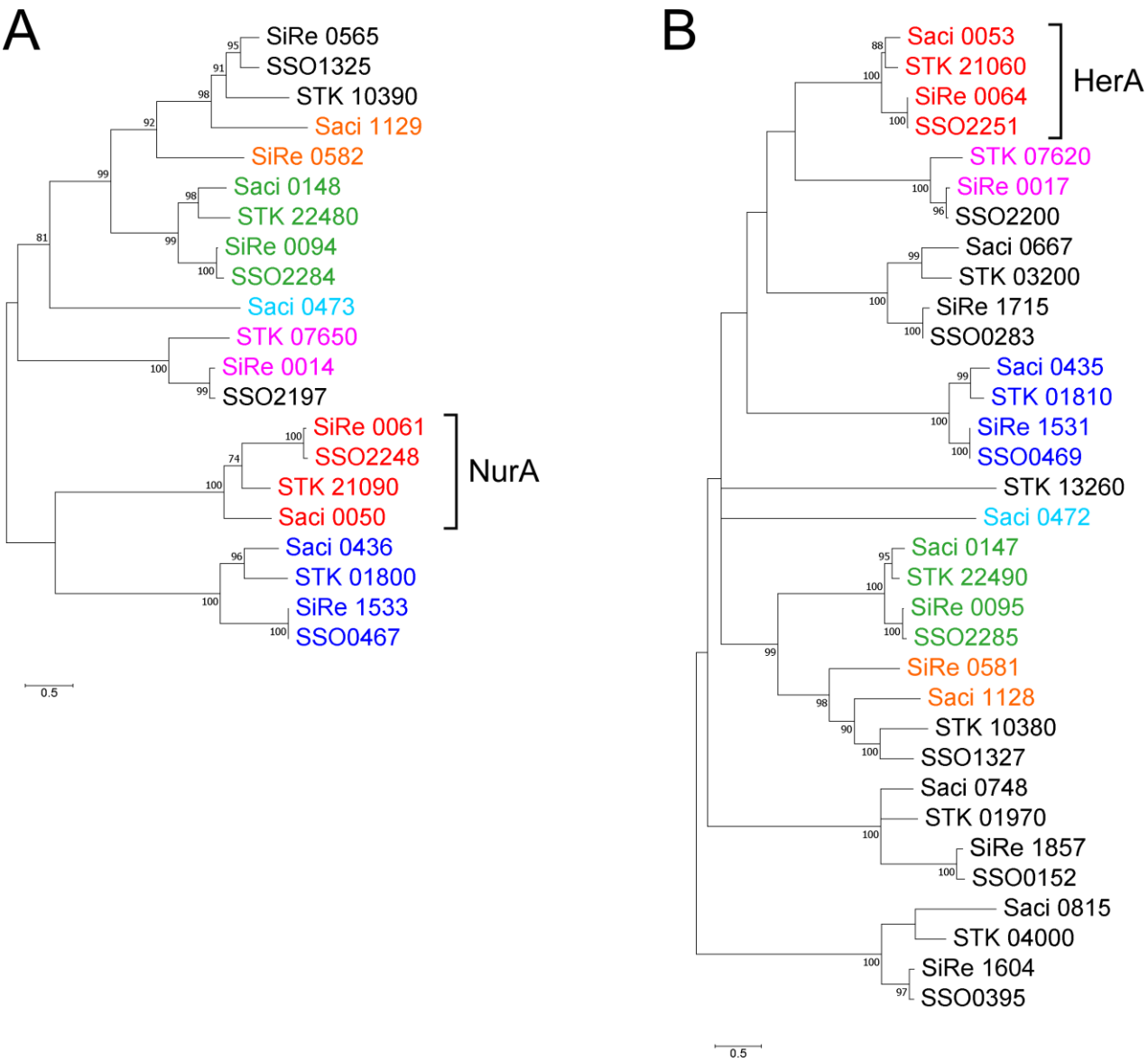

Fig. 33 Diversification of NurA and HerA. Phylogenetic trees of (A) NurA- and (B) HerA-like proteins in *Sulfolobus* species. All gene IDs and amino acid sequences were obtained from KEGG (https://www.genome.jp/kegg/) via motif search. These sequences were aligned by multiple-alignment tool MUSCLE, and molecular phylogenetic trees were generated by maximum likelihood method with a phylogenetic analysis software MEGA7 (https://www.megasoftware.net/). Trees were drawn to scale with branch lengths measured in the number of substitutions per site. Boot strap values more than 70 are shown on the branches and expressed in percentages. The orthologous genes are coded by the same color in each tree, and the same color-coded genes between (A) and (B) indicate the *nurA*- and *herA*-like genes in the same operon-like gene cluster in each organism. Species corresponding to gene IDs are the following: Saci_(number), *Sulfolobus acidocaldarius* DSM 639; SiRe_(number), *S. islandicus* REY15A; STK_(number), *S. tokodaii*; and SSO(number), *S. solfataricus* P2.

References

1. **Morita R**, **Nakane S**, **Shimada A**, **Inoue M**, **Iino H**, **Wakamatsu T**, **Fukui K**, **Nakagawa N**, **Masui R**, **Kuramitsu S**. 2010. Molecular mechanisms of the whole DNA repair system: a comparison of bacterial and eukaryotic systems. J Nucleic Acids **2010**:179594.
2. **Kisker C**, **Kuper J**, **Van Houten B**. 2013. Prokaryotic nucleotide excision repair. Cold Spring Harb Perspect Biol **5**:a012591–a012591.
3. **Deaconescu AM**, **Sevostyanova A**, **Artsimovitch I**, **Grigorieff N**. 2012. Nucleotide excision repair (NER) machinery recruitment by the transcription-repair coupling factor involves unmasking of a conserved intramolecular interface. Proc Natl Acad Sci U S A **109**:3353–3358.
4. **Blackwood JK**, **Rzechorzek NJ**, **Bray SM**, **Maman JD**, **Pellegrini L**, **Robinson NP**. 2013. End-resection at DNA double-strand breaks in the three domains of life. Biochem Soc Trans **41**:314–320.
5. **Seitz EM**, **Brockman JP**, **Sandler SJ**, **Clark AJ**, **Kowalczykowski SC**. 1998. RadA protein is an archaeal RecA protein homolog that catalyzes DNA strand exchange. Genes Dev **12**:1248–1253.
6. **Bell JC**, **Kowalczykowski SC**. 2016. RecA: regulation and mechanism of a molecular search engine. Trends Biochem Sci **41**:491–507.
7. **Daley JM**, **Kwon YH**, **Niu H**, **Sung P**. 2013. Investigations of homologous recombination pathways and their regulation. Yale J Biol Med **86**:453–461.
8. **Sung S**, **Li F**, **Park YB**, **Kim JS**, **Kim A-K**, **Song O-K**, **Kim J**, **Che J**, **Lee SE**, **Cho Y**. 2014. DNA end recognition by the Mre11 nuclease dimer: insights into resection and repair of damaged DNA. EMBO J **33**:2422–2435.
9. **Mimitou EP**, **Symington LS**. 2011. DNA end resection-unraveling the tail. DNA Repair (Amst) **10**:344–348.
10. **Cejka P**, **Cannavo E**, **Polaczek P**, **Masuda-Sasa T**, **Pokharel S**, **Campbell JL**, **Kowalczykowski SC**. 2010. DNA end resection by Dna2–Sgs1–RPA and its stimulation by Top3–Rmi1 and Mre11–Rad50–Xrs2. Nature **467**:112–116.
11. **Nicolette ML**, **Lee K**, **Guo Z**, **Rani M**, **Chow JM**, **Lee SE**, **Paull TT**. 2010. Mre11–Rad50–Xrs2 and Sae2 promote 5′ strand resection of DNA double-strand breaks. Nat

Struct Mol Biol **17**:1478–1485.

12. **Mimitou EP**, **Symington LS**. 2008. Sae2, Exo1 and Sgs1 collaborate in DNA double-strand break processing. Nature **455**:770–774.
13. **Lengsfeld BM**, **Rattray AJ**, **Bhaskara V**, **Ghirlando R**, **Paull TT**. 2007. Sae2 is an endonuclease that processes hairpin DNA cooperatively with the Mre11/Rad50/Xrs2 complex. Mol Cell **28**:638–651.
14. **Mimitou EP**, **Symington LS**. 2009. DNA end resection: many nucleases make light work. DNA Repair (Amst) **8**:983–995.
15. **Zhu Z**, **Chung W-H**, **Shim EY**, **Lee SE**, **Ira G**. 2008. Sgs1 helicase and two nucleases Dna2 and Exo1 resect DNA double-strand break ends. Cell **134**:981–994.
16. **Krajewski WW**, **Fu X**, **Wilkinson M**, **Cronin NB**, **Dillingham MS**, **Wigley DB**. 2014. Structural basis for translocation by AddAB helicase–nuclease and its arrest at χ sites. Nature **508**:416–419.
17. **Wigley DB**. 2013. Bacterial DNA repair: recent insights into the mechanism of RecBCD, AddAB and AdnAB. Nat Rev Microbiol **11**:9–13.
18. **Singleton MR**, **Dillingham MS**, **Gaudier M**, **Kowalczykowski SC**, **Wigley DB**. 2004. Crystal structure of RecBCD enzyme reveals a machine for processing DNA breaks. Nature **432**:187–193.
19. **Amundsen SK**, **Fero J**, **Salama NR**, **Smith GR**. 2009. Dual nuclease and helicase activities of *Helicobacter pylori* AddAB are required for DNA repair, recombination, and mouse infectivity. J Biol Chem **284**:16759–16766.
20. **Kuzminov A**. 1999. Recombinational repair of DNA damage in *Escherichia coli* and bacteriophage λ. Microbiol Mol Biol Rev **63**:751–813.
21. **Morimatsu K**, **Kowalczykowski SC**. 2014. RecQ helicase and RecJ nuclease provide complementary functions to resect DNA for homologous recombination. Proc Natl Acad Sci U S A **111**:E5133–E5142.
22. **Rocha EPC**, **Cornet E**, **Michel B**. 2005. Comparative and evolutionary analysis of the bacterial homologous recombination systems. PLoS Genet **1**:e15.
23. **Buljubašić M**, **Repar J**, **Zahradka K**, **Đermić D**, **Zahradka D**. 2012. RecF recombination pathway in *Escherichia coli* cells lacking RecQ, UvrD and HelD helicases. DNA Repair

(Amst) **11**:419–430.

24. **Aravind L**, **Walker DR**, **Koonin E V.** 1999. Conserved domains in DNA repair proteins and evolution of repair systems. Nucleic Acids Res **27**:1223–1242.
25. **Seitz EM**, **Haseltine CA**, **Kowalczykowski SC**. 2001. DNA recombination and repair in the Archaea, p. 101–169. *In* Blum, P (ed.), Advances in applied Microbiology. Elsevier Inc.
26. **Hopfner K-P**, **Karcher A**, **Shin D**, **Fairley C**, **Tainer JA**, **Carney JP**. 2000. Mre11 and Rad50 from *Pyrococcus furiosus*: cloning and biochemical characterization reveal an evolutionarily conserved multiprotein machine. J Bacteriol **182**:6036–6041.
27. **Constantinesco F**, **Forterre P**, **Elie C**. 2002. *NurA*, a novel 5′-3′ nuclease gene linked to *rad50* and *mre11* homologs of thermophilic *Archaea*. EMBO Rep **3**:537–542.
28. **Constantinesco F**, **Forterre P**, **Koonin E V**, **Aravind L**, **Elie C**. 2004. A bipolar DNA helicase gene, *herA*, clusters with *rad50*, *mre11* and *nurA* genes in thermophilic archaea. Nucleic Acids Res **32**:1439–1447.
29. **Manzan A**, **Pfeiffer G**, **Hefferin ML**, **Lang CE**, **Carney JP**, **Hopfner K-P**. 2004. MlaA, a hexameric ATPase linked to the Mre11 complex in archaeal genomes. EMBO Rep **5**:54–59.
30. **Forterre P**. 2013. The common ancestor of archaea and eukarya was not an archaeon. Archaea **2013**:372396.
31. **Wei T**, **Zhang S**, **Zhu S**, **Sheng D**, **Ni J**, **Shen Y**. 2008. Physical and functional interaction between archaeal single-stranded DNA-binding protein and the 5′-3′ nuclease NurA. Biochem Biophys Res Commun **367**:523–529.
32. **De Falco M**, **Catalano F**, **Rossi M**, **Ciaramella M**, **De Felice M**. 2015. NurA is endowed with endo- and exonuclease activities that are modulated by HerA: new insight into their role in DNA-end processing. PLoS One **10**:e0142345.
33. **Chae J**, **Kim Y**, **Cho Y**. 2012. Crystal structure of the NurA–dAMP–Mn^{2+} complex. Nucleic Acids Res **40**:2258–2270.
34. **Blackwood JK**, **Rzechorzek NJ**, **Abrams AS**, **Maman JD**, **Pellegrini L**, **Robinson NP**. 2012. Structural and functional insights into DNA-end processing by the archaeal HerA helicase-NurA nuclease complex. Nucleic Acids Res **40**:3183–3196.
35. **Rzechorzek NJ**, **Blackwood JK**, **Bray SM**, **Maman JD**, **Pellegrini L**, **Robinson NP**. 2014. Structure of the hexameric HerA ATPase reveals a mechanism of translocation-coupled

DNA-end processing in archaea. Nat Commun **5**:5506.

36. **Byrne RT**, **Schuller JM**, **Unverdorben P**, **Förster F**, **Hopfner K-P**. 2014. Molecular architecture of the HerA-NurA DNA double-strand break resection complex. FEBS Lett **588**:4637–4644.
37. **Hopkins BB**, **Paull TT**. 2008. The *P. furiosus* Mre11/Rad50 complex promotes 5′ strand resection at a DNA double-strand break. Cell **135**:250–260.
38. **Zhang S**, **Wei T**, **Hou G**, **Zhang C**, **Liang P**, **Ni J**, **Sheng D**, **Shen Y**. 2008. Archaeal DNA helicase HerA interacts with Mre11 homologue and unwinds blunt-ended double-stranded DNA and recombination intermediates. DNA Repair (Amst) **7**:380–391.
39. **Quaiser A**, **Constantinesco F**, **White MF**, **Forterre P**, **Elie C**. 2008. The Mre11 protein interacts with both Rad50 and the HerA bipolar helicase and is recruited to DNA following gamma irradiation in the archaeon *Sulfolobus acidocaldarius*. BMC Mol Biol **9**:25.
40. **Cheng K**, **Chen X**, **Xu G**, **Wang L**, **Xu H**, **Yang S**, **Zhao Y**, **Hua Y**. 2015. Biochemical and functional characterization of the NurA-HerA complex from *Deinococcus radiodurans*. J Bacteriol **197**:2048–2061.
41. **Huang Q**, **Liu L**, **Liu J**, **Ni J**, **She Q**, **Shen Y**. 2015. Efficient 5′-3′ DNA end resection by HerA and NurA is essential for cell viability in the crenarchaeon *Sulfolobus islandicus*. BMC Mol Biol **16**:2.
42. **Zhang C**, **Tian B**, **Li S**, **Ao X**, **Dalgaard K**, **Gökce S**, **Liang Y**, **She Q**. 2013. Genetic manipulation in *Sulfolobus islandicus* and functional analysis of DNA repair genes. Biochem Soc Trans **41**:405–410.
43. **Fujikane R**, **Ishino S**, **Ishino Y**, **Forterre P**. 2010. Genetic analysis of DNA repair in the hyperthermophilic archaeon, *Thermococcus kodakaraensis*. Genes Genet Syst **85**:243–257.
44. **Fröls S**, **Gordon PMK**, **Panlilio MA**, **Duggin IG**, **Bell SD**, **Sensen CW**, **Schleper C**. 2007. Response of the hyperthermophilic archaeon *Sulfolobus solfataricus* to UV damage. J Bacteriol **189**:8708–8718.
45. **Lundgren M**, **Bernander R**. 2007. Genome-wide transcription map of an archaeal cell cycle. Proc Natl Acad Sci U S A **104**:2939–2944.
46. **Bernick DL**, **Cox CL**, **Dennis PP**, **Lowe TM**. 2012. Comparative genomic and transcriptional analyses of CRISPR systems across the genus *Pyrobaculum*. Front Microbiol

3:251.

47. **Liu T**, **Liu Z**, **Ye Q**, **Pan S**, **Wang X**, **Li Y**, **Peng W**, **Liang Y**, **She Q**, **Peng N**. 2017. Coupling transcriptional activation of CRISPR-Cas system and DNA repair genes by Csa3a in *Sulfolobus islandicus*. Nucleic Acids Res **45**:8978–8992.
48. **Cheng K**, **Zhao Y**, **Chen X**, **Li T**, **Wang L**, **Xu H**, **Tian B**, **Hua Y**. 2015. A novel C-terminal domain of RecJ is critical for interaction with HerA in *Deinococcus radiodurans*. Front Microbiol **6**:1302.
49. **Inoue M**, **Fukui K**, **Fujii Y**, **Nakagawa N**, **Yano T**, **Kuramitsu S**, **Masui R**. 2017. The Lon protease-like domain in the bacterial RecA paralog RadA is required for DNA binding and repair. J Biol Chem **292**:9801–9814.
50. **Wakamatsu T**, **Kitamura Y**, **Kotera Y**, **Nakagawa N**, **Kuramitsu S**, **Masui R**. 2010. Structure of RecJ exonuclease defines its specificity for single-stranded DNA. J Biol Chem **285**:9762–9769.
51. **Shimada A**, **Masui R**, **Nakagawa N**, **Takahata Y**, **Kim K**, **Kuramitsu S**, **Fukui K**. 2010. A novel single-stranded DNA-specific 3′-5′ exonuclease, *Thermus thermophilus* exonuclease I, is involved in several DNA repair pathways. Nucleic Acids Res **38**:5692–5705.
52. **Yamagata A**, **Kakuta Y**, **Masui R**, **Fukuyama K**. 2002. The crystal structure of exonuclease RecJ bound to Mn^{2+} ion suggests how its characteristic motifs are involved in exonuclease activity. Proc Natl Acad Sci U S A **99**:5908–5912.
53. **Masui R**, **Mikawa T**, **Kato R**, **Kuramitsu S**. 1998. Characterization of the oligomeric states of RecA protein: Monomeric RecA protein can form a nucleoprotein filament. Biochemistry **37**:14788–14797.
54. **Kickstein E**, **Harms K**, **Wackernagel W**. 2007. Deletions of *recBCD* or *recD* influence genetic transformation differently and are lethal together with a *recJ* deletion in *Acinetobacter baylyi*. Microbiology **153**:2259–2270.
55. **Jiao J**, **Wang L**, **Xia W**, **Li M**, **Sun H**, **Xu G**, **Tian B**, **Hua Y**. 2012. Function and biochemical characterization of RecJ in *Deinococcus radiodurans*. DNA Repair (Amst) **11**:349–356.
56. **Cao Z**, **Julin DA**. 2009. Characterization *in vitro* and *in vivo* of the DNA helicase encoded by *Deinococcus radiodurans* locus DR1572. DNA Repair (Amst) **8**:612–619.

57. **Bentchikou E**, **Servant P**, **Coste G**, **Sommer S**. 2010. A major role of the RecFOR pathway in DNA double-strand-break repair through ESDSA in *Deinococcus radiodurans*. PLoS Genet **6**:e1000774.

58. **Zhou Q**, **Zhang X**, **Xu H**, **Xu B**, **Hua Y**. 2007. A new role of *Deinococcus radiodurans* RecD in antioxidant pathway. FEMS Microbiol Lett **271**:118–125.

59. **Hashimoto Y**, **Yano T**, **Kuramitsu S**, **Kagamiyama H**. 2001. Disruption of *Thermus thermophilus* genes by homologous recombination using a thermostable kanamycin-resistant marker. FEBS Lett **506**:231–234.

60. **Agari Y**, **Kuramitsu S**, **Shinkai A**. 2010. Identification of novel genes regulated by the oxidative stress-responsive transcriptional activator SdrP in *Thermus thermophilus* HB8. FEMS Microbiol Lett **313**:127–134.

61. **Hoseki J**, **Yano T**, **Koyama Y**, **Kuramitsu S**, **Kagamiyama H**. 1999. Directed evolution of thermostable kanamycin-resistance gene: a convenient selection marker for *Thermus thermophilus*. J Biochem **126**:951–956.

62. **Ohtani N**, **Tomita M**, **Itaya M**. 2010. An extreme thermophile, *Thermus thermophilus*, is a polyploid bacterium. J Bacteriol **192**:5499–5505.

63. **Fukui K**, **Nishida M**, **Nakagawa N**, **Masui R**, **Kuramitsu S**. 2008. Bound nucleotide controls the endonuclease activity of mismatch repair enzyme MutL. J Biol Chem **283**:12136–12145.

64. **Luria S**, **Delbrück M**. 1943. Mutations of bacteria from virus sensitivity to virus resistance. Genetics **28**:491–511.

65. **Tanaka T**, **Mega R**, **Kim K**, **Shinkai A**, **Masui R**, **Kuramitsu S**, **Nakagawa N**. 2012. A non-cold-inducible cold shock protein homolog mainly contributes to translational control under optimal growth conditions. FEBS J **279**:1014–1029.

66. **Studier FW**. 2005. Protein production by auto-induction in high-density shaking cultures. Protein Expr Purif **41**:207–234.

67. **Kuramitsu S**, **Hiromi K**, **Hayashi H**, **Morino Y**, **Kagamiyama H**. 1990. Pre-steady-state kinetics of *Escherichia coli* aspartate aminotransferase catalyzed reactions and thermodynamic aspects of its substrate specificity. Biochemistry **29**:5469–5476.

68. **Kumarathasan P**, **Mohottalage S**, **Goegan P**, **Vincent R**. 2005. An optimized protein

in-gel digest method for reliable proteome characterization by MALDI-TOF-MS analysis. Anal Biochem **346**:85–89.

69. **Tomoike F**, **Tsunetou A**, **Kim K**, **Nakagawa N**, **Kuramitsu S**, **Masui R**. 2016. A putative adenosine kinase family protein possesses adenosine diphosphatase activity. Biosci Biotechnol Biochem **80**:2138–2143.

70. **Vargas-Uribe M**, **Rodnin M V.**, **Öjemalm K**, **Holgado A**, **Kyrychenko A**, **Nilsson I**, **Posokhov YO**, **Makhatadze G**, **von Heijne G**, **Ladokhin AS**. 2015. Thermodynamics of membrane insertion and refolding of the diphtheria toxin T-domain. J Membr Biol **248**:383–394.

71. **Inoue J**, **Shigemori Y**, **Mikawa T**. 2006. Improvements of rolling circle amplification (RCA) efficiency and accuracy using *Thermus thermophilus* SSB mutant protein. Nucleic Acids Res **34**:e69.

72. **Laemmli UK**. 1970. Cleavage of structural proteins during the assembly of the head of bacteriophage T4. Nature **227**:680–685.

73. **Melançon P**, **Lemieux C**, **Brakier-Gingras L**. 1988. A mutation in the 530 loop of *Escherichia coli* 16S ribosomal RNA causes resistance to streptomycin. Nucleic Acids Res **16**:9631–9639.

74. **Springer B**, **Kidan YG**, **Prammananan T**, **Ellrott K**, **Böttger EC**, **Sander P**. 2001. Mechanisms of streptomycin resistance: selection of mutations in the 16S rRNA gene conferring resistance. Antimicrob Agents Chemother **45**:2877–2884.

75. **Demirci H**, **Murphy F V.**, **Murphy EL**, **Connetti JL**, **Dahlberg AE**, **Jogl G**, **Gregory ST**. 2014. Structural analysis of base substitutions in *Thermus thermophilus* 16S rRNA conferring streptomycin resistance. Antimicrob Agents Chemother **58**:4308–4317.

76. **Gregory ST**, **Dahlberg AE**. 2009. Genetic and structural analysis of base substitutions in the central pseudoknot of *Thermus thermophilus* 16S ribosomal RNA. RNA **15**:215–223.

77. **Gregory ST**, **Cate JH.**, **Dahlberg AE**. 2001. Streptomycin-resistant and streptomycin-dependent mutants of the extreme thermophile *Thermus thermophilus*. J Mol Biol **309**:333–338.

78. **Bernardo-Filho M**, **Leitao AC**, **Alcantara-Gomes R**. 1992. Neighbour restoration: a possible explanation for some “broken” survival curves of UV-irradiated *Escherichia coli*

K12 cells. J Basic Microbiol **32**:373–380.

79. **Rastogi RP**, **Richa**, **Kumar A**, **Tyagi MB**, **Sinha RP**. 2010. Molecular mechanisms of ultraviolet radiation-induced DNA damage and repair. J Nucleic Acids **2010**:592980.

80. **Tomasz M**, **Lipman R**, **Chowdary D**, **Pawlak J**, **Verdine G**, **Nakanishi K**. 1987. Isolation and structure of a covalent cross-link adduct between mitomycin C and DNA. Science **235**:1204–1208.

81. **Imlay JA**. 2013. The molecular mechanisms and physiological consequences of oxidative stress: lessons from a model bacterium. Nat Rev Microbiol **11**:443–454.

82. **Sugino A**, **Peebles CL**, **Kreuzer KN**, **Cozzarelli NR**. 1977. Mechanism of action of nalidixic acid: purification of *Escherichia coli nalA* gene product and its relationship to DNA gyrase and a novel nicking-closing enzyme. Proc Natl Acad Sci U S A **74**:4767–4771.

83. **Gellert M**, **Mizuuchi K**, **O'Dea MH**, **Itoh T**, **Tomizawa J-I**. 1977. Nalidixic acid resistance: a second genetic character involved in DNA gyrase activity. Proc Natl Acad Sci U S A **74**:4772–4776.

84. **Wolfson JS**, **Hooper DC**. 1985. The fluoroquinolones: structures, mechanisms of action and resistance, and spectra of activity *in vitro*. Antimicrob Agents Chemother **28**:581–586.

85. **Aung HL**, **Samaranayaka CUK**, **Enright R**, **Beggs KT**, **Monk BC**. 2015. Characterisation of the DNA gyrase from the thermophilic eubacterium *Thermus thermophilus*. Protein Expr Purif **107**:62–67.

86. **Wei T**, **Zhang S**, **Hou L**, **Ni J**, **Sheng D**, **Shen Y**. 2011. The carboxyl terminal of the archaeal nuclease NurA is involved in the interaction with single-stranded DNA-binding protein and dimer formation. Extremophiles **15**:227–234.

87. **Gupta R**, **Unciuleac MC**, **Shuman S**, **Glickman MS**. 2017. Homologous recombination mediated by the mycobacterial AdnAB helicase without end resection by the AdnAB nucleases. Nucleic Acids Res **45**:762–774.

88. **Krokan HE**, **Bjoras M**. 2013. Base excision repair. Cold Spring Harb Perspect Biol **5**:a012583.

89. **Jasin M**, **Rothstein R**. 2013. Repair of strand breaks by homologous recombination. Cold Spring Harb Perspect Biol **5**:a012740.

90. **Krüger N-J**, **Stingl K**. 2011. Two steps away from novelty - principles of bacterial DNA

uptake. Mol Microbiol **80**:860–867.

91. **Averhoff B**. 2009. Shuffling genes around in hot environments: the unique DNA transporter of *Thermus thermophilus*. FEMS Microbiol Rev **33**:611–626.
92. **Van Houten B**. 1990. Nucleotide excision repair in *Escherichia coli*. Microbiol Rev **54**:18–51.
93. **Fuchs RP**, **Fujii S**. 2013. Translesion DNA synthesis and mutagenesis in prokaryotes. Cold Spring Harb Perspect Biol **5**:a012682.
94. **Ho TV**, **Schärer OD**. 2010. Translesion DNA synthesis polymerases in DNA interstrand crosslink repair. Environ Mol Mutagen **51**:552–566.
95. **Yamanaka K**, **Minko IG**, **Finkel SE**, **Goodman MF**, **Lloyd RS**. 2011. Role of high-fidelity *Escherichia coli* DNA polymerase I in replication bypass of a deoxyadenosine DNA-peptide cross-link. J Bacteriol **193**:3815–3821.
96. **Nevin P**, **Gabbai CC**, **Marians KJ**. 2017. Replisome-mediated translesion synthesis by a cellular replicase. J Biol Chem **292**:13833–13842.
97. **Belousova EA**, **Rechkunova NI**, **Lavrik OI**. 2006. Thermostable DNA polymerases can perform translesion synthesis using 8-oxoguanine and tetrahydrofuran-containing DNA templates. Biochim Biophys Acta **1764**:97–104.
98. **Pham P**, **Rangarajan S**, **Woodgate R**, **Goodman MF**. 2001. Roles of DNA polymerases V and II in SOS-induced error-prone and error-free repair in *Escherichia coli*. Proc Natl Acad Sci U S A **98**:8350–8354.
99. **Timms AR**, **Steingrimsdottir H**, **Lehmann AR**, **Bridges BA**. 1992. Mutant sequences in the *rpsL* gene of *Escherichia coli* B/r: mechanistic implications for spontaneous and ultraviolet light mutagenesis. Mol Gen Genet **232**:89–96.
100. **Ohta T**, **Tokishita S-I**, **Mochizuki K**, **Kawase J**, **Sakahira M**, **Yamagata H**. 2006. UV sensitivity and mutagenesis of the extremely thermophilic eubacterium *Thermus thermophilus* HB27. Genes Environ **28**:56–61.
101. **Iyer LM**, **Makarova KS**, **Koonin E V**, **Aravind L**. 2004. Comparative genomics of the FtsK-HerA superfamily of pumping ATPases: implications for the origins of chromosome segregation, cell division and viral capsid packaging. Nucleic Acids Res **32**:5260–5279.
102. **Han W**, **Shen Y**, **She Q**. 2014. Nanobiomotors of archaeal DNA repair machineries: current

research status and application potential. Cell Biosci **4**:32.

103. **Blesa A**, **Baquedano I**, **Quintáns NG**, **Mata CP**, **Castón JR**, **Berenguer J**. 2017. The transjugation machinery of *Thermus thermophilus*: Identification of TdtA, an ATPase involved in DNA donation. PLoS Genet **13**:e1006669.

104. **Kondo N**, **Nishikubo T**, **Wakamatsu T**, **Ishikawa H**, **Nakagawa N**, **Kuramitsu S**, **Masui R**. 2008. Insights into different dependence of dNTP triphosphohydrolase on metal ion species from intracellular ion concentrations in *Thermus thermophilus*. Extremophiles **12**:217–223.

105. **Shimada A**, **Kawasoe Y**, **Hata Y**, **Takahashi TS**, **Masui R**, **Kuramitsu S**, **Fukui K**. 2013. MutS stimulates the endonuclease activity of MutL in an ATP-hydrolysis-dependent manner. FEBS J **280**:3467–3479.

106. **Kad NM**, **Van Houten B**. 2012. Dynamics of lesion processing by bacterial nucleotide excision repair proteins, p. 1–24. *In* Doetsch, PW (ed.), Progress in Molecular Biology and Translational Science, 1st ed. Elsevier Inc.

107. **Dillingham MS**, **Kowalczykowski SC**. 2008. RecBCD enzyme and the repair of double-stranded DNA breaks. Microbiol Mol Biol Rev **72**:642–671.

108. **Đermić D**, **Halupecki E**, **Zahradka D**, **Petranović M**. 2005. RecBCD enzyme overproduction impairs DNA repair and homologous recombination in *Escherichia coli*. Res Microbiol **156**:304–311.

109. **Brock TD**, **Brock KM**, **Belly RT**, **Weiss RL**. 1972. *Sulfolobus*: a new genus of sulfur-oxidizing bacteria living at low pH and high temperature. Arch Mikrobiol **84**:54–68.

110. **Blesa A**, **Quintans N**, **Baquedano I**, **Mata C**, **Castón J**, **Berenguer J**. 2017. Role of archaeal HerA protein in the biology of the bacterium *Thermus thermophilus*. Genes (Basel) **8**:130.

111. **Paspaleva K**, **Thomassen E**, **Pannu NS**, **Iwai S**, **Moolenaar GF**, **Goosen N**, **Abrahams JP**. 2007. Article crystal structure of the DNA repair enzyme ultraviolet damage endonuclease. Structure **15**:1316–1324.

112. **Nelson-Sathi S**, **Sousa FL**, **Roettger M**, **Lozada-Chávez N**, **Thiergart T**, **Janssen A**, **Bryant D**, **Landan G**, **Schönheit P**, **Siebers B**, **McInerney JO**, **Martin WF**. 2014. Origins of major archaeal clades correspond to gene acquisitions from bacteria. Nature **517**:77–80.

Acknowledgements

I would like to express the great appreciation to Professor Ryoji Masui (Osaka City University), Professor Seiki Kuramitsu (Osaka University), Dr. Kenji Fukui (Osaka Medical College), and Dr. Masao Inoue (Kyoto University) for daily experimental advices and deep discussion. I thank Professor Masahiro Ueda (Osaka University) for permitting the continuation of this research when I transferred to Ueda laboratory from Kuramitsu laboratory. I thank Dr. Kwang Kim (Osaka University) for support in mass spectrometric analysis, and also thank Dr. Yuya Nishida (Osaka University) for providing me with recombinant RecJ. Finally, I thank my colleagues in Kuramitsu laboratory and Masui laboratory for their kind help in this study, and also thank my family for support in my research life.

Research achievement

Publication

Yuki Fujii, Masao Inoue, Kenji Fukui, Seiki Kuramitsu, and Ryoji Masui (2018) Resistance to UV irradiation caused by inactivation of *nurA* and *herA* genes in *Thermus thermophilus*. *Journal of Bacteriology*, **200**, e00201-18

Masao Inoue, Kenji Fukui, Yuki Fujii, Noriko Nakagawa, Takato Yano, Seiki Kuramitsu, and Ryoji Masui (2017) Structure of the Lon protease-like domain of RadA/Sms, a RecA paralog, and its DNA-binding role for DNA repair. *Journal of Biological Chemistry* **292**, 9801–9814

Presentation in academic conferences

Kensuke Tatsuta, Hiroki Okanishi, Norie Araki, Yuki Fujii, and Ryoji Masui
「高度好熱菌ピルビン酸キナーゼの活性調節機構の解析」
The 65th Japanese Biochemical Society, Kinki Branch, **C13**, Hyogo, Japan, May 26, 2018 (Poster and Oral presentation)

Kazuya Takao, Kenji Fukui, Yota Iio, Masao Inoue, Yuki Fujii, Takato Yano, Seiki Kuramitsu, and Ryoji Masui
"Structural analysis of a novel DNA-binding protein which is subject to regulation by phosphorylation"
Consortium of Biological Sciences 2017, **3P-0092**/**4LT25-02**, Hyogo, Japan, Dec. 6-9, 2017 (Poster and Oral presentation)

Yusuke Fujino, Masao Inoue, Yuki Fujii, Seiki Kuramitsu and Ryoji Masui
"Effects of ATP on structural stability of protein kinase TpkD from *Thermus thermophilus* HB8"
Consortium of Biological Sciences 2017, **3P-0133**/**4AT25-12**, Hyogo, Japan, Dec. 6-9, 2017 (Poster and Oral presentation)

Masao Inoue, Kenji Fukui, Yuki Fujii, Noriko Nakagawa, Takato Yano, Seiki Kuramitsu, and Ryoji

Masui

“The Lon protease-like domain that has a DNA-binding activity”

Consortium of Biological Sciences 2017, **3LBA-007**, Hyogo, Japan, Dec. 6- 9, 2017 (Poster)

Kazuya Takao, Yota Iio, Masao Inoue, Yuki Fujii, Seiki Kuramitsu, and Ryoji Masui

「翻訳後修飾を受ける機能未知 DNA 結合タンパク質の構造機能解析」

酵素・補酵素研究会 2017, **PP4**, Miyagi, Japan, June 23-24, 2017 (Poster)

Masao Inoue, Kenji Fukui, Yuki Fujii, Noriko Nakagawa, Takato Yano, Seiki Kuramitsu, and Ryoji Masui

「DNA 修復酵素 RadA の Lon プロテアーゼ様ドメインは DNA 結合活性を持つ」

酵素・補酵素研究会 2017, **PP11**, Miyagi, Japan, June 23- 24, 2017 (Poster)

Yusuke Fujino, Masao Inoue, Yuki Fujii, Seiki Kuramitsu, and Ryoji Masui

「高度好熱菌 protein kinase TpkD の構造安定性に対する ATP の効果」

酵素・補酵素研究会 2017, **PP14**, Miyagi, Japan, June 23-24, 2017 (Poster)

Kazuya Takao, Yota Iio, Masao Inoue, Yuki Fujii, Seiki Kuramitsu, and Ryoji Masui

“Structural and functional analysis of a novel DNA-binding protein TkaP from *Thermus thermophilus* HB8”

The 17th Annual Meeting of the Protein Science Society of Japan, **2P-017**, Miyagi, Japan, June 20-22, 2017 (Poster)

Yusuke Fujino, Masao Inoue, Yuki Fujii, Seiki Kuramitsu, and Ryoji Masui

“Effects of ATP on structural stability of protein kinase TpkD from *Thermus thermophilus* HB8”

The 17th Annual Meeting of the Protein Science Society of Japan, **2P-019**, Miyagi, Japan, June 20-22, 2017 (Poster)

Kazuya Takao, Yota Iio, Masao Inoue, Yuki Fujii, Yu-hei Tahara, Makoto Miyata, Seiki Kuramitsu, and Ryoji Masui

"Structural and functional analysis of a novel DNA-binding protein TkaP from *Thermus thermophilus* HB8"
8th OCARINA International Symposium, Osaka, Japan, Mar.7-8, 2017 (Poster)

Kazuya Takao, Yota Iio, Yusuke Fujino, Masao Inoue, Yuki Fujii, Seiki Kuramitsu, and Ryoji Masui
"Analysis of conserved hypothetical proteins with post-translational modifications in *Thermus thermophilus* HB8"
The 39th Annual Meeting of the Molecular Biology Society of Japan, **AS11-3/3P-0067**, Kanagawa, Japan, Nov. 30 - Dec. 2, 2016 (Symposium and Poster)

Yuki Fujii, Masao Inoue, Kenji Fukui, Seiki Kuramitsu, and Ryoji Masui
"Analysis of the cellular function of AddAB from *Thermus thermophilus* HB8"
17th annual meeting on The Japanese Society for Extremophiles, **P-07**, Kanagawa, Japan, Nov. 25-26, 2016 (Poster, poster award)

Kazuya Takao, Yota Iio, Masao Inoue, Yuki Fujii, Yusuke Fujino, Seiki Kuramitsu, and Ryoji Masui
"Structural basis of a novel DNA-binding protein TkaP from *Thermus thermophilus* HB8"
The 89th Annual Meeting of the Japanese Biochemical Society, **3P-106**, Miyagi, Japan, Sept. 25-27, 2016 (Poster)

Yusuke Fujino, Takero Miyagawa, Masao Inoue, Yuki Fujii, Seiki Kuramitsu, and Ryoji Masui
"Effects of ligands on structural stability of protein kinase TpkD from *Thermus thermophilus* HB8"
The 89th Annual Meeting of the Japanese Biochemical Society, **1P-128/1T11-05**, Miyagi, Japan, Sept. 25-27, 2016 (Poster and Oral presentation)

Yuki Fujii, Masao Inoue, Kenji Fukui, Seiki Kuramitsu, and Ryoji Masui
"NurA and HerA of the Extremely Thermophilic Eubacterium *Thermus thermophilus* HB8 Suppress the Repair of DNA Crosslinks"
11th International Congress on Extremophiles, **O16**, Kyoto, Japan, Sept. 12-16, 2016 (Selected oral presentation)

Yusuke Fujino, Takero Miyagawa, Masao Inoue, Yuki Fujii, Seiki Kuramitsu, and Ryoji Masui
"Effects of ligands on structural stability of protein kinase TpkD from *Thermus thermophilus* HB8"
The 16th Annual Meeting of the Protein Science Society of Japan, **2P-022**, Fukuoka, Japan, June 7-9, 2016 (Poster)

Kazuya Takao, Yota Iio, Masao Inoue, Yuki Fujii, Seiki Kuramitsu, and Ryoji Masui
"Structural basis of a novel DNA-binding protein TkaP from *Thermus thermophilus* HB8"
The 16th Annual Meeting of the Protein Science Society of Japan, **2P-025**, Fukuoka, Japan, June 7-9, 2016 (Poster)

Masao Inoue, Kenji Fukui, Yuki Fujii, Takato Yano, Seiki Kuramitsu, and Ryoji Masui
"Structure and function of Lon protease-like domain of RadA/Sms, a bacterial RecA paralog involved in homologous recombination"
The 16th Annual Meeting of the Protein Science Society of Japan, **2P-014**, Fukuoka, Japan, June 7-9, 2016 (Poster)

Kazuya Takao, Yota Iio, Masao Inoue, Yuki Fujii, Seiki Kuramitsu, and Ryoji Masui
「高度好熱菌 *Thermus thermophilus* HB8由来の新奇な DNA 結合タンパク質(TkaP)の構造・機能的解析」
The 63th Japanese Biochemical Society, Kinki Branch, **B19**, Hyogo, Japan, May 21, 2016 (Poster and Oral presentation)

Yusuke Fujino, Takero Miyagawa, Masao Inoue, Yuki Fujii, Seiki Kuramitsu, and Ryoji Masui
「高度好熱菌 Protein kinase TpkD の構造安定性に対するリガンドの効果」
The 63th Japanese Biochemical Society, Kinki Branch, **B20**, Hyogo, Japan, May 21, 2016 (Poster and Oral presentation)

Yuki Fujii, Masao Inoue, Kenji Fukui, Kwang Kim, Seiki Kuramitsu, Masahiro Ueda, and Ryoji Masui

“NurA and HerA play inhibitory roles in repairing DNA cross-link structure in thermophilic eubacterium *Thermus thermophilus* HB8”
The 5th Annual Meeting for Whole-Organism Science Society, **No. 8**, Osaka, Japan, Dec. 19-20, 2015 (Poster)

Masao Inoue, Kenji Fukui, Yuki Fujii, Takato Yano, Seiki Kuramitsu, and Ryoji Masui
“Structure and function of Lon protease-like C-terminal domain of DNA repair protein RadA/Sms”
The 5th Annual Meeting for Whole-Organism Science Society, **No. 17**, Osaka, Japan, Dec. 19-20, 2015 (Oral presentation)

Yuki Fujii, Masao Inoue, Kenji Fukui, Kwang Kim, Seiki Kuramitsu, Masahiro Ueda, Ryoji Masui
“Analysis of cellular functions about archaeal-type nuclease NurA and helicase HerA from bacteria”
BMB2015, **2P0681**, Hyogo, Japan, Dec. 1-4, 2015 (Poster)

Masao Inoue, Kenji Fukui, Yuki Fujii, Takato Yano, Seiki Kuramitsu, and Ryoji Masui
「RecA 様タンパク質 RadA/Sms C 末端ドメインの構造と機能」
BMB2015, **2P0683**, Hyogo, Japan, Dec. 1-4, 2015 (Poster)

Yuki Fujii, Masao Inoue, Kenji Fukui, Kwang Kim, Seiki Kuramitsu, Masahiro Ueda, and Ryoji Masui
“Analysis of cellular function of NurA and HerA from *Thermus thermophilus* HB8”
16th annual meeting on The Japanese Society for Extremophiles, **S6-03**, Tokyo, Japan, Nov. 8-9, 2015 (Oral presentation)

Yuki Fujii, Masao Inoue, Kenji Fukui, Kwang Kim, Seiki Kuramitsu, Masahiro Ueda, and Ryoji Masui
“Functional analysis of archaeal type nuclease and helicase from bacteria”
The 62th Japanese Biochemical Society, Kinki Branch, **A8**, Shiga, Japan, May 16, 2015 (Poster and Oral presentation)

Masao Inoue, Yuki Fujii, Kenji Fukui, Noriko Nakagawa, Ryoji Masui, and Seiki Kuramitsu
"Functional Analysis of a Bacterial RecA Paralogue, RadA/Sms"
The 4th Annual Meeting for Whole-Organism Science Society, **No. 24**, Osaka, Japan, Sept. 26-27, 2014 (Poster)

Yuki Fujii, Masao Inoue, Kenji Fukui, Noriko Nakagawa, Kwang Kim, Ryoji Masui, Masahiro Ueda, and Seiki Kuramitsu
"Roles of Archaeal-Type End Resection Enzymes in *Thermus thermophilus* HB8"
The 4th Annual Meeting for Whole-Organism Science Society, **No. 25**, Osaka, Japan, Sept. 26-27, 2014 (Poster)

Yuki Fujii, Masao Inoue, Kenji Fukui, Ryoji Masui, and Seiki Kuramitsu
"Functional analysis of archaeal-type nuclease/helicase, NurA/HerA, from *Thermus thermophilus* HB8"
The 36th Annual Meeting of the Molecular Biology Society of Japan, **P3-0148**, Hyogo, Japan, Dec. 3-6, 2013 (Poster)

Masao Inoue, Yuki Fujii, Kenji Fukui, Noriko Nakagawa, Ryoji Masui, and Seiki Kuramitsu
"Functional analysis of RadA/Sms, a bacterial RecA paralog involved in homologous recombination"
The 3th Annual Meeting for Whole-Organism Science Society, **No. 21**, Osaka, Japan, Sept. 21-22, 2013 (Poster)

Yuki Fujii, Masao Inoue, Kenji Fukui, Ryoji Masui, and Seiki Kuramitsu
"Archaeal-type nuclease/helicase, NurA/HerA, are involved in decreased tolerance to UV irradiation in *Thermus thermophilus* HB8."
The 3th Annual Meeting for Whole-Organism Science Society, **No. 22**, Osaka, Japan, Sept. 21-22, 2013 (Poster)

Yuki Fujii, Masao Inoue, Kenji Fukui, Ryoji Masui, and Seiki Kuramitsu

“Analysis of nuclease and helicase like proteins involved in homologous recombination from extreme thermophile”

The 60th Japanese Biochemical Society, Kinki Branch, **C3**, Osaka, Japan, May 18, 2013 (Poster and Oral presentation)

Yuki Fujii, Masao Inoue, Kenji Fukui, Ryoji Masui, and Seiki Kuramitsu

“Genetic analysis of putative nucleases and helicases involved in double-strand break repair in *Thermus thermophilus* HB8”

The 85th Annual meeting of the Japanese Biochemical Society, **3P-971**, Fukuoka, Japan, Dec. 14-16, 2012 (Poster)

Yuki Fujii, Masao Inoue, Kenji Fukui, Ryoji Masui, and Seiki Kuramitsu

“Genetic analysis of putative nucleases and helicases involved in double-strand break repair in *Thermus thermophilus* HB8”

The 2th Annual Meeting for Whole-Organism Science Society, **No. 40**, Hyogo (SPring-8), Japan, Sept. 21-22, 2012 (Poster)